Design of Rubble-mound Foundations for Vertical Seawalls: Scour, Screed Layer and Berm Width

By

Esmé van Wageningen

UNIVERSITEIT
iYUNIVESITHI
STELLENBOSCH
UNIVERSITY

100
1918·2018

*Thesis presented in fulfilment of the requirements for
the degree of Master of Engineering in Civil Engineering in
the Faculty of Engineering at Stellenbosch University*

Supervisor: Prof JS Schoonees

December 2018

DECLARATION

Plagiarism is the use of ideas, material and other intellectual property of another's work and to present is as my own.

I agree that plagiarism is a punishable offence because it constitutes theft.

I also understand that direct translations are plagiarism.

Accordingly, all quotations and contributions from any source whatsoever (including the internet) have been cited fully. I understand that the reproduction of text without quotation marks (even when the source is cited) is plagiarism.

I declare that the work contained in this assignment, except where otherwise stated, is my original work and that I have not previously (in its entirety or in part) submitted it for grading in this module/assignment or another module/assignment.

_____

Esmé van Wageningen

_____

Student number

_____

Date

ABSTRACT

Coastal erosion has always been a challenging problem to solve for coastal engineers since it is such a complex process that threatens valuable environments and properties along the coastline. Structural erosion, or scour, develops due to the presence of a marine structure that interrupts the natural sediment transport processes. Scour is one of the most common mechanisms of failure of marine structures and therefore it is vital to gain a better understanding of the scour process in order to design marine structures that can withstand the adverse effects of scour.

The objective of this study is to gain more knowledge of the scour process that develops in specifically the screed layer directly underneath the concrete elements of a vertical seawall that is protected by a rubble-mound berm. This was accomplished by investigating existing literature on marine structures, their failure mechanisms, the processes of sand and granular scour as well as research on physical modelling. A physical experiment was then set up in a 2D wave flume in the hydraulic laboratory of the CSIR in Stellenbosch, South Africa to test the influences of different aspects of the scour process in the screed layer underneath a model seawall. The influence of the wave period, the rubble-mound berm width, the screed layer thickness, the armour rock stability and the reflection coefficient was investigated.

The scour damage in the model screed layer was measured with wooden dowels, as was done in previous research, as well as with a new method developed by the author that uses sonar technology to create a submerged image of the scour pattern that developed in the screed layer. The scour measurements for each different test set-up were analysed. Firstly, it was found that a shorter wave period resulted in more scour damage since the interaction between the incident and reflected waves was more significant near the seawall and occasionally superimposed due to the rapid change in wave direction and orbital velocities, which disturbs the screed material. The rubble-mound berm width, however, did not have as significant an influence on screed layer scour as expected. A wider berm did provide more scour protection, but the optimal berm design must balance protection and construction and material costs and therefore a narrower berm of $4D_{n50}$ is recommended. A minimised screed layer thickness of 100 mm is recommended since it resulted in the least amount of scour whilst still being able to be constructed at an adequate accuracy. As expected, a more stable armour layer resulted in less scour damage in the screed layer. Lastly, it was interesting to observe that a test that resulted in less scour, had a higher reflection coefficient. This is probably due to less wave energy that was absorbed by the berm (causing scour in the screed layer) but reflected back seaward instead.

OPSOMMING

Kuserosie was nog altyd 'n uitdagende probleem om op te los vir ingenieurs aangesien dit so 'n ingewikkelde proses is wat die waardevolle omgewing en eiendomme langs die kuslyn bedreig. Strukturele erosie, of uitskuring, is die proses wat ontwikkel as gevolg van die teenwoordigheid van 'n mariene struktuur wat die natuurlike sedimentvervoerprosesse onderbreek. Uitskuring is een van die mees algemene swigmeganismes van mariene strukture en dus is dit van uiterste belang om die uitskuringsproses beter te verstaan ten einde mariene strukture te ontwerp wat teen die skade wat uitskuring bestand is.

Die doel van hierdie studie is om die uitskuringsproses te ondersoek wat spesifiek plaasvind in die vlaklaag direk onder die betonelemente van 'n vertikale seemuur wat deur ruklip beskerm word. Dit is verwesenlik deur 'n literatuurstudie te doen oor kusstrukture, hul swigmeganismes en sand- en klipuitskuringsprosesse asook navorsing oor fisiese modelering. 'n Fisiese eksperiment in 'n 2D golfkanaal is toe in die hidrouliese laboratorium van die WNNR in Stellenbosch, Suid-Afrika, opgestel om die invloede van verskillende aspekte van die uitskuringsproses in die vlaklaag onder 'n modelseemuur te toets. Die invloed van die spits-golfperiode, die ruklip se kruinwydte, die vlaklaagdikte, die stabiliteit van die beskermende rukliplaag en die weerkaatsingskoëffisiënt is ondersoek.

Soos met vorige navorsingseksperimente, is die uitskuring met houtstokkies gemeet, asook met 'n nuwe metode wat deur die skrywer ontwikkel is. Hierdie metode behels om sonartegnologie te gebruik om onderwaterbeelde van die uitskuringspatrone wat in die vlaklaag ontwikkel het, te skep. Die uitskuringsmetings is vir elke verskillende toetsopstelling geneem en ontleed. Eerstens is daar gevind dat 'n korter golfperiode meer uitskuring veroorsaak omdat die interaksie tussen die invallende en weerkaatste golwe superponeerde golwe veroorsaak wat die golf- en orbitaalsnelhede se rigtings vining verander en sodoende die vlaklaag beskadig. In teenstelling het die ruklipkruinwydte nie so 'n beduidende invloed op die uitskuringsproses gehad soos verwag nie. 'n Wyer kruinwydte het meer beskerming teen uitskuring gebied, maar die optimale kruinontwerp moet 'n balans tref tussen effektiewe beskerming en konstruksie- en materiaalkoste en dus word 'n nouer kruinwydte van $4D_{n50}$ aanbeveel. 'n Minimale vlaklaagdikte van 100 mm word aanbeveel ten einde uitskuring te beperk terwyl dit nogsteeds moontlik is om dit met voldoende akkuraatheid te bou. 'n Meer stabiele beskermingskliplaag het ook, soos verwag, minder uitskuring tot gevolg gehad. Laastens, was dit interessant om te let dat toetse wat minder uitskuring gehad het, het hoër weerkaatsingskoëffisiënte gehad. Dit is moontlik omdat minder golfenergie deur die kruin en vlaklaag geabsorbeer is en die energie eerder seewaarts weerkaats is.

ACKNOWLEDGEMENTS

First and foremost, I want to thank my Heavenly Father for entrusting me with the capabilities to have undertaken this thesis. This thesis is for Him and would not have been possible without Him.

I am also indebted to the following people and would like to express my gratitude:

- Prof Koos Schoonees, my supervisor, for his guidance and mentorship throughout the research process and for always being patient, constructively critical and motivating with his words "Jy is mos slim, man" and for generously sharing his unrivalled knowledge in the coastal engineering field.
- Ross Jarvis, my laboratory partner, for his company and entertaining stories during the long days of physical modelling tests, his selfless hard work and help, for enduring blisters to do the heavy lifting and for always pitching at the laboratory earlier and leaving later.
- Johan Kieviet, Petro Uys, Carl Wehlitz, Rafick Jappie, Reagan Solomon, William Prins, Theuns Koopman and Sipho Masebala at the CSIR hydraulics lab and Johan Nieuwoudt and Iliyaas Williams at the Stellenbosch University's Civil Engineering Hydraulics laboratory for their generosity with their laboratory equipment, knowledge, time and labour as well as their interest and enthusiasm for the project.
- My father, Gerrit van Wageningen, for his enthusiasm and interest in my work, for coming up with the idea of incorporating sonar technology in the experimental methodology (refer to Section 3.10.3), for his love and support and the example of excellence that he sets.
- Belinda Muller at TECMED, for the interest shown in my work and for the generosity with their ultrasound sonar equipment that I could use for the entire duration of the physical modelling tests.
- My mother, Marietjie and brothers, Gerrit and Pine van Wageningen, for their constant encouragement and support throughout my Master's degree, for listening ears and for always providing a feeling of home when rest is needed.
- My Masters colleagues, Bettina Botha, Erica Braun, Andreas Brooks, Franco de Bondt, Stephan Dreyer, Jaco Koen, Hannes Viljoen, Janeke Volkmann and Janine Vonkeman that made Room S419 a (mostly) productive, but always enjoyable environment to work in.
- My friends and family, for their support and my fiancé, Josua Roux, for his love, support and for providing me with the motivation to hand in on time for our wedding right after graduation.

CONTENTS

LIST OF FIGURES

LIST OF TABLES

NOMENCLATURE

B	-	Width or diameter of coastal structure (m)
C_r	-	Refection coefficient
D	-	Characteristic linear dimension of unit (mm)
$D_{n,50}$	-	Median stone diameter (m)
Δ	-	$(\rho_r / \rho_w) - 1$
ε_p	-	Surf similarity parameter or Iribarren number
g	-	Gravitational acceleration (m/s^2)
γ	-	Enhancement factor for HR Wallingford Wave-maker
H_b	-	Breaking wave height (m)
H_s	-	Significant wave height (m)
H_{mo}	-	Significant wave height from variance of record (m)
h	-	Local water depth or water depth in front of structure toe(m)
h_t	-	Depth of foundation toe or berm (m)
h'	-	Depth of toe berm excluding the armour layer (m)
KC	-	Keulegan-Carpenter number
k_p	-	wave number associated with T_p
L_b	-	Breaking wavelength (m)
$L_{p,0}$	-	Deep-water wavelength (m) associated with T_p
L_p	-	Wavelength (m) associated with T_p
M_{50}	-	Median stone mass (kg)
m	-	Slope of seabed
μ	-	Dynamic viscosity (N.s/m^2)
N_{od}	-	Number of stones displaced within a strip of one D_{n50} width
N_s	-	Stability factor
ν	-	Kinematic viscosity (N.s/m^2)
P	-	Fluid density (kg/m^3)
φ	-	Shield's parameter
R^2	-	Coefficient of determination
ρ_r	-	Density of armour unit (kg/m^3)
ρ_w	-	Density of water (kg/m^3)
S_A	-	Horizontal scour area (m^2)

S_D	-	Horizontal scour depth (m)
s_{om}	-	Fictitious wave steepness based on T_m
s	-	Specific gravity
$\tan\beta$	-	Beach slope
T_p	-	Peak wave period (s)
T	-	Wave period (s)
u_m	-	Maximum undisturbed orbital velocity of water particles (m/s)
$u_{rms,m}$	-	Root-mean-square of horizontal velocity (m/s)
θ	-	Wave incident angle (°)
w	-	Particle fall velocity (m/s)
y_s	-	Maximum depth of scour (m)

1. INTRODUCTION

1.1 BACKGROUND

Coastal erosion is an everyday problem for properties and infrastructure located on the coastline and a complex problem to solve from an engineering perspective. Seawalls are marine structures, usually concrete, that protect these coastal properties against wave attack and erosion and stabilize the beach profile, as shown in Figure 1-1. However, seawalls are robust structures that disrupt the natural coastline and processes that form it. Seawalls induce wave breaking and reflected waves that create unnatural magnitudes of turbulence that disturb and suspend sediment or seabed material from the seabed at the toe of the seawall structure so that the material eventually washes out. This process is referred to as scour. The scoured material reduces the contact surface between the base of the seawall and the foundation. The reduction in contact surface results in a reduction in friction so the seawall may destabilise and eventually fail.
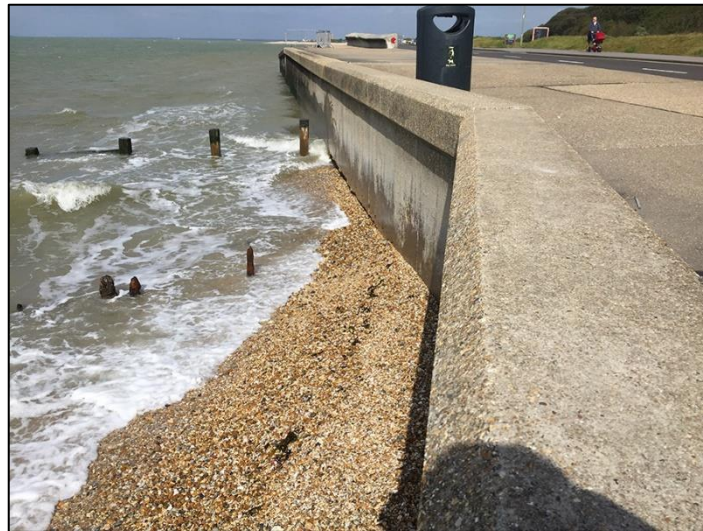
Figure 1-1: Vertical seawall on sediment foundation (SCOPAC, 2017)

Scour is alleged to be one of the main causes of failure in breakwaters and seawall structures (Bruun, 1985). Post disaster investigations that were conducted after the 2011 Japan earthquake and tsunami, indicated that catastrophic failures of coastal retaining structures along the eastern shoreline were caused by severe scour at the toe of the structures (Huang, 2017). Scour is therefore a major issue in the coastal construction environment so thorough research must be dedicated to understanding the scour process and effectively counteracting it.

The focus of this thesis will be on optimising the design of a rubble-mound foundation underneath a vertical seawall in order to effectively protect the seawall against scour. Scour mainly occurs in the screed layer of the rubble-mound foundation. The screed layer is a thin layer of finer granular material directly underneath the concrete seawall element that ensures a level surface for placement and sufficient contact area for friction for maximum stability of the structure.

1.2 OBJECTIVES

The objectives of this study were identified as follows:

- To investigate literature on the **standard design guidelines** of **vertical seawalls** and **scour protection** in order to design a model seawall and rubble-mound berm structure for specifically protecting the screed layer against scour.
- To investigate literature on physically modelling **scour processes** and measuring and **quantifying scour damage** in a laboratory set-up.
- To determine the effect the **wave period** has on the scour damage that develops directly underneath a vertical L-seawall in the screed layer with the aid of physical modelling.
- To determine the effect of the **berm width** in front of the seawall as well as the **screed layer thickness** on the scour damage in the screed layer with the aid of physical modelling.
- To investigate whether the **armour rock stability** of the berm in front of the seawall correlates in some way with the scour damage that develops.
- To use the results from the modelling tests to recommend an **equation for scour prediction** as well as an **optimised standard design** for a rubble-mound foundation of a vertical seawall, focusing on scour protection of the screed layer as well as realistic construction methods.

1.3 MOTIVATION

Scour is a major problem in the coastal construction industry, especially since it is such an unpredictable process and the effects only become evident once a coastal structure is in operation for long enough for the process to develop to a point of causing failure. Research on scour and especially granular scour has been found to be relatively insufficient compared to its significance in the coastal environment. Therefore, this study was motivated to be executed in order to gain more insight in the scour process.

A case study in coastal engineering practice provided more specific direction for this study: An L-shaped seawall in the Middle East nearly failed due to scour damage in the screed layer of the rubble-mound foundation (see more detail in 2.2.4). It was realised that there was no comprehensive design standard for the screed layer of a rubble-mound foundation and protecting it against scour. Therefore, this study attempts to fill that knowledge gap in coastal design standards by specifically testing the effect of the wave conditions and rubble-mound berm structure design on the scour damage that develops in the screed layer directly underneath a seawall structure.

1.4 SCOPE

The scope of this study extended to investigating literature on vertical seawalls, scour behaviour and physical modelling techniques in order to design a composite seawall structure that consists of an L-shaped seawall and rubble-mound berm and foundation. The design was then set up as a 2D flume experiment so that several tests could be executed in order to test the effect of the wave period, the rubble-mound berm width and the screed thickness on the extent of scour damage that developed directly underneath the seawall.

The wave periods that were tested ranged from 8 to 14 seconds, which are characteristic to the South African coastline (Rossouw, Coetzee and Visser, 1982). The berm widths that were tested ranged from 2 to 8 times the mean diameter of the armour units used in the berm, since this range covered the berm widths that are usually used in practice to just below the standard minimum berm width to test the validity of the standard. The screed thicknesses that were tested were 100, 200 and 300 mm in prototype since this range of thicknesses is realistic when used in practice.

These tests together with preparatory tests resulted in a total of 32 tests that had to be conducted.

1.5 LIMITATIONS

The following aspects limited the study to the scope mentioned above:

(i) Time

The experiment process was limited to one test per day since the set-up and execution took most of the day to complete and silicon was used in the set-up that had to dry overnight. The slow rate of test execution meant that the number of tests that could be conducted, was very limited in the available time at the test facilities. The number of tests that could be repeated and verified, was therefore also very limited.

(ii) Resources

Resources like labour, equipment and materials were limited to what the University of Stellenbosch and the test facility could offer and what the budget made available for this study could cover. The test facility had a 2D wave flume with a width of 750 mm available for testing and a team supported the author in constructing the experimental test set-up.

(iii) Data acquisition

Data that was acquired during the experiments was limited to scour depths, deep-water wave probe data (wave heights, periods and reflection coefficients) and visual observations. The shallow-water wave probe data at the toe of the structure could only be acquired during calibration without the seawall model structure in place (refer to Section 3.9 for more detail). Overtopping would have been a useful set of data, but due to the open system set-up of the experiments, overtopping could not be measured effectively and was therefore only visually observed and determined qualitatively.

1.6 LAYOUT OF THESIS

The layout of this study is described according to chapter content:

Chapter 1 - Introduction: describes the background of the study and the motivation behind why it is being conducted and what the study aims to achieve.

Chapter 2 - Literature Review: consists of an extensive investigation of previous research done on seawalls, specifically vertical L-shaped walls, sediment and granular scour and physical modelling techniques to inspire an original 2D model design for an L-element seawall on a rubble-mound foundation and berm.

Chapter 3 - Methodology: The methodology of preparing for, setting up and conducting the physical 2D model tests are described in detail.

Chapter 4 - Results and Analysis: The raw results are processed and analysed for each test set that was conducted. Graphs and trend lines are developed in an attempt to predict scour under the specific wave conditions and berm set-ups for future application in practice.

Chapter 5 - Conclusions and Recommendations: Conclusions are made from the result analysis and finally recommendations on a design standard for an anti-scour rubble-mound foundation of a vertical seawall are made.

2. LITERATURE REVIEW

2.1 INTRODUCTION

The literature review was conducted in order to gain sufficient insight and understanding regarding seawall structures, sediment and rock, coastal processes like erosion and scour as well as the science of physical modelling. The main focus of the literature review was on scour processes underneath vertical seawalls and the design of a standard rubble-mound foundation to protect a vertical seawall against scour.

2.2 SEAWALL STRUCTURE

2.2.1 General

Seawalls are defined as onshore marine structures with the primary purpose of protecting landside environment, property and infrastructure against coastal conditions like wave action, storm surge and flooding. Seawalls act as the boundary between the land and sea and run parallel to the shoreline in order to reinforce the coastal profile. This is done by stabilising the backfill on the landside while reflecting wave energy back to the seaside (Burchart and Hughes, 2012). Seawalls are categorized as "hard engineering" coastal protection, which can be defined as the controlled disruption of natural processes by man-made structures (Definitions.net, 2017). Every seawall is designed uniquely and specific for each site. The type of seawall that should be used, is determined by the surrounding coastal conditions, the coastal protection required and the construction methods, materials and finances available (Burchart and Hughes, 2012).

2.2.2 Types of Seawalls

There are numerous types of seawalls that are used across the globe that can generally be categorized as either vertical, curved or stepped concrete seawalls or gravity mound seawalls.

(i) Vertical seawalls

Vertical seawalls, as shown in Figure 2-1, are used in environments with high wave energy since a vertical seawall provides a high degree of protection against wave action and coastal flooding, given that the structure is accurately designed. Vertical seawalls are specifically suitable where limited space is available for the structure, since the structure can reach deep waters with minimum lateral space requirements. The drawbacks of vertical seawalls are that minimum energy dissipation occurs against the vertical face of the seawall so the seawall is exposed to intense

wave attack and requires regular maintenance (Sumer, Whitehouse and Tørum, 2001). Major wave reflection and turbulence occurs against the vertical face which contributes to erosion at the toe of the structure. This process will be discussed in detail in Section 2.3 (French, 2001).
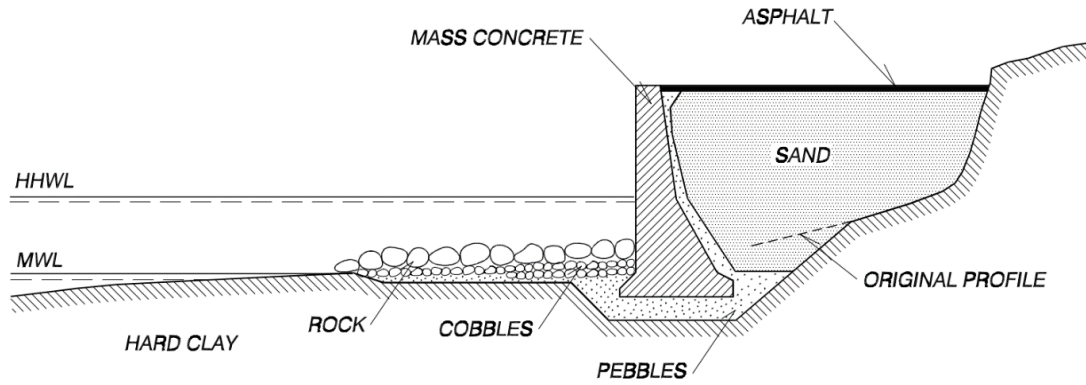
Figure 2-1: Cross-section of vertical seawall (Burchart and Hughes, 2012)

(ii)   Curved seawalls

Curved seawalls are concrete marine structures with a concave seaside face. The curved face, as shown in Figure 2-2, is designed to dissipate wave energy by increasing contact area so that reflected waves and turbulence is minimised. The curved wall is designed to transmit waves back towards the sea in order to minimise overtopping and wave run-up as well. Curved seawalls are much more complex to design and construct and therefore more expensive. It is vital to design the curve of the seawall accurately in order to provide efficient protection against overtopping and flooding. Incorrect curve designs can result in worse overtopping conditions. Every seawall design is unique to its location on the shoreline and the site conditions (Burchart and Hughes, 2012).
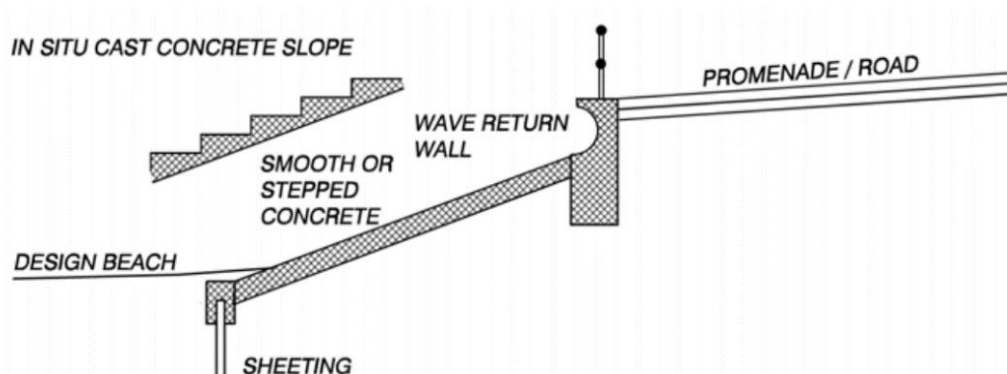
Figure 2-2: Cross-section of stepped and sloped seawall (Burchart and Hughes, 2012)

(iii)   Stepped seawalls

Stepped seawalls are alternative designs to curved seawalls to minimise wave run-up and overtopping. The seaside face, as shown in Figure 2-2, is designed in a stepped pattern to dissipate wave energy and transmit the waves back to the sea. An additional advantage of stepped seawalls is that the steps can serve a dual purpose of coastal protection as well as recreational facilities for pedestrians. As with curved seawalls, stepped seawalls require space along the shoreline, a lot of material and accurate design to be effective (Burchart and Hughes, 2012).

(iv)   Gravity mound seawalls

Gravity mound seawalls, as shown in Figure 2-3, are constructed by placing materials that range from rocks to concrete blocks to sandbags, on top of each other and rely on the material weight for structural integrity. Gravity mound seawalls are relatively low in cost and easy to construct and can therefore be used when required for emergency situations. However, these structures are generally only used in low wave energy conditions or as temporary protection. Dikes can also qualify as large gravity mound seawalls that provide wide coastal protection boundaries for the long term (Malan, 2016).
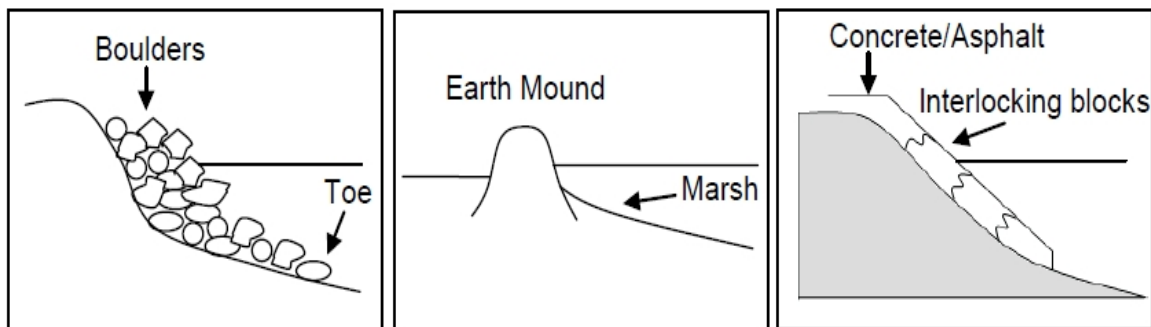
Figure 2-3: Cross-sections of gravity mound seawalls (Adapted from French, 2001)

This thesis will focus on the design and construction of vertical seawalls.

2.2.3   Types of Vertical Seawalls

There are various types of vertical seawalls that can be constructed, depending on the geotechnical and coastal conditions, financial investments and design and construction expertise available.

(i)   Embedded walls

Embedded walls usually consist of sheet piles that are driven into the seabed along the shoreline to retain backfill and provide coastal protection, as shown in Figure 2-4. The sheet piles form a continuous wall in order to resist

primary horizontal forces exerted by the backfill on the landside and wave and tidal action on the seaside. When necessary, sheet piles can be anchored by horizontal rods into the backfill for additional stability. Embedded walls are usually required when the geotechnical conditions of the local seabed does not provide the necessary bearing capacity of gravity seawalls (Malan, 2016).
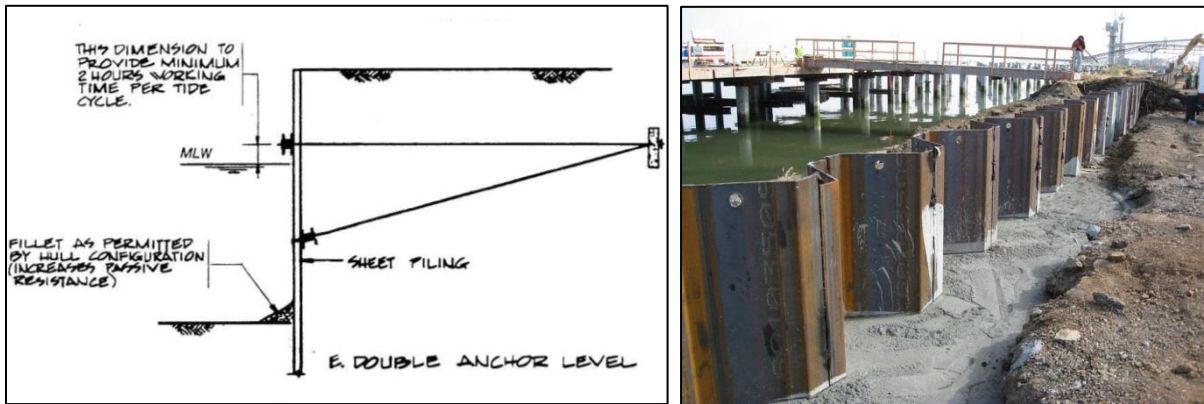
Figure 2-4: Embedded sheet pile seawall (Liftech Consultants inc, 2013)

(ii)   Counterfort and L-shaped seawalls

The use of L-shaped concrete units as retaining structures is a relatively new method of constructing seawalls. A unit consists of a horizontal bottom slab and a vertical retaining wall cast together in an L-shape and some wall elements are even constructed with webs for strength and stability. L-elements are precast separately onshore for effective quality control and then placed and fixed together to form a continuous wall structure. The units can either be placed in the dry in a cofferdam as shown in Figure 2-5 or directly into the sea. The joints between the units are then sealed with either geotextiles, in-situ cast concrete or plaster (Pitkala, 1986).
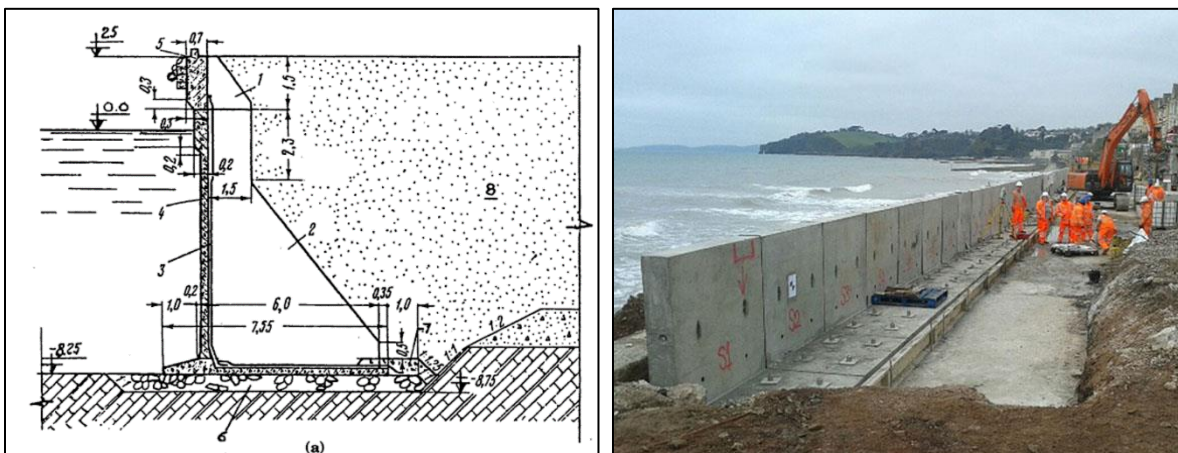
Figure 2-5: L-wall (Liftech Consultants inc, 2013)

(iii)   Caisson and cellular walls

Caisson walls consist of enormous hollow concrete blocks that are cast onshore and then generally placed in wet conditions. The hollow cells within a caisson are filled with sand in order to minimise concrete volumes and to control the weight of the caisson so the structure can be floated to the location and then filled up to sink the caisson into position. After the separate caisson units have been placed, an in-situ concrete cap is cast to join the caissons into a monolithic structure and to accommodate for construction tolerances and settlement. Due to its size, caissons are reinforced and therefore adequate steel cover and suitable concrete design is vital. A cross-section and example of a caisson wall is shown in Figure 2-6 (Alexander, 2016).
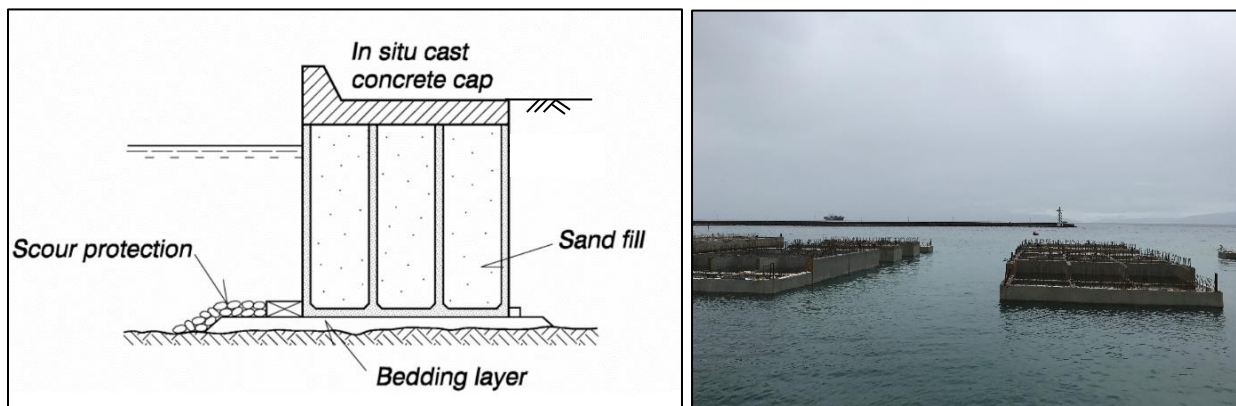
Figure 2-6: Caisson seawall cross-section (Burchart & Hughes, 2012) and caisson under construction

This thesis will focus on L-shaped vertical seawalls, although the research and experimental set-up is applicable to any seawall structure with a vertical face.

2.2.4   L-shaped seawalls (L-walls)

L-walls became popular retaining structures in the 1970s since the concept offered a balance between durable strength and economical and effective use of concrete. The design of L-elements is relatively flexible and can be adjusted according to the site conditions and requirements since the elements are cast in custom made moulds. The maximum dimensions of simple L-elements are generally 7 m in height and 3 – 12 m in breadth. When the elements exceed these dimensions, diagonal rib walls have to be constructed to stiffen the element structures. Stiffened elements can reach heights of up to 21 m and the mass of the individual elements can range between 60 and 450 tons. An example of an L-wall with backfill anchorage is shown in Figure 2-7 (Pitkala, 1986).

The bottom slabs ensure stability against horizontal forces, but if the elements are anchored to the back earth or joined to each other, stability can be improved and the bottom slab width can be reduced in order to ultimately

reduce the mass of the elements. The mass of the concrete elements determines the required bearing capacity of the foundation underneath the elements and, like all gravity structures, L-walls' foundation bearing capacity is a vital precondition. If the local seabed does not provide sufficient bearing capacity, it must be removed and replaced with a geotechnically stronger foundation like approved quarry run. The foundations of the L-wall elements are therefore vital to the stability of the entire structure so great care has to be taken when designing and especially constructing the foundation (Pitkala, 1986).
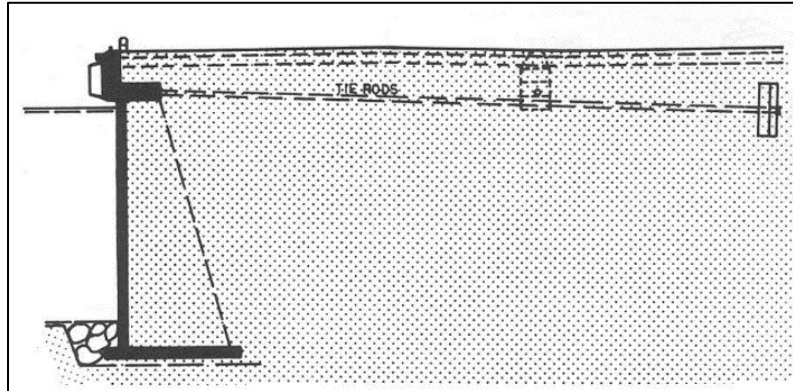
Figure 2-7: L-wall element anchored to backfill (Pitkala, 1986)

According to Alexander (2016) and Pitkala (1986), there are numerous advantages to using precast concrete L-walls as retaining structures in the coastal environment:

- L-walls (b) are quicker and more economical to construct compared to other gravity seawalls like block walls (a), as shown in Figure 2-8.
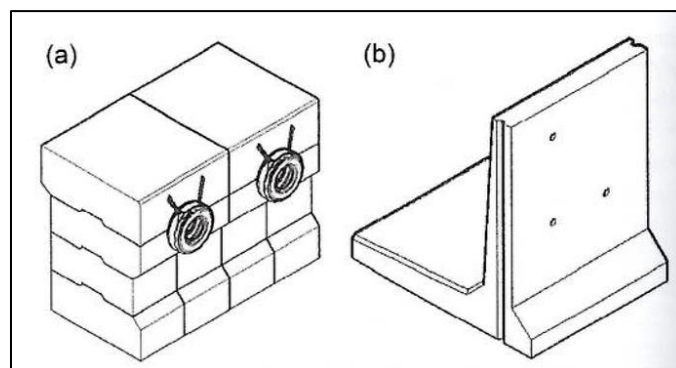
Figure 2-8: Block seawall and L-wall element (Alexander, 2016)

- Much less concrete per linear meter of seawall is required to ensure the stability of an L-wall, compared to a block wall.

- The bearing capacity of the seabed or stone foundation can be less due to the reduced mass of the concrete L-wall.
- Placement of L-wall segments is much quicker than placing block walls since an L-segment can generally replace several stacked block units.
- The concrete curing process can be carefully controlled since the L-elements are cast in the dry, as shown in Figure 2-9. This is so that sufficient durability and strength can be achieved.
- Elements can be shaped and altered without limitations in terms of corners, curves, slopes and fillets.

Figure 2-9: L-element cast mould (Alexander 2016)

Examples of L-walls from 1975 to the modern day can be investigated in terms of design and construction methods that were used. Pitkala (1986) conducted extensive research on L-elements as quay structures and focused on Finnish quay walls from 1970s to 1980s:

- The Buskö quay was constructed in 1975 in Pietarsaari, Finland. The total height of the stiffened L-wall is 10 m with a quay length of 180 m and a mass of 90 ton per element. The structure was founded on a sand bank.
- The Inkoo coal quay, Finland, was constructed in 1982 and was the deepest L-element structure at that time with a wall height of 18.6 m, quay length of 240 m and mass of 450 ton per element. The foundation was on even rock bed as shown in Figure 2-10.
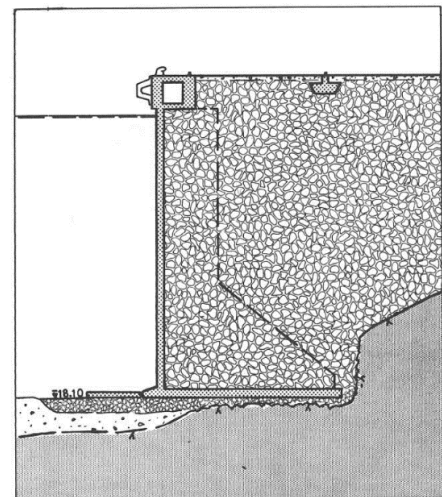
Figure 2-10: Inkoo quay wall cross-section (Pitkala, 1986)

- The Zliten fishing port, Libya, was constructed in shallow water with small L-elements, 2.5 – 3.5 m in height, mass of 20 – 30 ton/pc and 450 m in length.

- The Kristiina coal quay, Finland, was built in 1983 with a quay length of 155 m, L-element height of 18.5 m and a mass of 360 ton/pc on a levelled bedrock foundation.

- The Veitsiluoto quay wall, Finland, was constructed in 1985 with a quay length of 190 m and an element height of 11.5 m. The L-elements were anchored to the backfill so the bottom slab widths could be minimised, as mentioned above.

- A more recent example of an L-element quay wall was constructed in 2012 in Al Raha in the Arabian Gulf. This major project encompassed a 19 km perimeter quay wall around the Western precinct islands that consists of 6340 50-ton precast L-elements with a height of 5 – 6 m. The seabed consists of silty sand and had to be reinforced with stone columns and an anti-scour rock foundation with a screed layer as shown in Figure 2-12. The units were precast in moulds on dry land and then transported and lifted onto barges by a 250-ton crawler crane. The units were then placed in position from the barges onto the submerged foundation as shown in Figure 2-11 (Wehr, Freitag and Köhler, 2015).

Figure 2-11: Casting and placement of L-elements at Al Raha, Western precinct (Wehr, Freitag and Kohler, 2015)
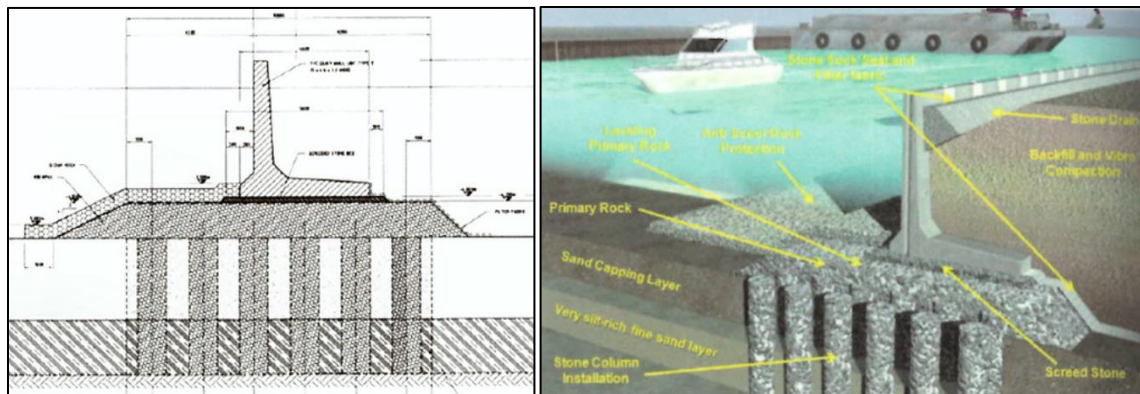
Figure 2-12: Cross-section and 3-D representation of Al Raha L-wall (Wehr, Freitag and Köhler, 2015)

- Finally, Figure 2-13 shows schematically how an L-element seawall was constructed in the Middle East. It was constructed with reinforced concrete elements that were placed on a rubble-mound foundation with a wide berm to protect the toe and a 100 mm screed layer to ensure a level surface for element placement.

Details of the rock layers that make up the foundation are shown in Table 2-1, with M_{50} representing the median mass of the rocks of the specific layer (Schoonees, 2018).

Table 2-1: Rubble-mound foundation details

Rock Layer	Grading range	Layer thickness
Armour (Class 4)	0.5 – 1 t (M_{50} = 0.7 t)	1500 mm
Filter (Class 2)	1 – 500 kg (M_{50} = 60 kg)	600 mm
Core (Class 1)	50 – 150 mm	300 – 900 mm
Screed	19 mm	100 mm minimum

During operation, scour occurred underneath the wall, mainly in the screed layer directly underneath the concrete L-elements. In some areas, the screed was flushed away into the filter layers due to wave and current action and caused the L-elements to become unstable and move. The behaviour of the screed material sparked interest in researching granular scour and ways to ensure stability of the screed layer as part of detailed foundation design (Schoonees, 2018).
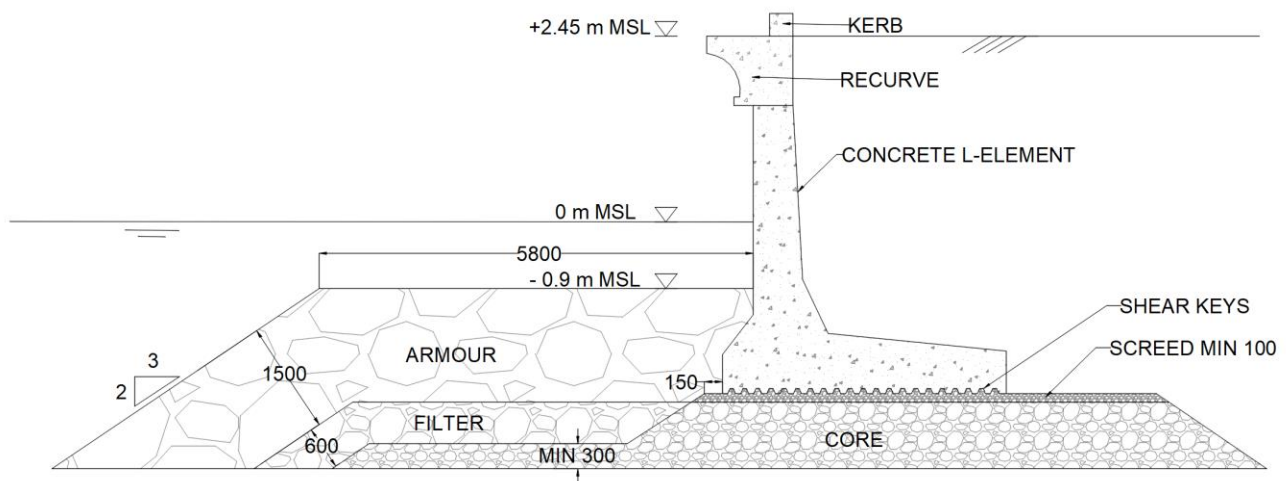
Figure 2-13: Cross-section of L-element and rubble-mound foundation design of Middle East case study (Schoonees, 2016)

2.2.5 **Failure Modes**

Marine structures are subject to various modes of failure that include hydrodynamic and geotechnical factors. According to the *Coastal Engineering Manual* (Burchart and Hughes, 2012)*,* a structure fails when it is damaged to the extent that the structural performance and functionality of the structure is below the minimum that was intended by design. Failure may occur due to the several reasons:

- Design failure occurs when either components of a structure, or the structure as a whole does not perform as expected in terms of withstanding design loads.
- Load exceeding failure occurs when the loads exerted on the structure exceed the design load conditions.
- Construction failure refers to when construction is executed inaccurately or construction materials are substandard and eventually cause the failure of the structure.
- Deterioration failure arises when the structure is not maintained sufficiently so that the structure deteriorates below design strength (Burchart and Hughes, 2012).

In the coastal environment, failure of seawalls poses a significant problem since seawalls generally serve an important purpose of protecting the landside against coastal conditions and therefore have to be stable, reliable and long lasting. As shown in Figure 2-14, there are various modes of failure that occur in the case of seawalls, with the focus on vertical seawalls and the stability of the seawall's foundation, namely:

- Toe or berm instability
- Sliding of the seawall
- Settlement of the seawall
- Seaward overturning due to toe scour
- Landward overturning due to overwash scour
- Rotational slip failure due to loads on backfill

Diagrams of failure methods are from the *Coastal Engineering Manual* (Burchart and Hughes, 2012).
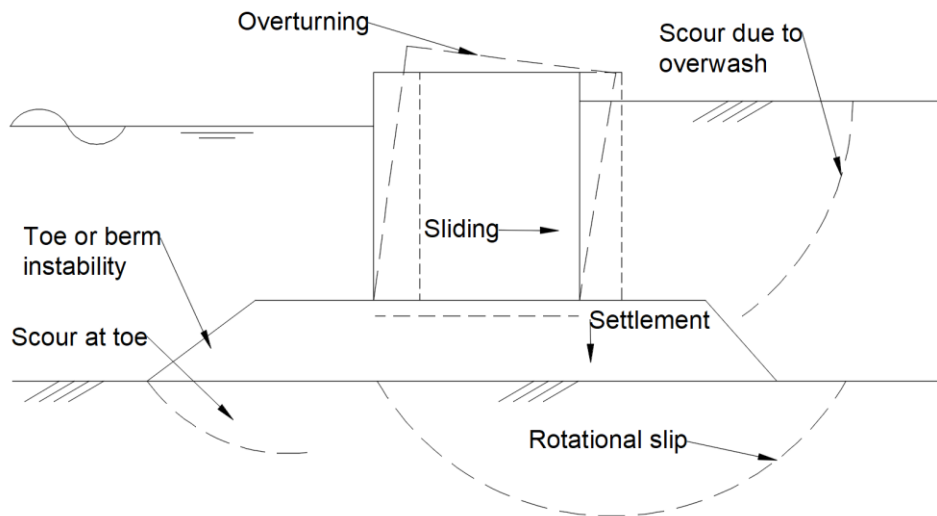
Figure 2-14: Summary of failure modes of vertical seawalls or breakwaters (adjusted from CIRIA, 2007)

(i)   Toe or berm instability in shallow water

When the toe of a marine structure is placed on hard seabed and in shallow water, it is exposed to wave breaking forces that may cause displacement of armour units, as shown in Figure 2-15. Toe blocks can either be placed in a trench, anchored or bolted in order to prevent damaged or displacement (Burchart and Hughes, 2012).
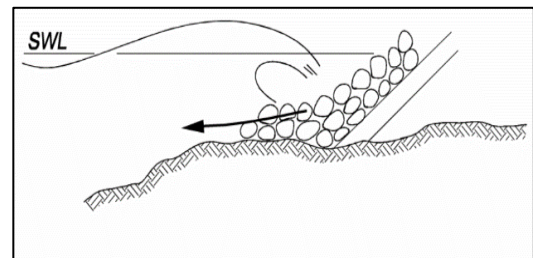
Figure 2-15: Toe or berm instability

(ii)   Sliding of seawall

Sliding, as shown in Figure 2-16, is the result of when the active soil and groundwater pressures of the backfill exceed the sum of the passive toe resistance and frictional resistance at the base of the structure. The toe can either be buried deeper or serrations at the base can prevent sliding (Burchart and Hughes, 2012).
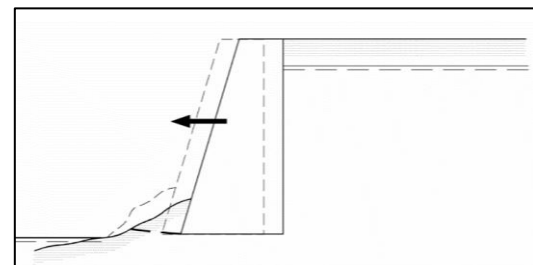
Figure 2-16: Seawall sliding

(iii)   Settlement of seawall

Gravity structures can be subject to settlement when the gravity load exceeds the bearing capacity of the soil or when consolidation or failure of the soil foundation occurs, as shown in Figure 2-17. The natural seabed can be replaced with material with a sufficient bearing capacity in order to prevent settlement (Burchart and Hughes, 2012).
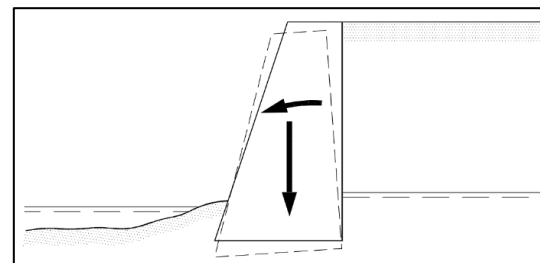
Figure 2-17: Seawall settlement

(iv)   Seaward overturning due to toe scour

Scour in front of the toe of the structure reduces the bearing capacity and passive resistance of the foundation soil. Overwhelming active backfill and groundwater pressures together with bearing capacity failure can result in seaward overturning and settlement of the marine gravity structure, as shown in Figure 2-18. Scour protection at the toe can reduce risk of scour related failure (Burchart and Hughes, 2012).
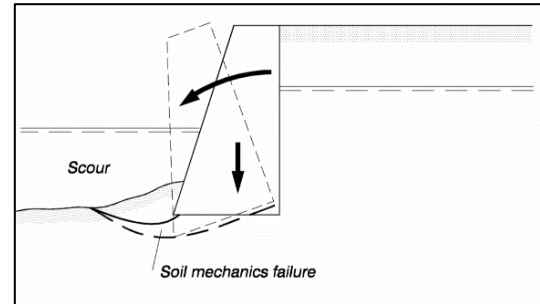
Figure 2-18: Overturning due to scour

(v)   Landward overturning due to overwash scour

Figure 2-19 shows how overwash scour is the result of severe overtopping of waves that damage the backfill material and eventually reduce the passive resistance of the backfill. Wave loads from the seaside can then overcome the backfill resistance and cause landward overturning. A higher crest level can reduce overtopping and prevent overwash scour (Burchart and Hughes, 2012).
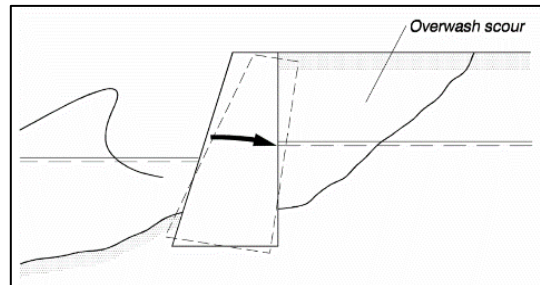
Figure 2-19: Overturning due to overwash scour

(vi)   Rotational slip failure

Slip failure occurs when the moment caused by the backfill, groundwater and surcharge loads exceeds the restoring moment from the passive toe soil resistance, as shown in Figure 2-20. Rotational slip can be prevented by constructing a geotechnical stable toe in front of the gravity structure (Burchart and Hughes, 2012).
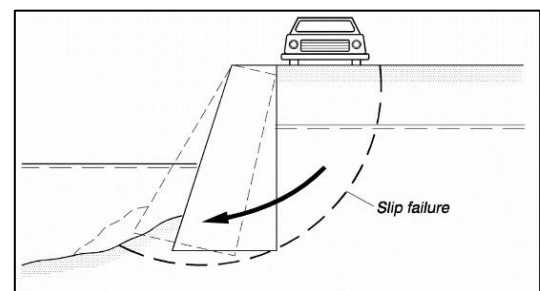
Figure 2-20: Rotational slip failure

According to UK studies, around 34 percent of seawall failures are due to the erosion of the beach or foundation material and a further 14 percent of failures can be partially attributed to local scour. Scour protection of marine structures must therefore be a principal objective during the design process. This study will focus solely on the processes around scour as failure mode of vertical seawalls (CIRIA, 2007b).

2.2.6 Foundation and Toe Design

The precast concrete elements, like L-elements or blocks, that vertical seawalls consist of, have to be placed on foundations that adhere to certain specifications. These foundations are generally constructed by placing multiple layers of varying stone gradings on the seabed. The main function of the foundation is to ensure that the concrete seawall elements are placed on bedding with sufficient bearing capacity. The stone foundation also provides a level bed for the concrete elements to be accurately placed and provides tolerance for if settlement of the seabed occurs under the weight of the seawall (CIRIA, 2007b).

The foundation is the arrangement of stone layers underneath the concrete structure and the foundation toe or berm is the extension of the foundation past the toe of the concrete structure. The main function of the toe is to protect the foundation from scour and the concrete structure from sliding, slipping and overturning. The toe also keeps the armour rock layers of the foundation berm in place (CIRIA, 2007b).

The stone layers of the foundation usually consist of a bedding layer on the bottom, followed by a core layer that consists of quarry run. The core of the toe is covered by one or more under-layers with a larger stone grading. The under-layers on the toe are then covered by an even larger grading of armour rock that is exposed to wave and current action. A screed layer is placed on the remaining exposed core layer that does not form part of the toe. More detail on the screed layer is discussed in Section 2.2.8 (CIRIA, 2007b).
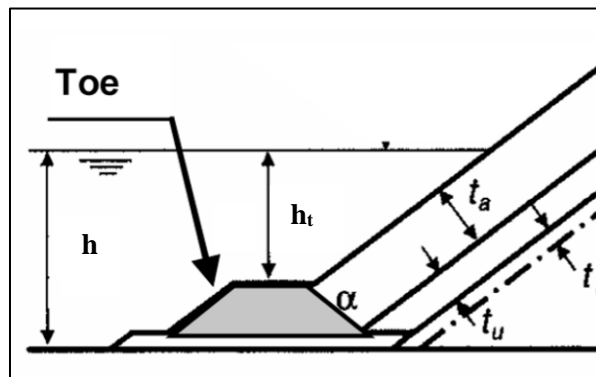
Figure 2-21: General cross-section detail of a toe at a coastal structure (CIRIA, 2007)

According to *The Rock Manual* (2007) the depth of the toe, h_t, with respect to the depth of the seabed, h, determines how the toe has to be designed, as shown in Figure 2-21. The type of marine structure, whether it is a rubble-mound or vertical face structure, also determines how the toe is designed (CIRIA, 2007b):

(i)   Toe design for rubble-mound structures

A lower or deeper toe with a ratio of $h_t/h = 0.5\text{-}0.8$ is less susceptible to wave action and is designed according to stability relationships and damage factors. Several studies have been conducted on the design and stability of low toe berms that are part of a rubble-mound marine structure. Madrigal and Valdés (1995) tested this subject specifically and yielded the following equation in terms of N_{od}, which represents the number of stones displaced within a strip of one D_{n50} width (Burchart and Hughes, 2012):

$$N_s = \frac{H_s}{\Delta\, D_{n,50}} = \left(5.8\,\frac{h_t}{h} - 0.6\right) N_{od}^{0.19} \qquad (2\text{-}1)$$

Where

$$D_{n,50} = \left(\frac{M_{50}}{\rho_r}\right)^{1/3} \qquad (2\text{-}2)$$

$$N_{od} = \begin{cases} 0.5 & \text{start of damage } (1-3\% \text{ units displaced}) \\ 2 & \text{moderate damage } (5-10\% \text{ units displaced}) \\ 5 & \text{severe damage } (20-30\% \text{ units displaced}) \end{cases} \qquad (2\text{-}3)$$

Van der Meer (1993) developed a formula for toe stability that can be used in the ranges $0.4 < h_t/h < 0.9$ and $3 < h_t/D_{n50} < 25$:

$$N_s = \frac{H_s}{\Delta\, D_{n,50}} * N_{od}^{-0.15} = 2 + 6.2 \left(\frac{h_t}{h}\right)^{2.7} \qquad (2\text{-}4)$$

However, a higher toe ($h_t/h<0.4$) tends to berm design and must have the stability of the armour layer, which is $H_s/D_{n50} = 2$. Therefore, the origin of Equation (2-4) is not at zero, as shown in Figure 2-22 (Van der Meer, 1993):
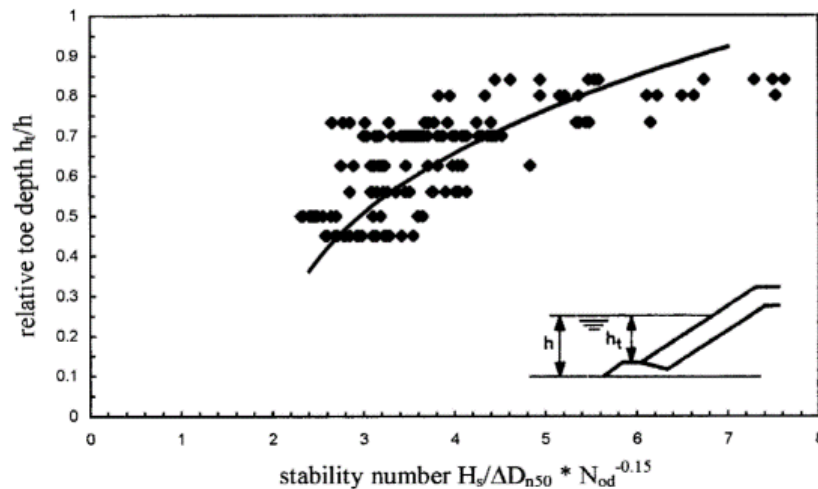
Figure 2-22: Toe stability as a function of h_t/h and N_{od} (Van der Meer, 1993)

Van Gent and Van der Werf (2014) conducted more recent studies on toe stability of rubble-mound structures, specifically structures with a slope of 1:1.5, which is applicable to this thesis. The results were used to develop Equation (to predict damage to rock toe structures (van Gent and van der Werf, 2014):

$$N_s = 0.032 \left(\frac{t_t}{H_s}\right)\left(\frac{B_t}{H_s}\right)^{0.3} \left(\frac{H_s}{\Delta\,D_{n,50}}\right)^3 \left(\frac{\hat{u}_\delta}{\sqrt{gH_s}}\right) \tag{2-5}$$

Where
$$\hat{u}_\delta = \frac{\pi\,H_s}{T}\frac{1}{\sinh kh_t} \tag{2-6}$$

$$k = \frac{2\pi}{L} = \frac{2\pi}{\frac{g}{2\pi}T^2} \tag{2-7}$$

(ii)   Toe design for vertical face structure

A higher or shallower toe, with a smaller ratio of h_t/h = 0.3-0.5, is more exposed to wave action on the water surface and should be designed as a berm or stepped structure (CIRIA, 2007b). Japanese research has focused on testing the stability of high toe structures that are usually used to protect vertical face structures. The following equation was yielded by Tanimoto *et al.* (1990) in terms of *h'*, the water depth on top of the berm excluding the armour layer (Burchart and Hughes, 2012):

$$N_s = \frac{H_s}{\Delta\,D_{n,50}} = max\left\{1.8, 1.3\,\frac{1-\kappa h'}{k^{1/3}\,H_s} + 1.8\,exp\left(-1.5\,\frac{(1-\kappa)^2}{\kappa^{1/3}}\frac{h'}{H_s}\right)\right\} \tag{2-8}$$

Where
$$\kappa = \kappa_1\kappa_2 \tag{2-9}$$

$$\kappa_1 = 2\frac{2\pi}{L_p}/\sinh\left(2\frac{2\pi}{L_p}h'\right) \tag{2-10}$$

$$\kappa_2 = max\left\{0.45\sin^2\theta\,\cos^2(\frac{2\pi}{L_p}B\cos\theta),\cos^2\theta\,\sin^2(\frac{2\pi}{L_p}B\cos\theta)\right\} \tag{2-11}$$

2.2.7 **Berm Design**

Berms are usually stepped structures on the seaside of a coastal structure like a breakwater or seawall and the function of a berm is normally to support the armour layer of the sloped structure. As mentioned in Section 2.2.6, foundation toes can also be designed according to berm specifications if the toe is shallow or high. When accurate construction methods are used, it is generally defined that the berm width must be 5 to 10 times the stone dimension of the berm (Gravesen, 2008). A wider berm can be required with more difficult site conditions when less accurate

methods, like dumping, are used. The stone size for a berm can be determined according to the damage factor, N_{od} (Gravesen, 2008):

$$N_s = \frac{H_s}{\Delta D_{n,50}} = \frac{1.6}{N_{od}^{-0.15} - 0.4 \frac{h_t}{H_s}} \tag{2-12}$$

The gradation of the stones that should be used in berm construction, is determined by a specified mass percentile of the entire gradation of material. The mass percentiles are acquired from the specific material's cumulative block weight distribution, as shown in Figure 2-23. The gradations that should be used for different stone layers in terms of cube length, are shown in Table 2-2 (Gravesen, 2008):
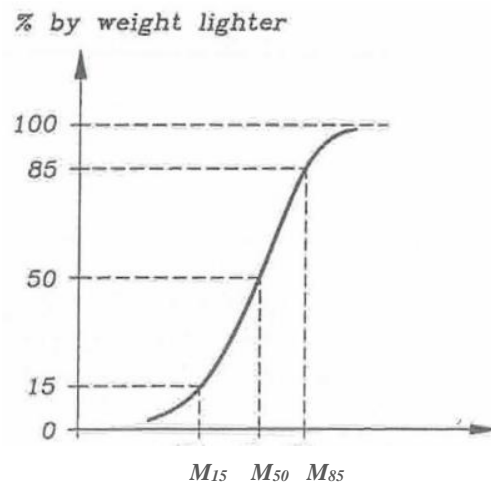
Figure 2-23: Material cumulative block mass distribution (adjusted from Gravesen, 2008)

Table 2-2: Gradation for stone layers and berms (Gravesen, 2008)

Gradation	$D_{85/15}$	Conventional Application
Narrow	< 1.5	Armour layers, filter layers and berms
Medium	1.5 – 2.5	Filter layers (sometimes armour layers and berms)
Wide	2.5 – 5 or more	Core material

2.2.8 Screed Layer

The screed layer, as mentioned in Section 2.2.6, is a thin layer that consists of fine rock (around 19 mm) that smoothens out the core layer to create a uniform and level surface for concrete elements to be placed on. An additional function of the screed layer is to provide additional contact area between the concrete element and the underlying rock foundation. This is done by casting serrations into the bottom surface of the concrete element so

that the element can be effectively embedded into the finer screed stones. More contact area ensures more friction between the foundation and the concrete element and thus improves stability (Schoonees, 2018).

Research does not yield much on specifications and codes for screed layer designs so it is assumed that screed layer design is based on engineering judgment, site conditions and constructability. The case study mentioned in Section 2.2.4, has a typical screed layer design that will be used in this thesis as guideline, with a thickness of 100 mm and a screed toe width of 150 mm. The screed layer thickness has to be optimised since the minimum thickness is limited by constructability and the maximum thickness is limited by scour susceptibility (Malan, 2016).

The screed layer is particularly susceptible to scour since it consists of finer and lighter material that can easily be flushed into the coarser filter and armour layers by wave or current action. Severe scour of the screed layer can result in structural instability or failure as mentioned in Section 2.2.4. Therefore, it is important to consider the design and construction of the screed layer when designing a rubble-mound foundation for concrete seawall elements (Schoonees, 2018).

2.3   SCOUR OF SAND

2.3.1   Erosion

Coastal erosion is one of the most prominent problems in coastal engineering and development since it is a continuous and powerful process that is not yet fully understood and predictable. Coastal erosion forms part of the dynamic processes that shape the valuable, yet vulnerable shoreline. The morphological and hydraulic processes that contribute to the erosion of a shoreline have to be understood in order to predict and control the erosion problems (Burchart and Hughes, 2012).

Waves, wind and tide are the primary factors that determine the morphological and hydraulic processes that shape the coastline. Tides cause the rise and fall of the water level and create tidal currents which result in erosion and shaping of the coastline. Wind also generates currents, waves, fluctuation in water levels as well as the transportation of sediment along the coast and strong winds result in storms, large waves and storm surge, which eventually can cause coastal erosion and severe damages and changes of the coastline. Coastal erosion is usually caused by either severe storm surges or by the presence of structures that is known as structural erosion or scour. The focus of this study will be on structural erosion (Pilarczyk, 2003).

2.3.2   Structural Erosion

Structural erosion, or scour, can be defined as the change of the profile of a coastline due to the presence of an artificial structure on the boundary between land and sea. The coastal structure disrupts the natural interaction between the ocean and the shoreline, specifically between the waves and sediment. The natural flow patterns around the structure are altered due to waves that are reflected from the structure instead of a natural profile that usually absorbs the wave energy. The result is an increase in turbulence and bed shear stress that scours away at the seabed underneath the structure, as shown in Figure 2-24. Reflected waves increase the depth to which the waves influence the seabed, which results in the scour of the local foundation material. Once the resisting force of the scoured foundation is overcome by wave forces, pressure from the backfill and gravity, failure of the structure occurs (Fowler, 1992).
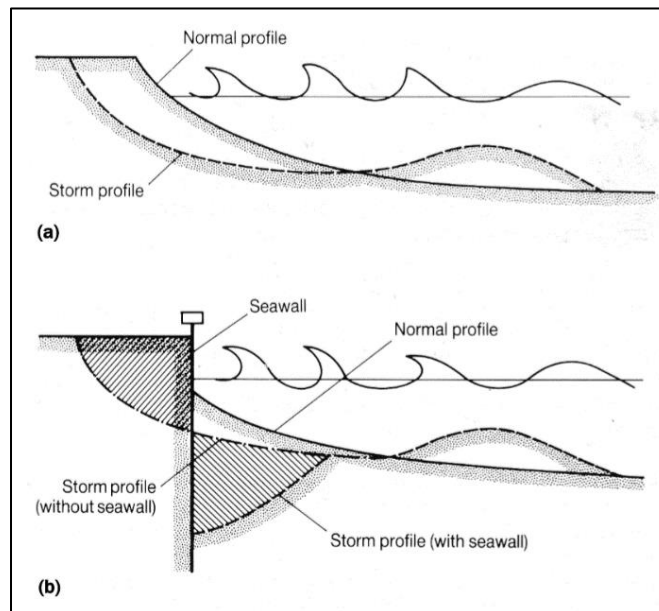
Figure 2-24: Scour at marine structure due to storms (Dean and Dalrymple, 2001)

2.3.3   Scour Development

Scour can be categorized as either general scour or local scour. General scour is the change in the natural profile and bed-level as a result of natural sediment transport and flow processes like waves, currents and tides. General scour develops over a long period of time so the effect of natural cycles can become evident. Local scour, however, develops in a much shorter time-scale with the introduction of an artificial marine structure on the natural seabed. The Hydraulic Engineering division of the *US Department of Transport* defines local scour as the removal of

material from around artificial hydraulic structures caused by an acceleration of flow and resulting vortices induced by the obstructions to the flow (Arneson *et al.*, 2012).

Mechanisms of scour are generally described in terms of the process that develops in rivers due to streams but it can also be applied to scour processes in marine environments. Mechanisms of scour can be characterized as either clear-water scour or live-bed scour. Clear-water scour occurs when sediment is removed from the scour hole through fluid flow, but the sediment is not replaced or supplied by the approaching flow, because the upstream bed material is at rest. Therefore, a scour depth equilibrium can be reached asymptotically once sediment particles are no longer dislodged from the scour hole by the fluid induced force. Live-bed scour, in contrast, occurs when the upstream bed's sediment is suspended and continuously replaces the sediment that has been dislodged at the downstream scour hole. An equilibrium will form once the rate of the upstream sediment supply equals the rate of sediment dislodgement from the scour hole downstream, but the scour depth continuously fluctuates about a mean value. Live-bed scour initially tends to develop faster, but the equilibrium scour depth is generally larger for clear-water scour, as shown in Figure 2-25. (Pagliara, Palermo and Carnacina, 2012).
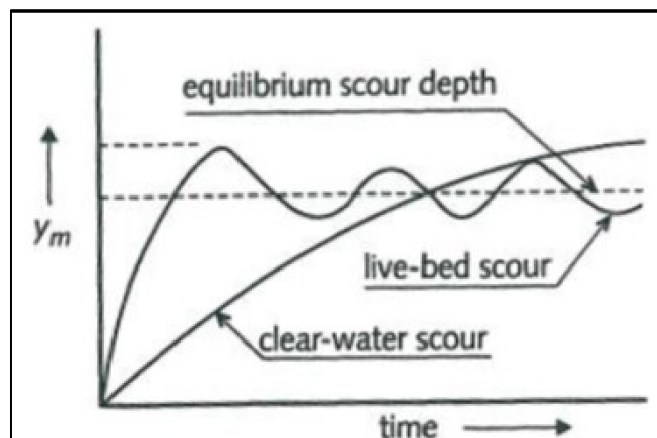
Figure 2-25: Scour depth development over time (Hoffmans, G.J. & Verheij, H. 1997)

The timescale of a scour experiment refers to the time that has to elapse for a scour process to fully develop. Xie (1981) performed more than 50 flume experiments on sand scour in order to determine the behaviour of the scour process. The sand particle diameters, wave periods, water depths and wave heights were varied, as well as the timescale or number of waves. It was found that the depth of the scour hole developed as a function of the number of waves the sediment was exposed to. The first 1000-2000 waves induced a rapid increase in scour depth that reached up to half the equilibrium scour depth. Equilibrium was reached within 7000 waves for steep waves (H/L>0.02) and 10 000 waves for flat waves (H/L<0.02) (Xie, 1981).

The scour depth at a vertical seawall is described by Xie (1981) in terms of the timescale (Xie, 1981):

$$y_m = y_{m,e}\left(\frac{t}{t_m}\right)^\gamma \quad for \quad t < t_m \qquad (2\text{-}13)$$

Where
t = time(s)

t_m = time when $y_m \approx y_{m,e}$ (s)

y_m = maximum scour depth (m)

$y_{m,e}$ = equilibrium scour depth (m)

γ = 0.3 – 0.4 (γ=0.3 for fine sediment)

Sumer and Fredsøe (1997) conducted 3-D experimental studies on the development of scour around vertical structures that include pipelines, rubble-mound and vertical breakwater heads. In terms of the timescale, it was found that the time required for substantial scour development in the 3-D experiments, was significantly shorter (10 minutes or 200 waves) than the 2-D trunk scour experiments that were conducted by Xie (1981), (10 000 waves). This is because scour around breakwater heads mainly develop due to lee-wake vortices, while trunk scour in Xie's 2-D case develops due to steady streaming, which is known to be a much slower process (B. M. Sumer and Fredsøe, 1997).

2.3.4   Scour Conditions

Except for the mere presence of marine structures that can result in scour, coastal conditions also contribute to the propensity of scour to occur. There are various coastal factors that govern the scour process and determine the extent of scour damage to marine structure foundations specifically. According to Hughes (2001), scour can result from the following conditions, either acting singularly or in combination (Hughes, 2001):

- Waves that reflect off a vertical structure increase the localised orbital velocities.
- Structures focus wave energy that induces breaking.
- Structure alignments and flow constrictions accelerate flows and redirect currents.
- Breaking waves that are directed downward mobilise sediment from the seabed.
- Vortices are created due to flow separation.
- Transitions from a hard bottom to an erodible bed.
- Wave pressure differentials and the presence of groundwater flow.

The way in which waves generally break around a site determines the amount of wave energy that penetrates to the depth of the seabed and consequently how much sediment is stirred up. According to Chadwick, Morfett and Borthwick (2013) here are three main types of wave breakers:

- ▪ Spilling breakers
- ▪ Plunging breakers
- ▪ Surging breakers

The main difference between the types of breakers is the steepness of the beach slope on which the waves break, as shown in Figure 2-26. The steepness of the incoming waves also determines the type of breaker that forms.
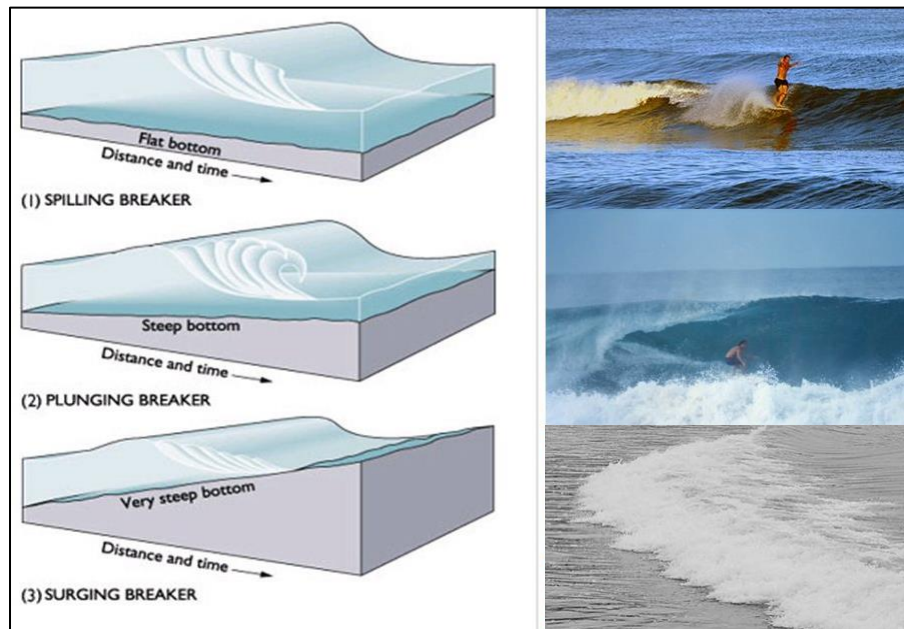
Figure 2-26: Types of wave breakers (Cameron, 2014)

(i)   Spilling breakers

Spilling breakers usually occur when relatively steep incoming waves break on a flat beach slope. Spilling waves break when the forward slope of the wave becomes unstable so plumes of air bubbles and water slide down the crest slope. Wind generated spilling breakers are also common in deep water (Fredsøe and Deigaard, 1992).

(ii)   Plunging breakers

Plunging breakers form when less steep incoming waves break on steeper seabed slopes. The waves break when the crest of the wave plunges forward as a single mass of water into the preceding trough. The plunging water jet can create a splash-up as well as coherent vortices that can reach the seabed and stir up sediment. Therefore,

plumes of sediment are generally observed around plunging breakers. As a result, plunging breakers tend to cause the most sediment erosion of all the wave breaker types (Fredsøe and Deigaard, 1992).

(iii)   Surging breakers

Surging breakers are found on very steep beach slopes. Unlike the breakers mentioned above, the wave crest does not become unstable and cause the wave to break. The foot of the steep face of the wave rushes forward onto the steep beach slope and causes the wave crest to decrease and eventually disappear as the wave breaks (Fredsøe and Deigaard, 1992).

Wave breakers can be characterized by the ration between the beach slope and the square root of the wave steepness, known as the surf similarity parameter or Iribarren number (Battjes, 1974; Chadwick, Morfett and Borthwick, 2013):

$$\varepsilon_b = \frac{\tan \beta}{\sqrt{H_b/L_b}} \tag{2-14}$$

The surf similarity parameter for the respective wave breakers are as follows:

Table 2-3: Iribarren numbers for types of breakers (Chadwick, Morfett and Borthwick, 2013)

Wave breaker	Breaking Iribarren number	Deep water Iribarren number
Spilling	$\varepsilon_b < 0.4$	$\varepsilon_b < 0.5$
Plunging	$0.4 < \varepsilon_b < 2.0$	$0.5 < \varepsilon_b < 3.3$
Surging	$\varepsilon_b > 2.0$	$\varepsilon_b > 3.3$

Sumer and Fredsøe (1997) have conducted extensive studies on the conditions and parameters that have significant effects on scour at coastal structures, specifically rubble-mound and vertical breakwaters. It was found that the *Keulegan-Carpenter* number (KC) is a major parameter in the scour process. The KC number is defined as follows (B. M. Sumer and Fredsøe, 1997)

$$KC = \frac{U_m T}{B} \tag{2-15}$$

Where U_m = maximum undisturbed orbital velocity of the water particles at the bed (m/s)

T = wave period (s)

B = width of the coastal structure, like a breakwater roundhead (m)

The KC number governs the flow patterns at the structure toe and equilibrium scour depth that will develop. The equilibrium scour depth increases with the increase of the KC number. However, the *Keulegan-Carpenter* number is only applicable to measure the scour around the head of coastal structures and not the trunk sections or quay walls, since the *B* parameter has to be defined. Empirical formulae for the width of the stone protection layer at the foundation of a coastal structure is also determined in terms of the KC-number (Sumer *et al.*, 1994; B. Sumer and Fredsøe, 1997).

The angle of wave attack and the reflective coefficient of the relevant structure also have major influences on the extent of scour that develops underneath the structure. Sumer and Fredsøe's (1997) experiments revealed that maximum scour damage occurs when the angle of wave attack is perpendicular to the face of a coastal structure and when the face of the structure is vertical (B. M. Sumer and Fredsøe, 1997).

2.3.5   **Scour Prediction**

Toe scour is defined as localized erosion directly at the seaside toe of a coastal structure. The maximum depth that can be scoured into the seabed, relative to the initial bed level, is referred to as the scour depth, y_s. There are simple methods available to predict the y_s that can form at the toe, that take into consideration incident conditions like the significant wave height, H_s, the water depth, d, and the geometry and reflective coefficient, C_r, of the coastal structure in question. However, these methods are only suitable for preliminary designs since the methods do not consider the effect of angled wave attacks or currents. More sophisticated and complex methods are required to accurately predict the scour depth that might form at coastal structures. The *Rock Manual* (CIRIA, 2007b) suggests that prediction methods can be categorised as either rule of thumb methods, semi-empirical methods that are based on hydraulic models, as well as simple and complex morphodynamical models. Simple rule of thumb methods include that the maximum depth of scour is equal to the maximum unbroken wave height, H_{max}, that occurs locally (CIRIA, 2007b):

$$y_s = H_{max} \qquad\qquad\qquad (2\text{-}16)$$

However, further studies have revealed that this method of prediction would underestimate the scour that may take place at a coastal structure. Three general observations have been made in an attempt to acquire more accurate scour depth predictions:

- For a mean wave steepness, s_{om}, of 0.02 – 0.04, Equation (2-16) is a sufficient approximation.
- Maximum scour occurs at the structure if the structure is located at the plunge point of the local breaking waves.

▪ The scour depth that can be reached at a structure is directly proportionate to the reflection coefficient of the structure and therefore vertical structures result in maximum scour (CIRIA, 2007b).

There are numerous trends and formulae that have been acquired by various authors to predict scour at vertical marine structures under different conditions. Hughes (2001) suggested formulae for scour prediction at vertical structures for both breaking and non-breaking waves. The maximum scour depth, S_m, for breaking waves can be predicted as follows (Hughes, 2001):

$$\frac{S_m}{H_{mo,0}} = \sqrt{22.72 \frac{h}{L_{p,0}} + 0.25}$$
(2-17)

Where $\qquad H_{mo,0}$ = Significant deep-water wave height (m)

$\qquad\qquad h$ = pre-scour water depth (m)

$\qquad\qquad L_{p,0}$ = deep-water wavelength associated with peak wave period, T_p.

The range of validity for this prediction method is (Hughes, 2001):

$$0.011 < \frac{h}{L_{p,0}} < 0.045 \quad and \quad 0.015 < \frac{H_{mo,0}}{L_{p,0}}$$
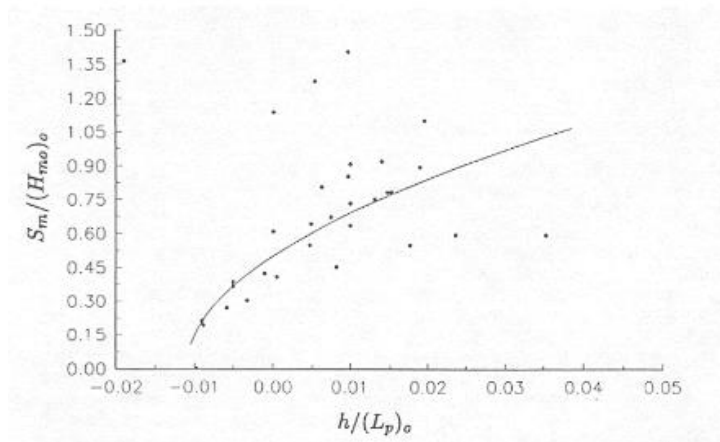
Figure 2-27: Prediction of scour for breaking waves (Hughes, 2001)

For non-breaking waves, Xie (1981) performed regular wave tests, which can be compared to Hughes's (2001) irregular wave tests of which the formula is as follows:

$$\frac{S_m}{u_{rms,m} T_p} = \frac{0.05}{\left[\sinh(k_p h)\right]^{0.35}}$$
(2-18)

where

$$\frac{u_{rms,m}}{g\,k_p\,T_p\,H_{mo}} = \frac{\sqrt{2}}{4\pi\,\cosh(k_p h)}\left[0.54\,\cosh\left(\frac{1.5 - k_p h}{2.8}\right)\right] \tag{2-19}$$

Where $u_{rms,m}$ = Root-mean-square of horizontal velocity (m/s)

k_p = wave number associated with T_p
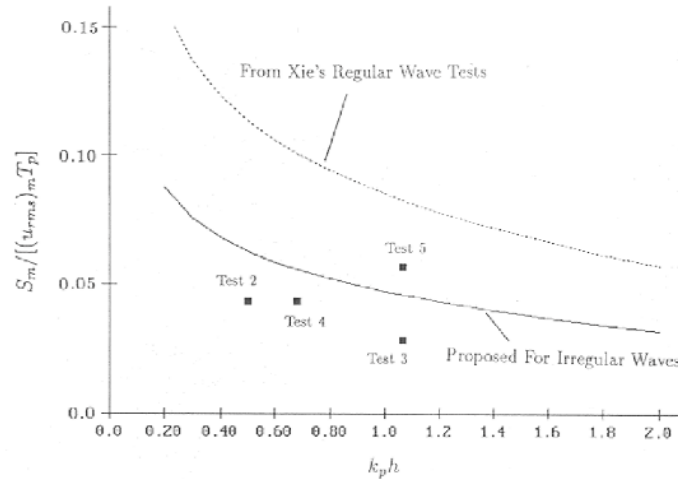
Figure 2-28: Prediction of scour for non-breaking waves (Hughes, 2001) (Xie, 1981)

Sumer and Fredsøe (1997) conducted numerous studies on scour around marine structures and specifically investigated the effect of plunging breakers on the scour process. It was found that maximum scour was induced with plunging type of breakers, which confirms what is mentioned in Section 2.3.4. Equation (2-20) and Figure 2-29 was developed to predict scour depth specifically at the lee side of a breakwater roundhead under plunging breaker conditions:

$$\frac{S}{H_s} = 0.01\,C_2\left(\frac{T_p\sqrt{g\,H_s}}{h}\right)^{1.5} \tag{2-20}$$

Where C_2 = uncertainty factor with a mean value of 1 and standard deviation of 0.34 (B. M. Sumer and Fredsøe, 1997).
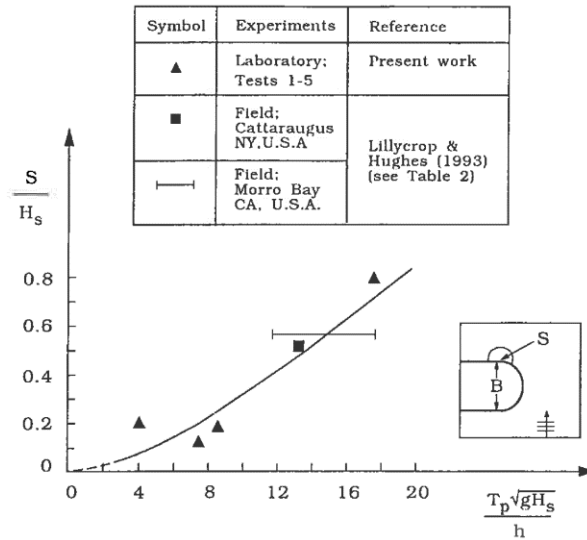
Figure 2-29: Maximum scour depth induced by plunging breaker at lee side of breakwater (Sumer and Fredsøe, 1997)

2.3.6   **Scour Control**

It is clear that scour poses a significant threat to the reliability of seawalls and therefore scour control forms an important part of the design process of seawall foundations. Incorporating scour control in the design of coastal structures is renowned for being a very challenging activity from an engineering point of view. The reason for this is that scour control encompasses complex and multidisciplinary interactions and responses like hydraulic loading, geotechnical features, morphology and structural design. It is therefore important to incorporate multidisciplinary, multifunctional and integrated planning in order to design effective scour control measures for coastal structures like seawalls (Pilarczyk, 2003).

The most prominent problems caused by scour at coastal structures are geotechnical failures like sliding and liquefaction, as mentioned in Section 2.2.5. The following measures can be taken in order to counteract these phenomena to protect coastal structures at risk, however due to the complex nature of scour processes, these simple measures are not guaranteed to be effective (Hughes, 2001):

- Extension of bed protection increases the distance between the coastal structure and the threatening scour hole and reduces the flow velocities.
- Armour stone protection can reduce the risk of slide failure.
- Wave forces on the sea-bed can be minimised by reducing wave reflection from off the coastal structure. This can be achieved by constructing an energy dissipation revetment, toe or berm of irregular rock in front of the coastal structure.

- Placing a scour-control blanket along the problem area can aid in isolating the extent of the problem. Scour blankets are usually constructed from prefabricated flexible mats, gabion mattresses or rockfill.

- Regular scour monitoring during construction and operation ensures that the structure stability is up to standard.

- Grouting with asphalt or cement can improve the quality of the bed foundation and reduce scour, but grouting is an unnatural addition to the environment and can create other problems.

It is important to attempt to prevent the scour process from developing at coastal structures with the initial design and construction phases instead of incorporating mitigation or control measures. Construction and rehabilitation costs can consequently be minimised by monitoring the impact of scour on the natural coastal environment (Burchart and Hughes, 2012).

2.4   SCOUR OF GRANULAR MATERIAL

2.4.1   General

Sediment is classified according to particle size. Two different scales are described in the *Coastal Engineering Manual* (Burchart and Hughes, 2012): the *Modified Wentworth Classification* that is generally used in the geological field and the *Unified Soils Classification* that was developed by American engineering groups. The *Wentworth* scale will be used to classify sediment in this thesis. The majority of research done on scour processes focuses on the scour of sand and not on the scour of granular material, like the screed layer of a rubble-mound foundation. Sand is defined as geological material with a range of 0.06 – 2 mm in particle size, while geological particles with a size range of 2 – 80 mm, are characterized as granular material or gravel, as shown in Figure 2-30 (Burchart and Hughes, 2012).

Particle Size (mm)																		
80	40	10	5.0	2.0	1.0	0.8	0.6	0.4	0.3	0.2	0.1	0.08	0.04	0.02	0.01	0.005	0.002	0.001
Cobbles	Coarse gravel		Fine gravel		Very coarse sand	Coarse sand		Median sand		Fine sand	Very fine sand		Silt				clay	

Figure 2-30: Sediment classification by particle size (Dolui, Chatterjee and Das Chatterjee, 2016)

The focus of this thesis is on granular scour and how granular filters can be used to counter the scour process and protect a coastal structure against erosion failure. The *Coastal Engineering Manual* defines a filter layer as a layer

of a specific grading stone that protects the base material or soil against scour without causing an excessive build-up of pore pressure in the underlying layers. The detailed functions of a granular filter layer are the following (Burchart and Hughes, 2012):

- Turbulent flow and excessive pore pressure can cause core material to leech into the coarser armour layer. Voids will then develop in the core layer and differential settlement of the structure can occur as the overlaying tones settle into the voids. The intermediate particle size of the filter material will prevent the fine core material to flush into the coarse armour layer thus effectively keeping the core layer intact.
- The filter layer levels the foundation and effectively distributes the weight of the structure to ensure uniform settlement and baseplate loading on the structure.
- The granular filter layer can aid in dissipating flow energy and reduce the hydrodynamic loads on the outer layers.
- A granular filter layer can also serve as bedding for large coastal structures like caissons if the bearing capacity of the natural sea-bed is not sufficient. The bedding layer also retains geotextile filter cloth.

Geotextile filter cloth is an alternative to a granular filter layer to keep core material intact. Nevertheless, granular filter layers have numerous advantages over geotextile fabrics when used in coastal construction (Burchart and Hughes, 2012):

- Filter material is usually very durable.
- The filter layer provides a good contact surface between the base and armour layer.
- Bottom irregularities can be smoothed out by a granular filter layer for a uniform construction base.
- The porous granular layer dampens the wave energy.
- A granular layer can rely on self-weight for stability in wave and current action while geotextile fabrics have to be weighted.
- The loose structure of a granular layer can better withstand impacts from larger armour stones during construction or from stones that shift during settlement.
- The granular layer is relatively easy to construct and repair and can even be self-healing.
- Granular material is widely available and relatively inexpensive.
- If geotextile fabric is used with a filter layer, the filter layer protects the geotextile fabric from being punctured by larger armour stones.

2.4.2 **Types of Granular Filters**

Granular filters can be characterized as either traditional geometrically closed filters or geometrically open filters as shown in Figure 2-31. Geometrically closed filters are constructed with multiple rock layers of increasing particle size. The intermediate filter layer is placed in between the finer under-layer and coarse armour layer so the fine grains cannot flush through. Closed filters are difficult and time-consuming to construct due to the numerous layers of materials with different gradings that have to be place and

Figure 2-31: Geometrically closed (left) and open (right) filters (Warmink and Joustra, 2013)

local flow velocities from construction process can cause a loss of fine material (Warmink and Joustra, 2013).

The design of geometrically open filter layers combines the filter layer and the armour layer into one single grading. This means that the finer bed or core material can technically be transported through the pores of the filter when the hydraulic load exceeds the critical load. However, the hydraulic loads (from water flow over the filter layer for instance) are reduced within the pores of the filter layer so that the finer material cannot be flushed through. The filter layer has to have sufficient thickness to reduce the hydraulic loads within the pores. Otherwise if the fines flush through, scour will develop underneath the filter layers and result in settlement and eventually failure as shown in Figure 2-32. Open granular filters are easier and more economical to construct since it is a single layer that has to be placed (Warmink and Joustra, 2013).
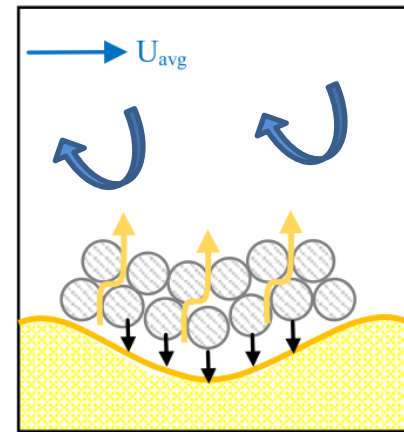
Figure 2-32: Failure of open filter (Warmink and Joustra, 2013)

2.4.3 **Design Criteria for Granular Filters**

The design criteria for granular filters are based on grain size distributions and the geometry of voids between particles. The retention criterion refers to preventing the core material to leach through the filter layer. This can be ensured if the grain size diameter exceeded by 85% of the filter material ($d_{15\,filter}$) is less than 4 to 5 times the grain size diameter exceeded by 15% of the foundation material ($d_{85\,foundation}$) (CIRIA, 2007b):

$$\frac{d_{15filter}}{d_{85foundation}} < 4 \; to \; 5 \qquad (2\text{-}21)$$

The design for a granular filter layer has to be optimized in order for the bed material and filter material to move simultaneously. If the filter layer is designed too thick, only the filter layer will move and possibly erode. On the other hand, if the layer is too thin, only the bed material will move and erode through the filter layer, which can cause the structure to fail. Warmink and Joustra (2013) conducted physical experiments at the Atlantic basin research facility of Deltares in Delft to test two equations from Hoffmans (2012) (Equation (2-29)) and Wörman (1989) (Equation (2-23)) for acquiring the optimal granular filter layer thickness. The important region in the graph in Figure 2-33 to consider when designing open filters in non-uniform flow, is found between these equations and adjacent to the zone representing geometrically closed filters (Hoffmans, 2012).

Hoffmans (2012):
$$\frac{D_F}{d_{f50}} = \frac{d_{f15}}{d_{f50}} \; \alpha_d \; \ln\left(\frac{d_{f50}}{d_{b50}}\right) = 1.2 \; \ln\left(\frac{d_{f50}}{d_{b50}}\right) \tag{2-22}$$

Wörman (1989):
$$\frac{D_F}{d_{f15}} = 0.16 \; \frac{n_f}{1-n_f} \frac{d_{f85}}{d_{b85}} \frac{\Delta_f}{\Delta_b} = 0.085 \; \frac{d_{f50}}{d_{b50}} \tag{2-23}$$

With
D_F = thickness of filter layer (m)

d_{f50}/d_{f15} = filter particle diameter ratio ≈ 1.25

α_d = load dampening coefficient = 1.5

d_{b50}/d_{f50} = base particle diameter ratio ≈ 1.25

n_f = porosity of filter layer = 0.4

Δ_f/Δ_b = relative density filter and base material= 1
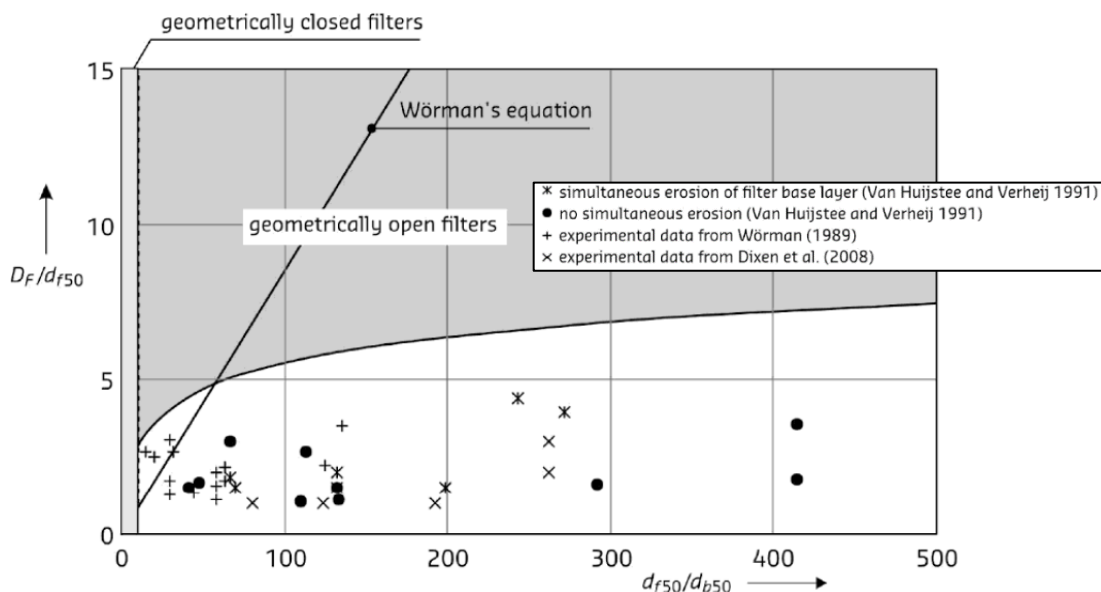
Figure 2-33: Design graph for optimal filter particle diameter (Hoffmans, 2012)

2.4.4   **Granular Filter Failure Modes**

According to Warmink and Joustra (2013), granular filter layers are regarded as failed when

- The filter layer does not prevent underlying geotextile fabric from getting punctured and consequently a loss of soil or bedding occurs.
- The base layer is eroded either perpendicularly through the filter layer due to outgoing flow as shown in Figure 2-34, or due to wave and current forces acting parallel to the filter layer.
- The filter layer becomes internally unstable due to a wide gradation that causes the filter layer to compact, settle differentially or become more permeable.
- Lateral shearing develops due to the interface between adjacent filter layers that become unstable.

U_{avg}	U_{avg}	U_{avg}	U_{avg}
I) Filter is *instable, bed is stable*.	II) Both filter and bed are *instable*.	IIII) Filter is stable, bed is *instable*.	IV) Both filter and bed are *stable*.
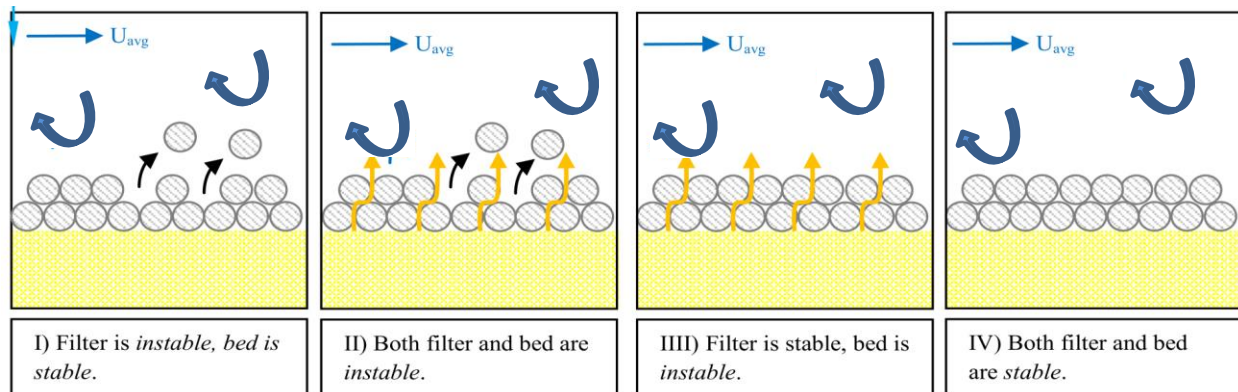
Figure 2-34: Filter layer and bedding stability mechanisms (Warmink and Joustra, 2013)

2.5   SCOUR DATA ACQUISITION

Scour experiments are generally physically modelled since sediment transport behaviour is difficult to model and predict numerically or mathematically. However, measuring scour physically is a difficult challenge that has arisen in the physical modelling field. Sand scour can be visually mapped by comparing top view or side view photographs or by physically measuring differences in levels in a grid system with a point gauge or bed profilers (Sumer and Fredsøe, 2000; Gislason, Fredsøe and Sumer, 2009). Granular scour is more difficult to map since the material particles are larger and the scour patterns that develop are not as distinct. Scour data acquisition becomes even more challenging when the scour damage underneath a structure has to be measured. Visual observations become either impossible or limited to the boundaries of the structure against the glass if the experiment is set-up in a 2D glass wave flume, as shown in Figure 2-35 (Malan, 2016).
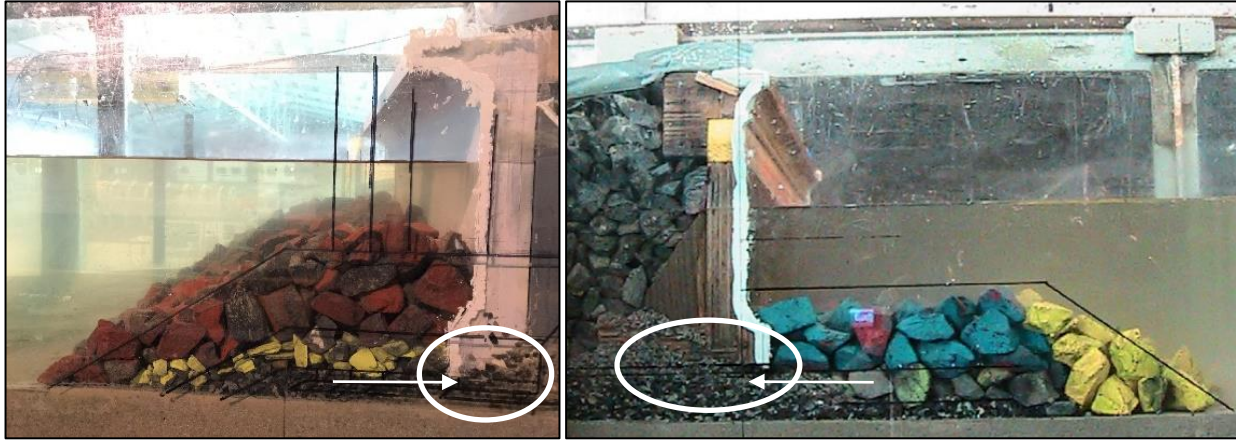
Figure 2-35: Visual observation of scour process against glass of flume (Malan, 2016)

A method of granular scour measurement underneath a model structure of a seawall was developed by the University of Stellenbosch in 2016 (Malan, 2016). The method used wooden dowels of different diameters to probe underneath the seawall where a screed layer was initially placed but was scoured away due to wave attack, as shown in Figure 2-36. The depth that the dowels penetrate underneath the seawall before reaching undisturbed screed, determines the scour depth that developed at that specific point. However, it is challenging to ensure the same amount of force is used to probe into the screed layer with the dowels and the screed layer is disturbed with this intrusive method of measurement. Consistency and accuracy is therefore difficult to guarantee with this method (Malan, 2016).

Figure 2-36: Scour measurement with wooden dowels (Malan, 2016)

An alternative method of granular scour measurement underneath a seawall structure had to be developed to improve the above-mentioned dowel method. Ultrasound technology is often used in marine engineering environments since it can create accurate images of underwater environments and topographies. The sonar technology generates a sound that is sent through a medium, such as water and the relevant objects or material that is being measured, reflects the sound back to the receiver. The time it takes to receive the reflected sound determines how far the object is from the sonar and so an image can be generated of the object. Sonar technology is often used in practice in the form of single-beam or multi-beam echo sounders for underwater surveys, as shown in Figure 2-37 (GNS, 2018).
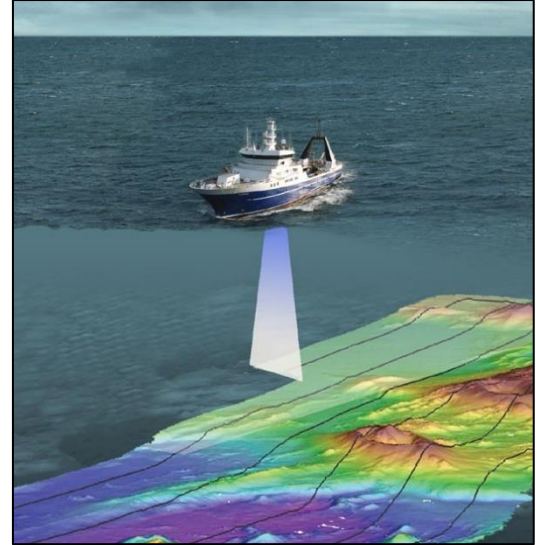
Figure 2-37: Eco sounder sonar technology used in underwater surveys (GNS, 2018)

This same principle can be applied when attempting to measure granular scour underneath a seawall structure. As long as there is access to a horizontal view underneath the base of the seawall, sonar technology can be used to measure how much scour occurred by detecting the location of undisturbed material underneath the base and how much material has been scoured out. This method is preferred above the dowel method since it is a non-intrusive method that does not disturb the material during data acquisition. The method is also more objective since the acquired scour depth is based on an image that is taken and can be measured off, instead of an inconsistent force with which a dowel is probed with. More detail on the sonar method is described in Section 3.10.3 (Van Wageningen, 2018).

2.6   PRECEDING PHYSICAL MODEL STUDY ON GRANULAR SCOUR

2.6.1   General

A physical model study was conducted by Malan (2016) that gave to rise to this thesis. Malan's study also focused on the seawall structure in the Middle East where significant scour occurred, as mentioned in Section 2.2.4. The aim of the study was to review existing methods of designing and constructing scour protection at the foundation of a vertical seawall with a specific focus on the screed layer directly underneath the concrete seawall structure (Malan, 2016).

A physical model was set up in the 2D model wave flume at the Council of Scientific and Industrial Research (CSIR) laboratory in Stellenbosch and 16 tests were conducted on a scale of 1 in 20 to test the following parameters (Malan, 2016):

Constant parameters:

- Wave conditions
- Bathymetry
- Grading of rock layers
- Position of vertical seawall structure

Variable parameters

- Screed layer thickness
- Screed toe width
- Construction method (with or without compaction)
- Addition of sediment (sand and clay) to screed layer.

The model structure, constructed from marine plywood, had a similar design to the L-element seawall in the Middle East case study. It was placed on a screed layer which covered a specifically graded rubble-mound foundation with a rubble-mound berm as shown in Figure 2-38. The model set-up was exposed to waves generated by the *HR Wallingford* wave-maker in the wave flume. Scour damage developed in the screed and foundation layer underneath the seawall structure. The scour damage underneath the seawall was measured by probing with wooden dowels and measuring the depth that the dowels penetrated (Malan, 2016).

Figure 2-38: Physical set-up and measurements for scour experiments (Malan, 2016)

2.6.2 **Conclusions**

The following conclusions were made after the execution of the physical tests (Malan, 2016):

- A thicker screed layer is more susceptible to scour since a greater area that consists of smaller grading rock (19mm) is exposed to wave and scour action as opposed to the larger core and filter gradings. However, the screed layer must still provide sufficient space for the structural element to settle into for stability and levelness.

- The screed toe directly in front of the concrete structure must be as narrow as possible while the layout still adheres to filter rules.

- The screed layer must not be compacted during construction since compaction may reduce the settlement of the structural element into the screed material. This can result in unwanted flows, scour action and a loss of friction between the element and the screed.

- Addition of sediment to the screed may result in poor quality control and therefore it is not recommended.

- Even though the design of the scour protection adheres to design guidelines, the effectiveness of the scour protection relies heavily on the quality and consistency of the construction methods and processes.

2.6.3 **Recommendations**

The following recommendations were made based on the knowledge obtained throughout the study (Malan, 2016):

- Tests should be repeated in order to reduce the confidence intervals of measured scour damage. However, time limitations did not allow for repetitions.

- Great care should be taken to ensure that the construction process is executed consistently since scour behaviour appears to be very sensitive to inconsistencies.

2.7   DIMENSIONAL ANALYSIS AND GOVERNING PARAMETERS

2.7.1 General

When hydraulic designs have to be done within physical systems, mathematical models are very convenient and useful in order to recreate these systems and predict behaviour and reaction of the system on the hydraulic design. However, some physical systems cannot be accurately modelled mathematically since it becomes too complex. Scale model physical experiments are alternative to mathematical models to simulate complex physical systems. Physical modelling, again, produces two new problems, namely the design of the model and experimental procedure as well as the correct interpretation of the results. In order to scale and interpret the physical model correctly and ensure similitude, physical laws and governing parameters have to be identified. The process of dimensional analysis then uses these parameters to create dimensionless factors that have to be kept constant within the physical model and prototype to ensure similitude. Dimensional analysis has been used in Section 4.6 to generate equations for scour predictions (Warnock, 1950).

2.7.2 Dimensionless Parameters of Processes

The following systems and processes are expected to govern the scour process underneath a vertical seawall with the parameters defined in Figure 2-39 (CIRIA, 2007b):
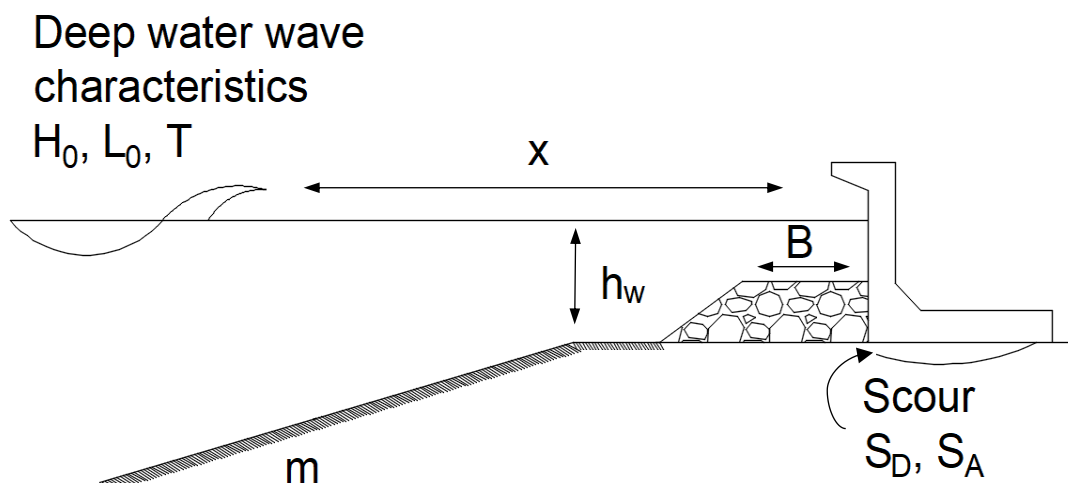
Figure 2-39: Definition sketch of parameters (adjusted from CIRIA, 2007)

- Sediment and granular material properties (Sumer and Fredsøe, 2000)

$$\varphi = \frac{U_m{}^2}{g(s-10)D_{50}} \; ; \; \frac{w}{U_m} \qquad (2\text{-}24)$$

Where φ = Shields parameter

         s = specific gravity

         w = particle fall velocity (m/s)

- Wave breaker type (Fredsøe and Deigaard, 1992) as mentioned in Section 2.3.4.

$$\frac{H_0}{L_0} \; ; \; m \qquad (2\text{-}25)$$

Where m = slope of seabed

- Seawall parameters (Burchart and Hughes, 2012)

$$\frac{h_w}{L_0} \; ; \; \frac{x}{L_0} \; ; \; \frac{T_p\sqrt{gH_0}}{h_w} \; ; \frac{L_0}{B} \qquad (2\text{-}26)$$

Where x = distance between breaking wave and seawall (m)

         B = Berm width (m)

- Scour process

$$\frac{S_D}{H_0} \; ; \; \frac{S_A}{H_0{}^2} \qquad (2\text{-}27)$$

Where S_D = scour depth underneath seawall (m)

         S_A = scour area underneath seawall (m²)

2.7.3 Governing Parameters

The variable parameters that will be applicable for this study are the parameters that include the wave period, which can be expressed as the wavelength, the scour process and the berm width in front of the seawall structure since these parameters form part of the objectives of the study, as mentioned in Section 1.2:

$$\frac{L_0}{B} \; ; \; \frac{S_D}{H_0} \; ; \; \frac{S_A}{H_0{}^2} \qquad (2\text{-}28)$$

The remaining dimensionless parameters are expected to remain constant throughout the experimental tests of the study.

2.8   PHYSICAL MODELLING

2.8.1   General

Modelling is the process of creating a representation of a real-life situation, referred to as the prototype. Physical modelling refers to the physical reproduction of a prototype in a controlled environment, like a laboratory and usually on a smaller scale. The advantages of physical modelling are as follows (Burchart and Hughes, 2012):

- The major dominant forces can be reproduced in proportion to the actual physical system of the prototype.
- The appropriate equations for the physical processes can be integrated without simplifying assumptions as with numerical or analytical modelling.
- The controlled environment and smaller scale of a physical model permits easier and cheaper data acquisition compared to field data collection
- The physical representation of prototype makes the observation of the effects of the processes clear and convenient to demonstrate.
- Most of the physical processes can be simulated simultaneously with physical modelling as opposed to numerical modelling for instance, where a single process usually has to be isolated in order to be modelled.

Physical modelling also poses challenges when used to simulate engineering problems, for instance (Hughes, 1995):

- Laboratory and scale effects are important to consider and to minimise when using physical models. More detail on this will be discussed in Section 2.8.4.
- The set-up and testing procedure of physical models are generally expensive and time-consuming, compared to analytical or numerical models.

This thesis will focus on the physical modelling of short wave tests on rubble-mound and vertical coastal structures and the scaling of wave characteristics and sediment.

2.8.2   Froude Model Scale

The major forces that govern prototype situation that is being modelled, has to be identified and considered when scaling a physical model. According to Warnock (1950), all physical engineering problems can be simplified to the interaction of two major forces with the remaining forces being classified as minor. According to Hughes (1995), there are four conditions that have to be conserved when conducting short wave physical modelling tests,

namely the Froude number, Strouhal number, Euler number and Reynolds number. In coastal engineering, the Froude criterion is mostly used where inertia (F_i) and gravitational forces (F_g) dominate as is the case for scour modelling. The Froude number expresses the influences of inertia and gravitational forces in a hydraulic environment (Hughes, 1995):

$$Froude\ Number = \sqrt{\frac{inertia\ force}{gravity\ force}} = \sqrt{\frac{\rho\ D^2 V^2}{\rho\ D^3 g}} = \frac{V}{\sqrt{g\ D}} \qquad (2\text{-}29)$$

Where   D = characteristic linear dimension (mm)

               V = flow velocity (m/s)

               g = gravitational acceleration (m/s^2)

In order to ensure similitude, the Froude number in the model ($_m$) must be the same as in prototype ($_p$). The general Froude scale ratio can be expressed as shown in Equation (2-30), and from there all the Froude similitudes can be derived as shown in Table 2-4 (Reynolds scaling laws are also shown) (Hughes, 1995):

$$N_x = \frac{X_p}{X_m} = \frac{Value\ of\ X\ in\ prototype}{Value\ of\ X\ in\ model} \qquad (2\text{-}30)$$

Table 2-4: Scaling laws for Froude and Reynolds (Hughes, 1995)

Characteristic	Dimension	Froude	Reynolds
Geometric			
Length	$[L]$	N_L	N_L
Area	$[L^2]$	N_L^2	N_L^2
Volume	$[L^3]$	N_L^3	N_L^3
Kinematic			
Time	$[T]$	$N_L^{1/2}N_\rho^{1/2}N_\gamma^{-1/2}$	$N_L^2N_\rho N_\mu^{-1}$
Velocity	$[LT^{-1}]$	$N_L^{1/2}N_\rho^{-1/2}N_\gamma^{1/2}$	$N_L^{-1}N_\rho^{-1}N_\mu$
Acceleration	$[LT^{-2}]$	$N_\gamma N_\rho^{-1}$	$N_L^{-3}N_\rho^{-2}N_\mu^2$
Discharge	$[L^3T^{-1}]$	$N_L^{5/2}N_\rho^{-1/2}N_\gamma^{1/2}$	$N_L N_\rho^{-1}N_\mu$
Kinematic viscosity	$[L^2T^{-1}]$	$N_L^{3/2}N_\rho^{-1/2}N_\gamma^{1/2}$	$N_\rho^{-1}N_\mu$
Dynamic			
Mass	$[M]$	$N_L^3N_\rho$	$N_L^3N_\rho$
Force	$[MLT^{-2}]$	$N_L^3N_\gamma$	$N_\rho^{-1}N_\mu^2$
Mass Density	$[ML^{-3}]$	$N_L^{3/2}N_\rho^{-1/2}N_\gamma^{1/2}$	N_ρ
Specific weight	$[ML^{-2}T^{-2}]$	$N_L^{3/2}N_\rho^{-1/2}N_\gamma^{1/2}$	$N_L^{-3}N_\rho^{-1}N_\mu^2$
Dynamic viscosity	$[ML^{-1}T^{-1}]$	$N_L^{3/2}N_\rho^{1/2}N_\gamma^{1/2}$	N_μ
Surface tension	$[MT^{-2}]$	$N_L^2N_\gamma$	$N_L^{-1}N_\rho^{-1}N_\mu^2$
Volume Elasticity	$[ML^{-1}T^{-2}]$	$N_L N_\gamma$	$N_L^{-2}N_\rho^{-1}N_\mu^2$
Pressure and stress	$[ML^{-1}T^{-2}]$	$N_L N_\gamma$	$N_L^{-2}N_\rho^{-1}N_\mu^2$
Momentum, impulse	$[MLT^{-1}]$	$N_L^{7/2}N_\rho^{1/2}N_\gamma^{1/2}$	$N_L^2N_\mu$
Energy, work	$[ML^2T^{-2}]$	$N_L^4N_\gamma$	$N_L N_\rho^{-1}N_\mu^2$
Power	$[ML^2T^{-3}]$	$N_L^{7/2}N_\rho^{-1/2}N_\gamma^{3/2}$	$N_L^{-1}N_\rho^{-2}N_\mu^3$

2.8.3   Model Scale Selection

With physical modelling, the largest possible model scale should be used in order to minimise scale effects that can influence the credibility of the tests. Practical considerations like the capacity of the modelling flume, the capabilities of the wave-maker and the sensitivity of the probes available, usually limit the model scale that can be used. Studies referenced by Hudson *et al.* (1979) suggest linear scales between 1:20 and 1:50 for vertical wall models while Jensen and Klinting (1983) and Oumeraci (1984) suggest a scale range of 1:10 – 1:80 for rubble-mound structures. However, since then larger test facilities have been developed to get the model scale as close to prototype as possible in order to minimise scale effects (Hughes, 1995).

2.8.4   Scale Effects

As mentioned in Section 2.8.2, physical models are scaled according to Froude's assumption that gravitational and inertia forces govern the physical processes being modelled. However, this assumption causes other forces like surface tension, elasticity and kinematic viscosity to be scaled incorrectly since these forces tend to become more prominent as the scale and flow decreases. When short-wave hydraulic models are scaled according to the Froude

criterion, the non-similitude of these forces can cause scale effects in terms of wave reflection, transmission energy dissipation and wave breaking. The following scale effects are common when physically modelling coastal processes and coastal structures (Hughes, 1995):

(i)   Wave Reflection

Waves that reflect from smooth surfaces like vertical walls are usually smaller in model scale due to frictional losses that are more prominent at the reflective surface than in prototype. However, relatively more wave reflection can be generated in model scale if rubble-mound materials are merely geometrically scaled from prototype, which can cause flow through the structure to become laminar instead of remaining turbulent. Wire mesh screens can be fixed into the model set-up to counter or reduce wave reflection. Larger scale models (1:10 – 1:20) generate less wave reflection scale effects since flow remains turbulent as in prototype (Hughes, 1995).

(ii)   Wave Transmission

In the case of porous rubble-mound structures, the flow is influenced by viscous model effects that results in the structure behaving less porous than in prototype. Therefore, if the core material sizes are geometrically reduced, frictional losses are greater in the model and wave transmission is not modelled accurately. Additional scaling methods for wave transmission are discussed in Section 2.8.5 (Keulegan, 1973).

(iii)   Surface Tension

Surface tension usually has a negligible effect on coastal models. However, when waves are less than 0.35 seconds apart or the water depth is less than 20 mm, surface tension becomes prominent enough to consider and account for in physical models. The restoring force of surface tension dampens the wave motion and influences the wave celerity, which in turn affects other prominent processes like wave refraction (Hughes, 1995; Hudson *et al.*, 1979).

(iv)   Viscosity and Friction

The scaling of short-wave models demands that the Froude number of the model and prototype is in similitude. However, frictional and viscous effects are then not necessarily correctly simulated since the similitude of the Reynolds number is not prioritised. Internal friction and bottom boundary layer friction can attenuate modelled wave heights over distances. However, short-wave models are usually modelled over short distances so that the effect of viscosity and friction becomes negligible. (Sumer, 2006)

(v)   Wave Breaking

Surface tension determines the size of air bubbles that get entrained in breaking waves. Since surface tension is not usually scaled down, air bubbles are not according to model scale, but larger and reach deeper under the water

surface. However, according to Le Méhauté (1976), the momentum equations express that energy dissipation during wave breaking remains in similitude regardless of the internal dissipation mechanisms. Battjes and Stive (1985) conducted physical tests scaled according to the undistorted Froude criterion and found that tests with a prototype wave height range between 0.1 m to 1.5 m, or model wave heights of more than 500 mm did not result in any significant scale effects in terms of air entrainment differences (Battjes and Stive, 1985).

(vi)   Air Compression

Wave breaking at a vertical wall structure results in significant air compression and shock pressures, which can only truly be simulated in a partial vacuum, so empirical corrections are required to account for air compression effects. (Le Méhauté, 1976; Hughes, 1995)

(vii)   Material Particle Sizes

The behaviour of sand or granular particles are influenced by their size. When rocks are scaled from prototype size, it is important that the model scale particles retain prototype soil behaviour (See Figure 2-30 in Section 2.4). Gravel and sand have similar characteristics in terms of internal forces and interaction with water. However, clay is a cohesive soil due to the small particle size and interaction with pore water is more significant. Therefore, once sediment is scaled down so that it can be classified as clay, the behaviour of the model soil will not accurately represent prototype anymore (CIRIA, 2007a).

The above-mentioned scale effects are the most prominent effects that have to be considered when physically modelling a vertical coastal structure with a rubble-mound foundation, although there are even more scale effects known to occur with the physical modelling process (CIRIA, 2007a).

2.8.5   Scale for Wave Transmission

Wave transmission becomes an important process to simulate when coastal rubble-mound structures are physically modelled. These semi-permeable structures dissipate wave energy within the voids and therefore wave reflection, transmission and run-up have to be modelled as close as possible to prototype processes. When considering wave transmission on downscaled granular material, the viscous forces will dominate the hydraulic flow processes. The inertia to viscous force ratio becomes important to keep constant from prototype to model scale and is referred to as the Reynolds number, R_n (Hughes, 1995):

$$R_n = \frac{inertia\ force}{viscous\ force} = \frac{\rho\ D\ V}{\mu} \tag{2-31}$$

With μ = Dynamic viscosity (N.s/m^2)

When the Reynolds number of armour units of geometrically scaled porous rubble-mound structure models is too low (R_n <2000), more wave energy will be reflected and less wave energy will be transmitted through the structure, when compared to prototype. This is due to the flow within the interior of the porous structure that becomes laminar instead of remaining entirely turbulent as in prototype. The downscaled diameter of the material of the finer rock layers of a rubble-mound structure, like the screed layer, can be determined with methods of Lé Mehauté (1965) and Keulegan (1973) in order to ensure similitude in the model and prototype in terms of wave transmission. Another method of ensuring similitude is to reduce wave reflection in the model with wire screens to create turbulent flow within the rock layers. However, the preferred measure is to model in the largest possible scale so that required corrections of geometrically scaled units can be minimised, as well as the effect of fluid viscosity on the model. (Hughes, 1995; Keulegan, 1973)

Lé Mehauté (1965) and Keulegan's (1973) methods focus on acquiring a distortion factor, K, which is bigger than unity, to increase the size of the finer rock layers, like the core and screed, in order to account for wave transmission and reflection as mentioned above. The diameter of the model material, D_m, can then be determined with the following equation (Le Méhauté, 1976; Keulegan, 1973):

$$N_L = \frac{L_p}{L_m} = K\frac{D_p}{D_m} \tag{2-32}$$

Hudson *et al.* (1979) recommended that an average between the K factors that are acquired from both the Lé Mehauté (1965) and Keulegan (1973) methods be used.

(i)   Lé Mehauté (1965)

Lé Mehauté developed a nomogram method to determine K, as shown in Figure 2-40. His method corrects scale affects that arise from flow through a porous core of a coastal structure. Assumptions for this method include that the scale effects of the outer armour layers are negligible and that the core material size gradation is similar for prototype and model. The solid lines of the nomogram represent constant values of the K factor. The ordinate is the geometric scale length scale $N_L = L_p/L_m$ and the abscissa is a dimensional factor that combines rubble-mound structure parameters (Le Méhauté, 1976):

$$\frac{H_i}{\Delta L}D_p^3\ P_p^5 \tag{2-33}$$

Where H_i = incident wave height (m)

                ΔL = average core material section width (m)

D_p = quarry stone diameter of prototype (cm), taken as 10% smaller than quarry stone from core material gradation curve

P = porosity of core ($0 < P < 1$)

$$P = P_m = P_p \qquad D_m = D_p K \frac{L_m}{L_p}$$

$$\frac{H_i}{\Delta L} D_p^3 \, P_p^5$$
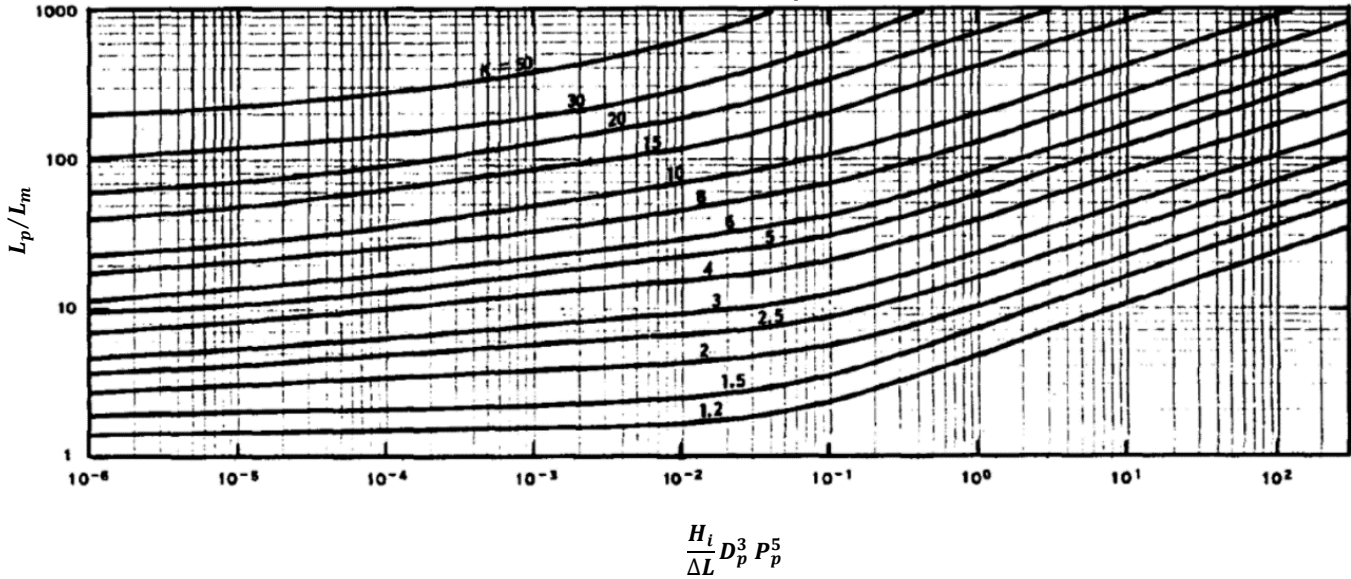
Figure 2-40: Nomogram for sizing rubble-mound structures for Wave Transmission (Hughes, 1995)

(ii)   Keulegan (1973)

Keulegan developed a series of empirical equations in order to determine the K factor. Two equations are used to give wave transmission, depending on the Reynolds number. If the Reynolds number is greater than 2000, the energy losses are assumed to be due to turbulent dissipation, and for a Reynolds number between 20 and 2000, viscous dissipation occurs within the structure. The equations are as follows (Keulegan, 1973):

For $R_n > 2000$

$$(\frac{H_i}{H_t})_p = 1 + \gamma_p \, (\frac{H_i}{2h})_p \, (\frac{\Delta L}{L})_p \qquad (2\text{-}34)$$

and

$$\gamma_p = \frac{P_p^{-4}}{10.6} \left(\frac{L}{D}\right)_p (g \, h \, \frac{T^2}{L^2})_p^{4/3} \qquad (2\text{-}35)$$

For $20 < R_n < 2000$

$$(\frac{H_i}{H_t})_m^{2/3} = 1 + \gamma_m \, (\frac{H_i}{2h})_m^{2/3} \, (\frac{\Delta L}{L})_m \qquad (2\text{-}36)$$

and

$$\gamma_p = \frac{P_m^{-4}}{1.52} \left(\frac{v \, T}{D \, L}\right)_m^{\frac{1}{3}} \left(\frac{L}{D}\right)_m (g \, h \, \frac{T^2}{L^2})_m^{4/3} \qquad (2\text{-}37)$$

where

$$R_n = \frac{P\,H_i\,L\,D}{2\,\nu\,h\,T}$$

(2-38)

and

$$V_{seepage} = \frac{P\,H_i\,L}{2\,h\,T}$$

(2-39)

Where H_t = transmitted wave height (m)

L = incident wavelength (m)

ν = kinematic viscosity (N.s/m^2)

Equation (2-39) represents the maximum seepage velocity at the face of the permeable structure and it is the velocity that is used in the Reynolds number from Equation (2-38). Finally, the wave transmission similarity entails that:

$$\left(\frac{H_i}{H_t}\right)_p = \left(\frac{H_i}{H_t}\right)_m$$

(2-40)

Thus, the ratio can be used in either prototype equations (2-34) and (2-35), or the model equations (2-36) and (2-37), depending on the Reynolds number, to determine D_m and eventually solve Equation (2-32) to determine K. As mentioned above, the average of the two K factors acquired from Lé Mehauté and Keulegan's methods should be calculated and then used to scale fine granular material with Equation (2-32) (Hughes, 1995).

2.8.6   Laboratory Effects

Laboratory effects refer to the non-similitudes that arise between prototype and the model due to the environment in which the model is set up. These effects are mainly related to the physical constraints of the boundaries of the model flow, the mechanical methods that generate nonlinear waves and currents and the oversimplification of prototype forces and processes (Hughes, 1995).

(i)   Inaccurate Wave Generation

When a mechanical wave board generates energetic waves, cross waves can develop within a narrow 2-D flume or unwanted nonlinear, irregular waves can form from a generating motion based on a linear wave transformation function (Wallingford, 2018).

(ii)   **Re-reflection of Waves**

Waves that are generated by the mechanical wave-maker, travel to the test end of the flume and are reflected off the structure being tested, as in prototype. However, when these reflected waves travel back to the wave-maker and re-reflect off the board again, a laboratory effect develops that is not in similitude with prototype. This effect can be minimised by either installing energy dissipation beaches at the test boundaries or active wave absorption can be implemented at the wave board with detection and absorption of unintentional reflected wave energy (Swart, 2016).

(iii)   **Fresh and Salt Water**

Hydraulic models are usually conducted with fresh water and in the case of coastal problems, prototype fluid is salt water, which differs by approximately 3% from fresh water in terms of density. This difference is estimated to result in a 15% error in stability studies if corrections are not made to account for this effect (Le Méhauté, 1976).

(iv)   **Absence of wind**

A common model effect is that wind is not modelled when conducting coastal experiments. Since waves are often generated or influenced by wind, it is usually an important model effect to consider. However, according to engineering judgment, the effect of wind on the scour of a submerged foundation will not be as prominent (Swart, 2016).

2.8.7 Probe Positioning

When conducting 2D physical tests in a wave flume, the incident and reflected wave heights have to be measured to ensure that the wave-maker is calibrated according to the conditions and bathymetry so that desired wave heights are obtained at the location of the structure being tested in the flume. Wave heights and periods are measured with wave probes that use capacitance variance. Probe positioning is important to determine for each unique experiment. A three-probe set-up is used to reduce the errors in amplitude and phase measurement that occur due to non-linearity in the waves in a two-probe set-up. This three-probe set-up has to be placed at least one wavelength from a reflective structure (such as the wave-maker in the flume) for fluctuations in wave heights and periods, induced by the reflective structure, to become negligible (Neelamani and Vedagiri, 2002).

Mansard and Funke (1980) specified limits that the spacing between the consecutive probes have to adhere to in order to avoid singularity in the estimation of the incident and the reflected wave heights that are recorded by the probes. According to them, these limits are as follows:

$$X_{12} = \frac{L_p}{10} \tag{2-41}$$

$$\frac{L_p}{6} < X_{13} < \frac{L_p}{3} \tag{2-42}$$

$$X_{13} \neq \frac{L_p}{5} \quad and \quad X_{13} \neq \frac{3L_p}{10} \tag{2-43}$$

With X_{12} = distance between Probe 1 and Probe 2 as shown in Figure 2-41 (m)

             X_{13} = distance between Probe 1 and Probe 3 as shown in Figure 2-41 (m)
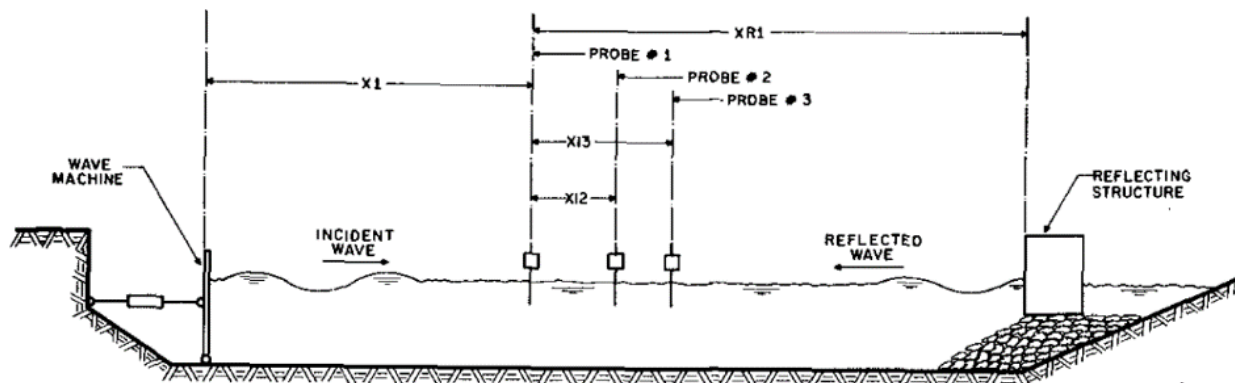
Figure 2-41: Probe positioning in wave flume (Mansard and Funke, 1980)

2.9   LITERATURE REVIEW SUMMARY

An extensive literature review was conducted in order to gain knowledge of vertical seawalls, rubble-mound berms, foundations and screed layers and the structural scour process. Research on dimensional analysis and physical modelling was also required in order to design an effective methodology and test set-up.

The research that was found to be the most important and relevant to this thesis, is summarised below:

(i)   Seawall structure

Different wall structures are used on coastlines around the world and the type of seawall is dependent on the specific site conditions and requirements. Vertical seawalls are used where the landside has to be protected against wave attack, but where limited space is available. Sufficient construction expertise and financial support is necessary for vertical seawalls, especially L-element seawalls. L-walls save on concrete volumes, but the elements have to be accurately and carefully placed on a foundation with sufficient bearing capacity and scour protection. This thesis specifically focuses on L-seawalls and the scour process that develops underneath the wall elements. However, scour under gravity block seawalls or caissons should be very similar compared to scour underneath L-walls provided the foundations on the seaward side of the walls are essentially the same (Pitkala, 1986).

(ii)   Rubble-mound berm and foundation

Rubble-mound berms and foundations are usually used to support L-wall structures. These berms and foundations consist of different gradings of rock namely armour, filter and core rock layers, all with different functions. The foundation core layer is covered with a thin screed layer that evens out the irregular core so that the L-element can be placed on a level surface. However, this screed layer consists of a small and narrow rock grading which makes it very susceptible to scour (CIRIA, 2007a).

(iii)   Scour

Scour refers to structural erosion that is caused by wave and current action at the base of a coastal structure. Scour development, conditions and predictions have been thoroughly studied by Xie (1981), Sumer and Fredsøe (1997 – 2006), Burchart and Hughes (2001 – 2012) among others. However, these studies mainly focused on scour of sand, while this thesis actually focuses on granular scour. There is limited information available on granular scour and therefore this thesis attempts to fill this gap in the literature.

(iv)   Dimensional analysis

Dimensional analysis is required for modelling coastal processes accurately. Dimensionless parameters have to be identified that will have a significant effect on a specific experimental set-up. The governing parameters for this study were identified as follows:

$$\frac{L_0}{B} \; ; \; \frac{S_D}{H_0} \; ; \; \frac{S_A}{H_0{}^2} \qquad\qquad (2\text{-}44)$$

(v)   Physical modelling

Malan's preceding scour tests that were conducted in 2016 with physical experiments had to be researched properly in order to expand the research with an original method in this thesis. The general guidelines of physical modelling were also considered as well as the scale and laboratory effects that could influence the results and credibility of the tests (Malan, 2016).

3. METHODOLOGY

3.1   PROBLEM STATEMENT

Previous research and existing literature show that numerous methods have been developed to predict scour under marine structures. *The Coastal Engineering Manual* and *Rock Manual* are generally used as a baseline for designing scour protection for marine structures. However, there are no standard guidelines specifically for the design and construction of granular scour protection at rubble-mound foundations underneath seawalls.

The purpose of this study is to design and test a standard layout for a rubble-mound foundation of a vertical seawall, focusing on minimizing scour of the screed layer directly beneath a L-shaped counterfort seawall. The functions of a screed layer are essentially to provide a level surface for placing a concrete element, like an L-wall element, as well as to ensure sufficient contact area between the base of the concrete element and the rubble-mound foundation for stability.

The experimental test set-up, as the preceding tests mentioned in Section 2.6, is roughly based on a case study of an L-wall in the Middle East where scour of the rubble-mound foundation occurred as mentioned in Section 2.2.4. It was identified that the design and construction methods of the screed layer had a significant influence on the extent of scour, so therefore the focus of the experiments is on the design and construction method of the screed layer.

Physical modelling of the vertical seawall and rubble-mound foundation set-up was conducted in order to test scour of the screed layer under varying conditions. The 2D physical model laboratory tests were conducted at the Council for Scientific and Industrial Research (CSIR) facilities in Stellenbosch. The general set-up consists of a rubble-mound foundation topped with a screed layer, a section of a model L-wall structure and a rubble-mound berm in front. The design water depth in which the set-up is constructed, is 4 m in prototype, based on a typical depth in front of a shallow seawall structure. Cross-sections of the layout are shown in Figure 3-1 and Figure 3-2.
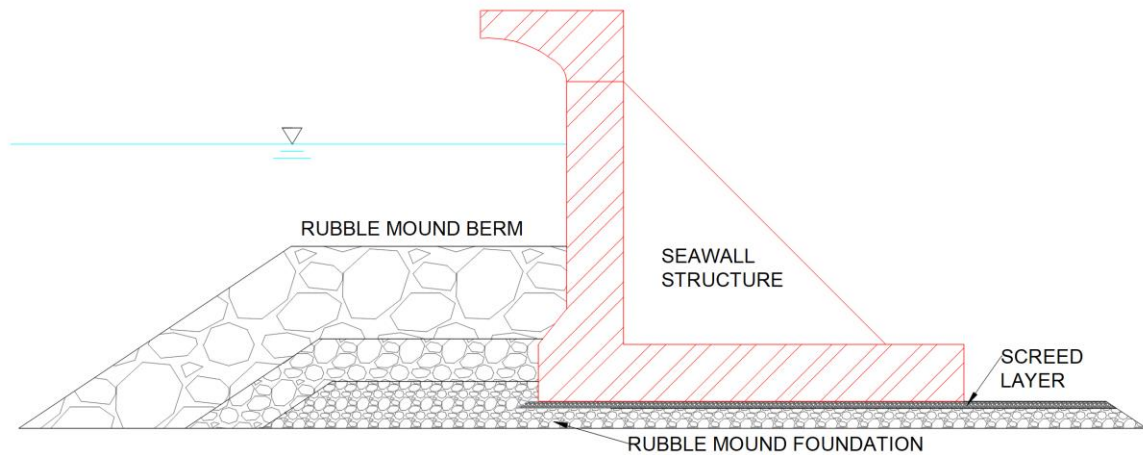
Figure 3-1: General design of cross-section of L-element on rubble-mound foundation with berm

Figure 3-2: Cross-section of set-up as built in the wave flume

3.2 PARAMETERS AND HYPOTHESIS

The parameters that may have a significant effect on the scouring of the screed layer of a rubble-mound foundation beneath an L-wall, were identified and it was decided which parameters will be kept constant and which will be varied in order to test the influence these variable parameters have on scour. Refer to Section 2.6 to identify the contrast between the parameters of the preceding experimental set-up by Malan (2016) and the set-up of this thesis.

3.2.1   Constant Parameters

- Bathymetry
- Position and design of seawall structure
- Wave height
- Water level
- Width of screed toe
- Rock gradings of screed, core, filter and armour material
- Construction methods

3.2.2   Variable Parameters

- Wave period
- Berm width
- Screed layer thickness

3.2.3   Hypothesis

The screed layer is the most susceptible to scour of all the layers in the rubble-mound foundation structure, since it consists of material with the smallest particle size. The objective of the physical tests is to determine which of the above-mentioned variable parameters will have a significant effect on the scour development in the screed layer and what extent of the effect is.

Firstly, the rate of scour development has to be determined, as with the preceding experiments. The rate of scour development can be determined by running continuous wave tests and measuring the scour depth throughout the tests as the scour depth develops. It is expected that the scour depth will increase as the number of waves increases, but that an equilibrium depth will be reached at some point after a specific number of waves.

A direct relationship between the wave period and the extent of scour that develops in the screed layer is expected: the longer the wave period, the more scour will develop. This is because longer waves result in higher orbital velocities of the water particles and is therefore expected to administer more damage to the rubble-mound foundation.

The berm width of the toe is hypothesized to also have a significant effect on the scour. A berm structure's main function is to protect the toe of a coastal structure against failure mechanisms like scour. Therefore, it is expected

that a wider berm would result in less scour of the screed layer because more wave energy is dissipated on the berm before reaching the seawall. However, a narrower berm is more economical to construct. Therefore, an ideal berm width has to be determined in terms of balancing protection and construction cost considerations.

The influence of the screed thickness has been tested in the preceding study (Malan, 2016) but will be repeated in this study to confirm that the thicker the screed layer, the more susceptible the screed would be to scour since a thicker face of the finer screed material is exposed to the scour process. However, the screed layer cannot be too thin since it becomes difficult to construct under water and it might not serve its primary purpose of providing a level surface for the L-wall structure to be placed on.

It is expected that there will be a correlation between the stability factors obtained from the berm stability tests and the extent of the scour damage from the scour tests. The less stable the armour protection of the berm (lower stability factor), the more exposed the whole foundation structure under the seawall becomes. Therefore, it is expected that more scour will also occur.

The reflection coefficient, which is determined by the height of the reflected wave in relation to the incident wave, was also considered when analysing the scour results. A high reflection coefficient means that most of the wave energy is not absorbed or dissipated, but reflected back off a reflective structure, like a vertical seawall. Therefore, it is expected that a higher reflection coefficient will result in less scour, since scour is a result of energy that penetrates the berm and is not reflected back seaward.

3.3   MODEL SCALE

The scale that was used for the model set-up, was 1:20, as it was mentioned in Section 2.8.3 that vertical seawall structures can be modelled effectively between 1:20 and 1:50 and the largest scale yields the most accurate results. The model was scaled according to the Froude similarity law. Wave parameters, water levels, structural dimensions and rock gradings were also achievable for this scale. The preceding scour tests also used a scale of 1:20 and therefore it was kept consistent for comparison.

The main scale factors are shown in Table 3-1.

Table 3-1: Scale factors according to Froude

Scalar	Parameter	Froude scale	Froude scale 1:20
Distance [m]	Wave height, water level	n	20
Time [s]	Wave period, test duration	$n^{1/2}$	$\sqrt{20} = 4.47$
Mass [kg]	Rock and sediment mass	n^3	8000
Area [m²]	Scour area	n^2	400
Volume [m³]	Rock and sediment volume	n^3	8000

3.4 HYDRAULIC RESEARCH FACILITY AND EQUIPMENT

3.4.1 Wave Flume

The experimental model was set up in a glass 2D wave flume in the CSIR model hall in Stellenbosch, South Africa. The flume is 30 m long, 1 m deep and 0.75 m wide. The flume in the CSIR facility is shown in Figure 3-3 (a). The facility and flume were simultaneously used for another research thesis by Ross John Jarvis titled "*Stability Analysis of Varying Berm Widths of a Composite Vertical Seawall*" so some parameters had to be adjusted to fit these experiments (Jarvis, 2018).

Figure 3-3: (a) 2D wave flume in CSIR facility and (b) HR Wallingford paddle wave-maker at CSIR laboratory (Malan, 2016)

3.4.2 Wave-maker

The wave flume is equipped with an *HR Wallingford* single-paddle wave-maker, as shown in Figure 3-3 (b) and Figure 3-4 (a). The wave-maker has an integrated Dynamic Wave Absorption System, shown in Figure 3-4 (b), which enables it to actively absorb and compensate for reflected waves off highly reflective structures like vertical

seawalls. The maximum water depth in which the wave-maker can operate effectively is 750 mm and the maximum wave height that it can produce is 400 mm between frequencies of 0.4 and 0.6 Hz. The wave-maker is capable of producing both regular and irregular wave spectrums. Two standard irregular wave spectral shapes can be produced, namely, JONSWAP and Pierson-Moskowitz (Malan, 2016). The JONSWAP spectral shape was used in the physical modelling experiments of this thesis, with an enhancement factor, γ, of 3.3, which is typical for sea state.

Figure 3-4: (a) HR Wallingford wave-maker and   *(b) Dynamic Wave Absorption System control panel*

3.4.3 **Probes**

Input parameters of the *HR Wallingford* wave-maker include a significant wave height and peak wave period desired for the relevant test. However, due to the unique bathymetry, the reflectiveness of the structure in the flume and the condition of the water, the resulting output values are not exactly equal to the input values. Capacitance probes are used to measure and record the output values that include the wave heights H_s, H_{m0}, (refer to Section 3.6.1 for when the different significant wave heights are used) and the peak period, T_p. The capacitance probes used during this thesis were custom built by CSIR. As the water level surrounding the probe varies, it is recorded through varying voltage readings that are recorded by the probes. These voltage variations are converted to time-series data to represent a sequence of surface elevations from which the above-mentioned wave parameters can be calculated. The probe set-up and an example of the probe output data is shown in Figure 3-5.
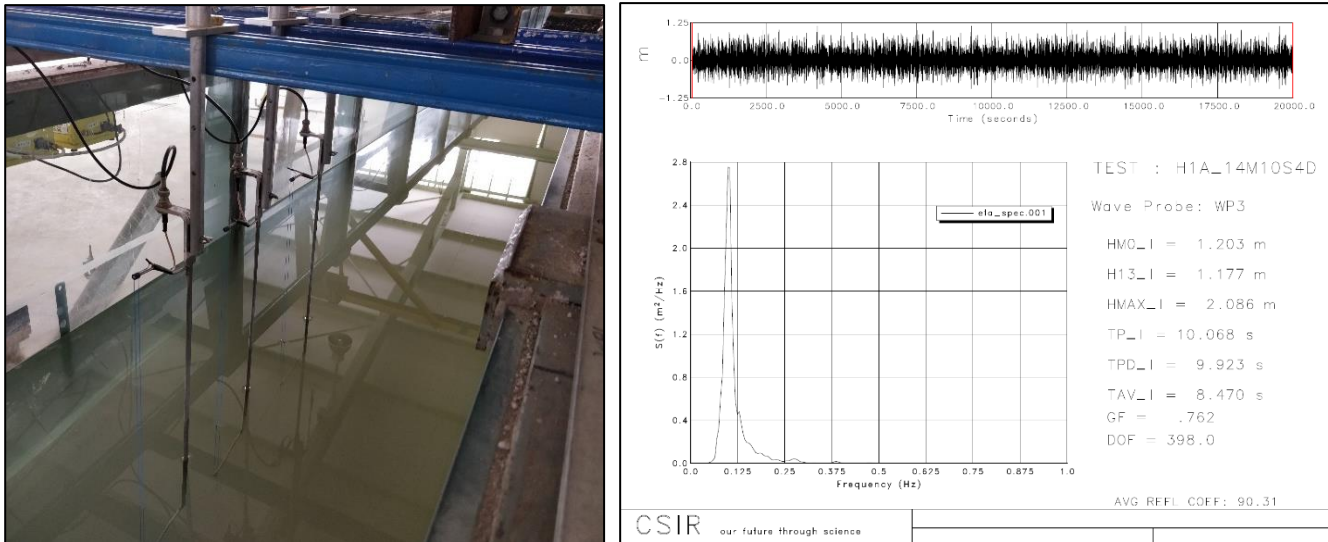
Figure 3-5: (a) Probe set-up in flume and (b) probe output data

Section 2.8.7 describes the requirements for the spacing configuration between the three probes in a set-up. These requirements were used to calculate the spacings for both the deep-water and shallow-water probe set-ups that were placed in the flume. The shallow-water probe set-up was only used during the calibration process without the structure (refer to Section 3.9). Each probe set-up (Probe 2) had to be placed at least one wavelength from a reflective structure and preferably on a flat slope to ensure accurate readings. Therefore, the deep-water probes were placed at 12 m (from the wave-maker) and the shallow-water probes were placed at 21.75 m or 8.25 m from the back end of the flume, where the toe of the berm would be situated during testing. This was to acquire wave data right where the seawall had to be placed. The spacings differed for every wave period since different wave periods result in different wavelengths that had to be accounted for.

The spacings for each probe set-up is shown in Table 3-2 in model dimensions. The spacing between Probe 2 and 3 (X_{23}) was kept constant in order to simplify the physical set-up when different wave periods were tested. The probe positioning is shown in Figure 3-6.

Table 3-2: Probes spacings in model dimensions [mm]

Wave Period	Deep water			Shallow water		
	X_{12}	X_{13}	X_{23}	X_{12}	X_{13}	X_{23}
8s	372	915	543	240	640	400
10s	488	1031	543	305	705	400
12s	600	1143	543	369	769	400
14s	710	1254	543	432	832	400
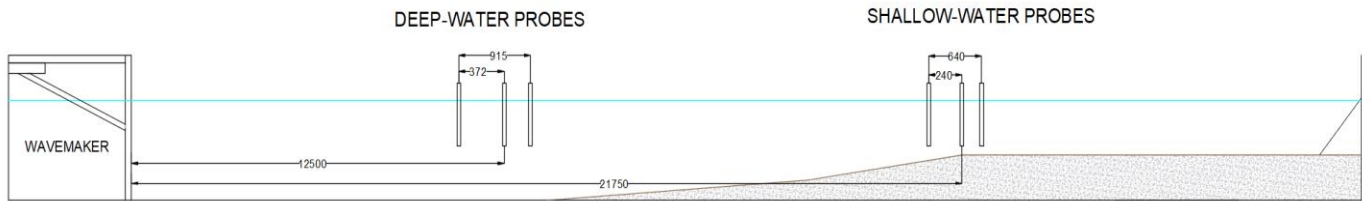
Figure 3-6: Probe positioning for 8s wave period in the flume in model dimensions [mm]

3.5   BATHYMETRY

This thesis focused on developing a standard design for a rubble-mound screed layer and therefore a realistic worst-case scenario had to be simulated, based on South African beach and nearshore profiles.

South African coastlines typically consist of steep slopes where plunging breakers occur regularly. As mentioned in Section 2.3.4, plunging breakers generally cause the most scour and therefore a design condition of the worst case can be modelled with plunging breakers breaking on a typically steep South African coastal bathymetry.

A slope of 1:18.6 was used as a shallow water slope since it is consistent with the average shallow water slope between -1 m and +1 m MSL along the south-western coast of South Africa and is therefore realistic (Schoonees, 2014). The length of the slope has to be as long as possible, but at least a wavelength for the desired design wave to develop (Mansard and Funke, 1980). The average wavelength of the longest period over the entire flume is calculated to be 118.5 m, which translates to 5.9 m in model scale. However, due to the limiting length of the flume and positioning of viewpoint windows, a slightly shorter length of 5.75 m could be allocated to the shallow water slope.

The deep-water slope of the test set-up was constructed at 1:50 since this is also a typical slope for South African deep waters. A model scale length of 3 m could be allocated for the deep-water slope for a smooth and realistic transition between the shallow water slope and the flume bed. A simplified long section of the flume and bathymetry is shown in Figure 3-7. Images of the bathymetry construction process are shown in Appendix C.

(a) Prototype [m]

(b) Model [mm]
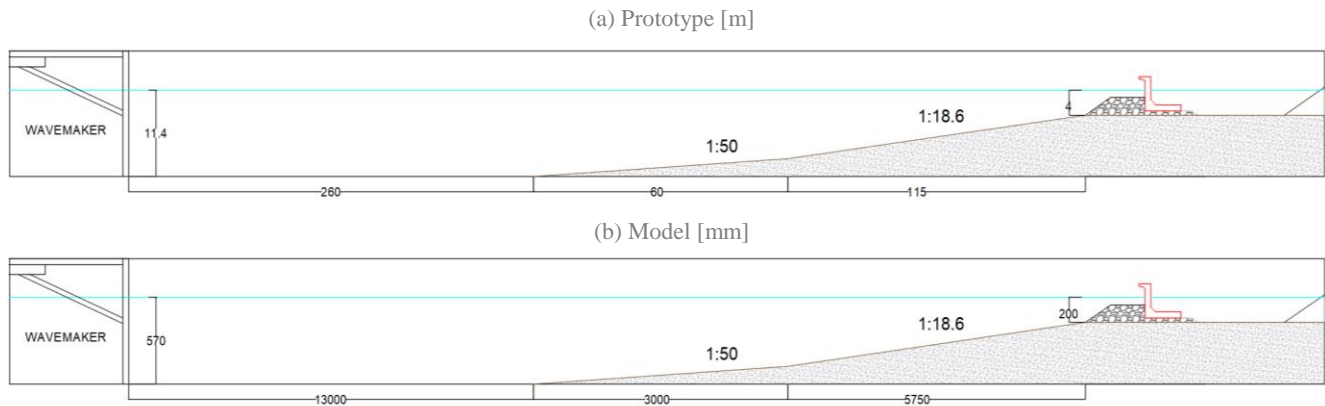
Figure 3-7: Long section of 2-D flume (a) in prototype [m] and (b) in model dimensioning [mm]   (not to scale)

According to Iribarren calculations, waves with periods of 12 seconds or more will result in plunging breakers over the above-mentioned bathymetry and with a wave height of 1.3 m (explained in Section 3.6.1) while the berm structure, with an even steeper slope of 1:1.5, will induce plunging breakers for waves with shorter periods. Calculations are shown in Appendix A.

3.6   WAVE CHARACTERISTICS

3.6.1   Wave period and height

The typical range of wave periods found around the coast of South Africa is 8 to 12 seconds. Therefore, this range was tested in the physical experiments. Storm conditions can result in waves with periods of up to 16 seconds. However, due to time limitations, only 14 second periods were used for longer wave period tests to represent storm conditions.

The significant wave height was kept constant at 1.3 m since it is a realistic wave height at the design depth of 4 m and is also valuable for the simultaneous stability tests mentioned in Section 3.4. The probes described in Section 3.4.3 record both the H_s and H_{m0} during a test. According to the *Coastal Engineering Manual,* H_s and H_{m0} are basically similar, but in shallow water near breaking H_s is a more accurate representation of the actual significant wave height and therefore the H_s values from the probe output were used to determine the significant wave heights during the tests (Burchart and Hughes, 2012).

3.6.2   Wave Spectra and Number

As mentioned in Section 3.4.2, the wave-maker that was used in this thesis can produce regular and irregular wave spectrums and the irregular waves can either be Pierson-Moskowitz or JONSWAP spectrums. The Pierson-Moskowitz wave spectrum is used for fully arisen sea states, while the JONSWAP wave spectrum, which was developed by the JOint North Sea WAve Project, is used for fetch limited sea states. The JONSWAP spectrum is characteristic around the South-African coast and therefore it was used when generating waves during the physical set-up (Chadwick, Morfett and Borthwick, 2013).

The wave-maker has to generate a sufficient number of waves in a sequence in order for the sequence to qualify as an accurate representation of a natural sea state where the average and peak wave period and wave height will occur. The number of waves required for an entire JONSWAP cycle is 512. Table 3-3 shows the duration required to reach 512 waves for each wave period that was tested.

Table 3-3: Duration for an entire JONSWAP cycle for different wave periods

Wave Period [s]	Duration in prototype [s]	Duration in model scale [s]
8	4096	916
10	5120	1145
12	6144	1374
14	7168	1603

The number of waves that is required for sufficient scour to occur is determined by when the scour process reaches equilibrium as described in Section 2.3.3. The point of equilibrium has to be determined experimentally since it is unique for each set-up. Scour development tests were run prior to the main berm tests in order to determine the number of waves required to reach that point of equilibrium. Tests ranged from 500 to 3000 waves in 500 wave increments.

3.7   SEAWALL STRUCTURE

The model structure for the L-wall was constructed with PVC sheets that are rigid and impermeable, as shown in Figure 3-8. The design of the cross-section is based on the preceding tests' L-element design tested by Malan (2016). However, the recurve shape on top of the wall was designed according to recommended specifications developed by Schoonees (2014), Swart (2016) and Kretschmer (2017) to minimise overtopping. Three webs were installed to ensure strength and stability since the wall had to be broken out and placed back into the flume after each test. The base of the PVC wall was serrated to represent serrations that sink into the screed layer to increase

the contact area and therefore increase the friction between the base of the wall and the screed layer. (Schoonees, 2014; Swart, 2016; Kretschmer, 2017).
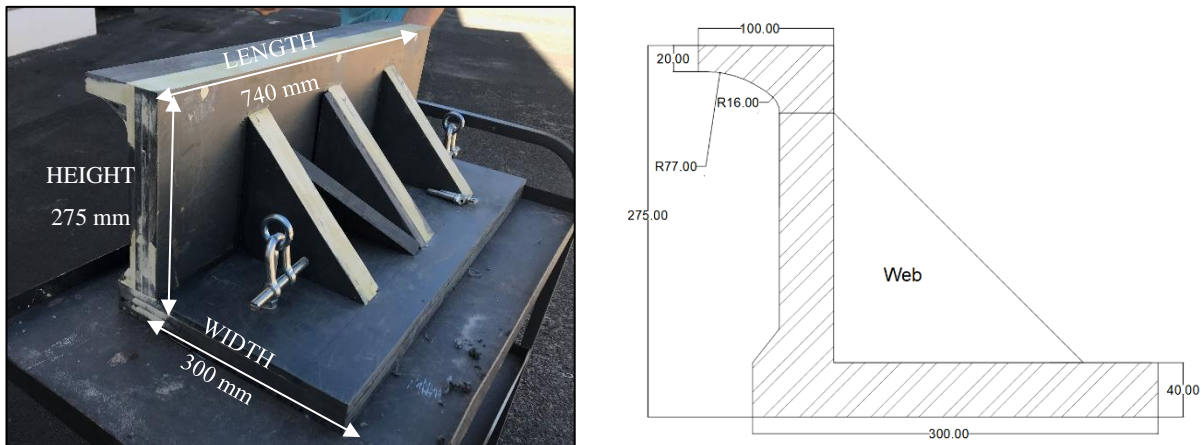
Figure 3-8: Model and cross-section of L-wall structure

During placement, a layer of core material had to be placed first, covered by a thin layer of screed material. It was imperative that these layers were placed precisely level so that the wall can be placed on a level bed. If any unevenness occurred that resulted in gaps between the base of the wall and the screed layer, more scour could occur that would have resulted in inaccurate readings. Care was taken to prevent these gaps.

Guidelines of the entire cross-section were drawn on both glass sides of the flume so that the wall could be accurately replaced after every test. After the wall was placed and the levels of the wall were checked, it was fixed to the glass walls with fast-curing waterproof silicon. *Sikaflex Sealing and Bonding Silicone* worked well for this purpose. The silicon was left to dry overnight before another test could commence. Great care was taken to ensure that as little as possible streams of water and screed material could pass through past the edges of the wall in order to minimise boundary effects.

The L-wall element was designed to be 5.5 m high and 6 m wide in prototype. The model dimensions were adjusted accordingly, as shown in Figure 3-8. The section had to fit snugly into the 750 mm wide flume, so the section was constructed to be 740 mm long in model scale resulting in 10 mm

Figure 3-9: Model backfill set-up

of free movement to place the wall. Apart from the silicon sealant, the seawall structure was fixed in position with concrete tiles and struts as the model equivalent to backfill. The set-up is shown in Figure 3-9.

3.8   FOUNDATION AND BERM STRUCTURE

The rubble-mound berm and foundation of the seawall was modelled with different layers and gradings of granular material. The general layout is based on typical rubble-mound marine structure with appropriate rock sizes, as shown in Figure 3-1 and Figure 3-2.

3.8.1   Layers

The berm and foundation consist of various layers of different rock gradings. The larger rocks provide stability against wave attack and sufficient interlocking between the rocks can be provided by the smaller underlying rock gradings. The rock layer sizes have to adhere to the filter rule to ensure that the finer material does not flush through the coarse rock layers. This filter rule refers to the median mass of a rock layer that must not be more than 10 times the median mass of the rock in the underlying layer (CIRIA, 2007b).

The core layer is the finest granular layer and was placed first as part of the berm and foundation. The screed layer, which is described in Section 2.2.8, is then placed where the seawall structure will be placed afterwards, but with an extended toe. The filter layer was then placed over the core as the next layer for the berm. Lastly, the armour layer was placed. These layers were placed according to cross-section guidelines that were drawn on both glass sides of the flume. The construction process is shown in Appendix C.

3.8.2   Grading

Custom grading curves were designed and graded for each of the rock layers according to the geometrically scaled down design grading ranges for each rock layer shown in Table 3-4 and Table 3-5. 300 samples were randomly picked and weighed from each chosen graded rock pile at the CSIR facility. The core material had to be measured with a Vernier Calliper since it was too small to weigh. These sample masses and dimensions were then combined in an attempt to create grading curves that fitted the custom theoretical grading curves. These grading curves are shown in Appendix B and the mixed rock gradings are shown in Figure 3-11.

The screed layer has to be scaled according to the Lé Mehauté (1965) and Keulegan's (1973) methods. This is because the screed layer should be scaled down geometrically because of the wave transmission that will be

influenced by frictional losses that are not modelled accurately on that small scale (refer to Section 2.8.5). In prototype the screed layer is designed to consist of 19 mm stone. With the above-mentioned methods, 19 mm stone is scaled down to 2.2 mm which can be classified as coarse sand. The calculations are shown in Appendix A. Filter sand, shown in Figure 3-10, with a grading of 0.9 – 3.4 mm was ordered from a supplier to model the screed material.

Figure 3-10: Filter sand used to model screed material

The tables below show the different layer gradings and how the berm is designed in terms of layer thicknesses. A layer thickness coefficient of 1.15 is used for the double layers of irregular rock that the berm consists of (Van der Meer, 1998). The different rock gradings are shown in Figure 3-11 and the berm structure with the gradings is shown in Figure 3-12.

Table 3-4: Prototype rock gradings for berm and foundation layers

Layer	Grading	Median mass M_{50} or dimension	Median diameter D_{n50}	Layer thickness ≈double with kt=1.15
Armour	40 kg – 1400 kg	465 kg	560 mm	1300 mm
Filter	2 kg – 200 kg	47 kg	260 mm	600 mm
Core	10 mm – 320 mm	121 mm	121 mm	280 mm
Screed	19 mm	19 mm	19 mm	100 mm

Table 3-5: Model rock gradings for berm and foundation layers

Layer	Grading	Median mass M_{50} or dimension	Median diameter D_{n50}	Layer thickness ≈double with kt=1.15
Armour	2 g – 250 g	58 g	28 mm	65 mm
Filter	0.1 g – 30 g	5.8 g	13 mm	30 mm
Core	1mm – 16mm	6 mm	6 mm	14 mm
Screed	0.9mm – 3.4mm	2.2 mm	2.2 mm	5 mm

ARMOUR	FILTER	CORE

Figure 3-11: Graded granular material for rock berms
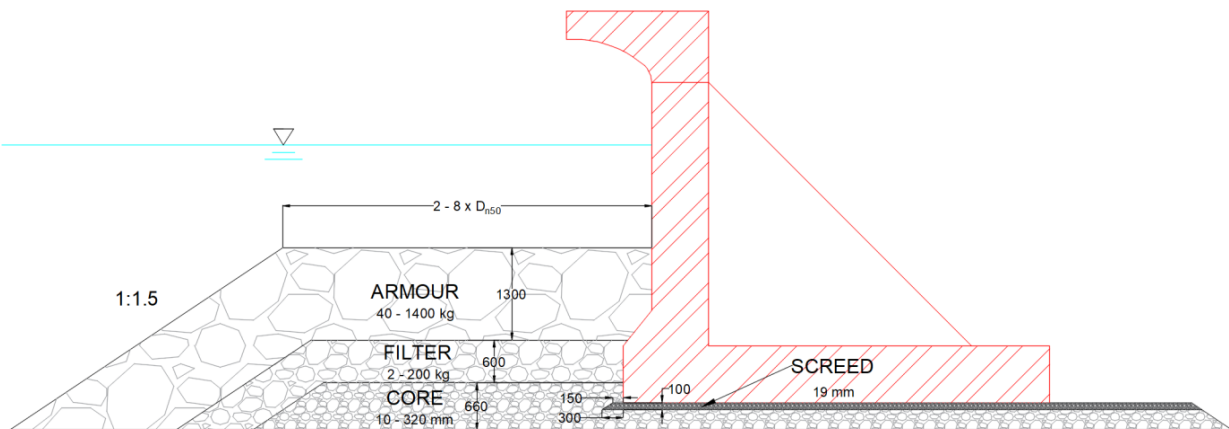
Figure 3-12: Prototype cross-section of berm with rock layers indicated

3.9   CALIBRATION

Wave conditions were initially calibrated before any structure was installed in order to accurately generate the design wave conditions with the wave-maker for a natural sea state with no reflective structure. For every different wave condition, different gains were entered into the wave-maker software so the output wave data, acquired from the probes, were the same as the input values. The gain values are shown in Appendix C.

Two sets of probes were placed in the flume during calibration: deep-water probes and shallow-water probes, as mentioned in Section 3.4.3. However, since the shallow-water probes were placed right on the structure's location, it could only be used during calibration. During tests, the shallow-water probes were removed to make space for the structure, but the deep-water probes remained to ensure the correct wave conditions were created and to record

the reflective coefficient that indicates the effect of the reflective structure on the wave conditions in the flume during the test.

The wave probes had to be calibrated daily before each test commenced due to possible changes in water temperature and purity that could have occurred overnight which influence the conductivity of the water. This was done by sampling three different water levels on the probes at known elevations and assigning those elevations to the probe software.

3.10   DATA ACQUISITION

3.10.1 Wave Probe Data

Wave data was acquired from the capacitance probes as described in Section 3.4.3. The Generalised Experiment control and Data Acquisition software package (GEDAP) is used by the CSIR hydraulics laboratory to convert the capacitance variances recorded by the probes in the flume to a time series of water level elevations that represent the irregular wave spectrum that was generated. The wave parameters that were required, could then be acquired from the GEDAP software's generated time series. The output data used for data analysis is shown in Figure 3-5 in Section 3.4.3.

3.10.2 Scour Depth: Dowel Measurements

Scour damage measurements were conducted with dowels to remain consistent with the data acquisition method of the preceding scour tests by Malan (2016) described in Section 2.5 and 2.6. This method involves probing underneath the seawall structure with wooden dowels to measure the depth that can be penetrated due to scour of the screed layer that has occurred, as shown in Figure 3-13. The length of the seawall was divided into 5 cm intervals, numbered 1 to 15, where the dowels were probed with, so that 15 data points could be acquired throughout the 75 cm wall length. Two dowels with different diameters were used to obtain an average scour depth: a smaller 5 mm diameter dowel (100 mm in prototype) and a bigger 10 mm diameter dowel (200 mm in prototype). These two sets of measurements as well as the average could then be plotted against the length of the seawall to obtain a scour pattern that developed underneath the wall. The 15 data points were also integrated over the length of the seawall in order to obtain an average area that scoured underneath the wall.

However, this dowel method is an intrusive method that disturbs the original scour pattern as the dowels are pushed underneath the seawall to probe the scour depth that developed. Therefore, an alternative, non-intrusive method had to be developed to measure the scour damage.

Figure 3-13: (a) Wooden dowels of 5 mm and 10 mm diameters and (b) measuring scour depth with the dowels

3.10.3 Scour Depth: Ultrasound Measurements

An alternative method to the dowels was developed for measuring scour damage, as mentioned in Section 2.5. Ultrasound sonar equipment was used to create an image of the extent of the scour damage that occurred underneath the submerged base of the seawall. An image of the scour damage could be captured in a non-intrusive way so the scour depth can be measured off the image.

Marine sonar equipment is not readily available or manoeuvrable when conducting physical experiments in a narrow 2D wave flume. However, the same sonar technology is also used in the medical field and medical sonar equipment is easier to handle and was accessible to the author during the execution of the physical experiments. *TECMED* supplied a *Toshiba Viamo* sonar machine with a 10 MHz probe from the Radiology department of *Medi Clinic* in Johannesburg for the duration of the experimental tests, as shown in Figure 3-14(a). The image that is generated is shown in Figure 3-14(b). The codename of the test, the date, the time and the type of test (MSK 1204 – refers to musculoskeletal that is used for smaller anatomical diagnostic tests in the radiology field and was used for scour measurements in this thesis) is shown in the top ribbon. Visual adjustment parameters are shown in the right column and the measurements that are taken on the centre screen image, are shown at the bottom of the screen.
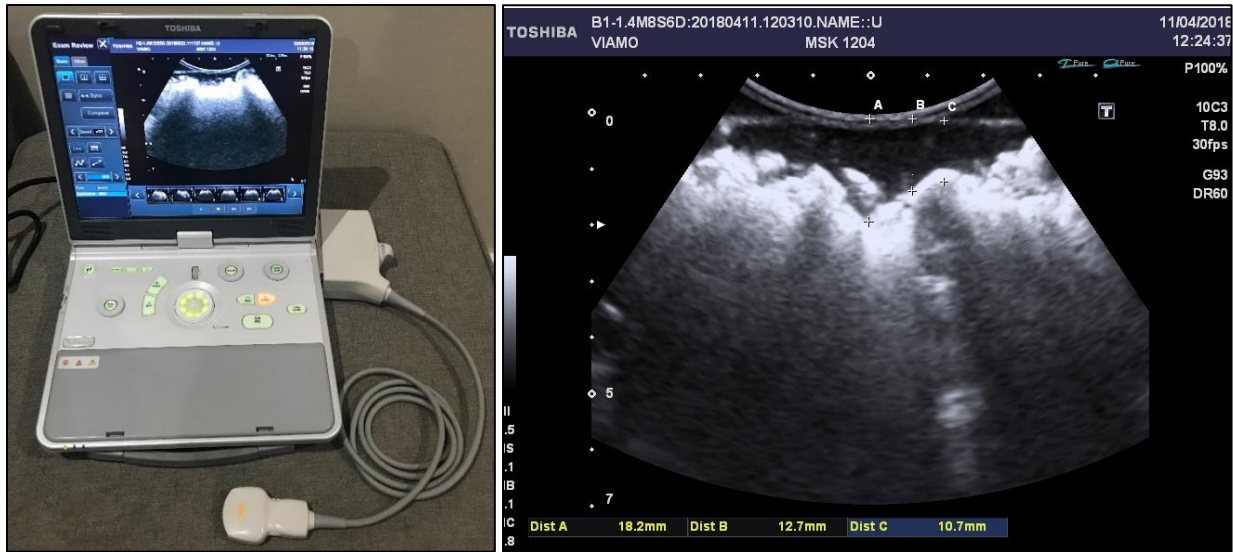
Figure 3-14: (a) Toshiba Viamo Sonar with (b) screen capture showing onscreen measurements

The sonar imaging equipment was initially calibrated to ensure that the onscreen distance measurements were accurate. River rocks of known dimensions were placed 200 mm from the sonar probe and images were taken and measured onscreen to see whether the distances and dimensions matched the true values, as shown in Figure 3-15. The true and measured values are shown in Table 3-6 and it can be seen that the percentage difference between the true values and measured values are negligibly small and therefore the onscreen sonar measurements could be used for the experiments.
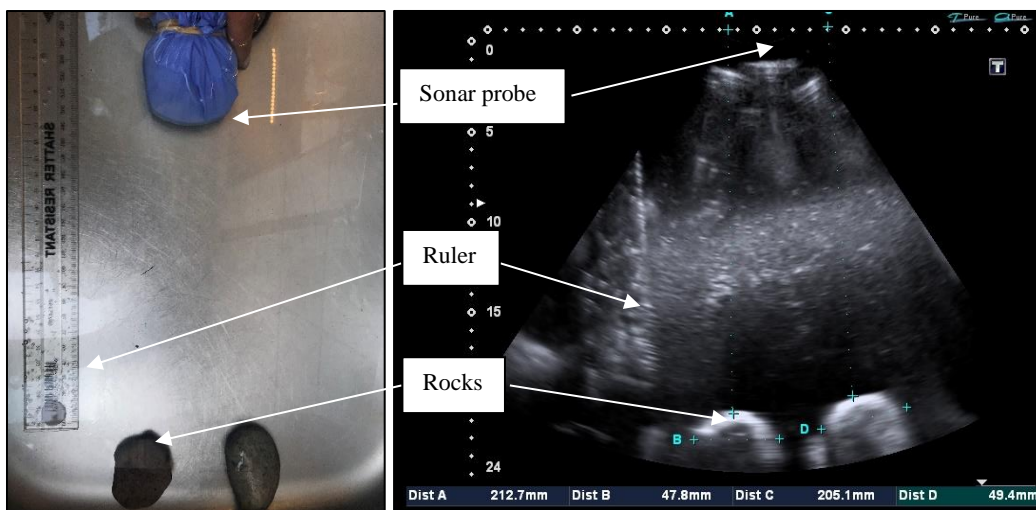
Figure 3-15: Sonar calibration with river rocks

Table 3-6: Calibration of sonar measurements

Object	True measurement [mm]	Sonar measurement [mm]	Difference
Distance from probe to rocks	200	205.1	2.6%
Rock B	47	47.8	0.4%
Rock D	50	49.4	1.2%

After the scour tests were completed the berm was locally removed rock by rock so the scour data could be acquired directly underneath the toe of the model seawall structure. For data acquisition, 15 images were taken in 5 cm intervals to create 15 data points along the length of the seawall. The probe was placed against the toe of the seawall structure so an image of the situation directly underneath the base could be taken. The data acquisition process is shown in Figure 3-16. Measurements were taken from the edge of the seawall (faint white line against the arch of the probe) to where the effect of the scour process visibly stops, the scour damage boundary (white edge of sediment) as seen in Figure 3-17.

Figure 3-16: Sonar measurement process
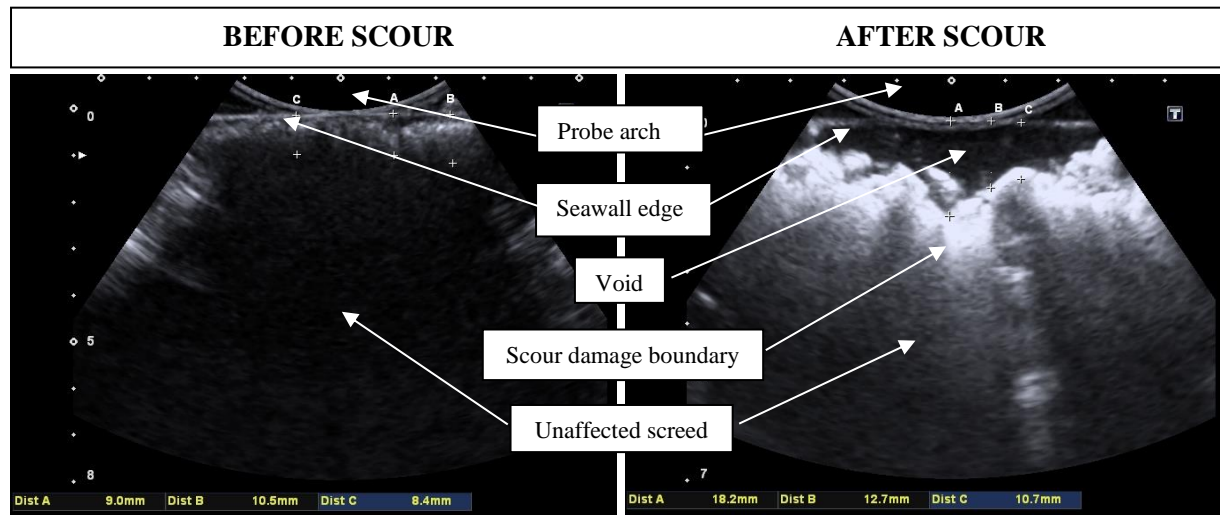
Figure 3-17: Sonar images of the effect of scour underneath seawall

These length measurements were also integrated over the length of the seawall to acquire the area of scour damage that developed during each experimental test. The 15 data points and average area could be directly compared to the dowel measurements to verify the scour damage that occurred. However, because the ultrasound method is a

non-intrusive method of data acquisition, the ultrasound measurements had to be taken prior to the dowel measurements so the scour pattern that developed in the screed, was not disturbed by the intrusive dowel method.

After all 15 images were taken, they had to be analysed and measured to obtain 15 scour depth data points. This measurement process may become subjective due to the fact that the scour pattern does not necessarily form a clear boundary between the void of the screed that was scoured out and the undisturbed screed. It is also important to be able to identify reverberations that become visible on the sonar images, as shown in Figure 3-18. These reverberations have to be distinguished from disturbed screed that also appears lighter, and should be ignored when taking measurements.
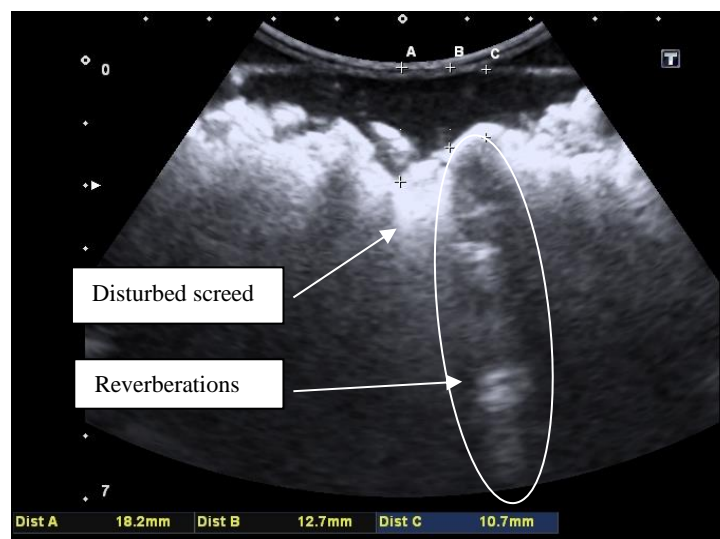
Figure 3-18: Sonar image showing reverberations and disturbed screed

In order to ensure that measurements were taken consistently and objectively, two different experimental set-ups were taken (Test Set H1 and H2, see Section 3.12.2) and the 15 images of each set-up were measured three times. Each set of measurements was done independently on different days so the author could not remember where the measurements were taken the previous time, but rather use fresh, independent and objective judgment of where measurements should be taken. These three independent measurements were then compared to judge whether they match and if measurements were taken consistently. The measurements are shown in Figure 3-19 and Figure 3-20 and the average differences between the measurements are summarised in Table 3-7. It can be observed that the measurements remain very similar over the three independent opportunities of analysis, with an average difference of 8.3% between the measurements for Test H1 and 13.9% for Test H2. Therefore, the method of data analysis was considered as objective and consistent.
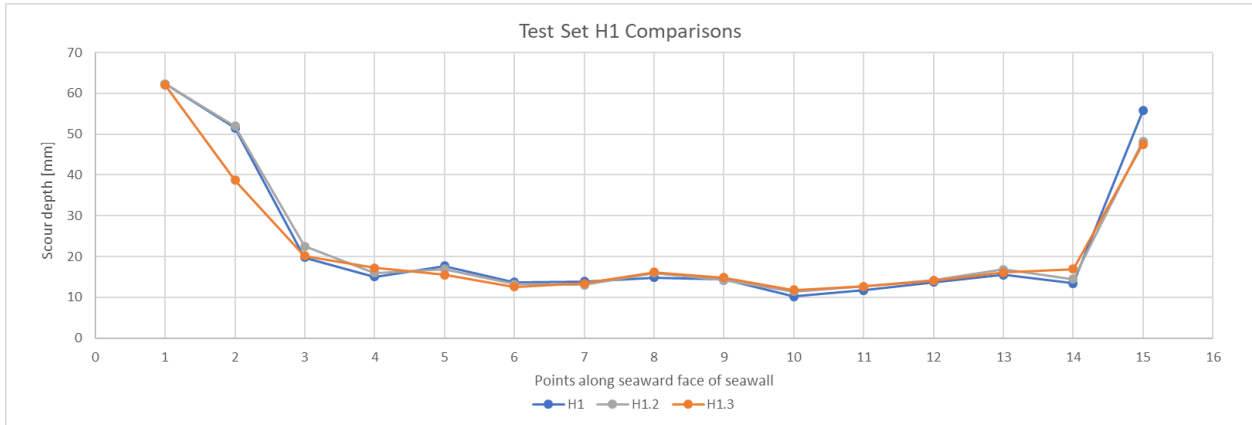
Figure 3-19: Three independent measurements for Test H1
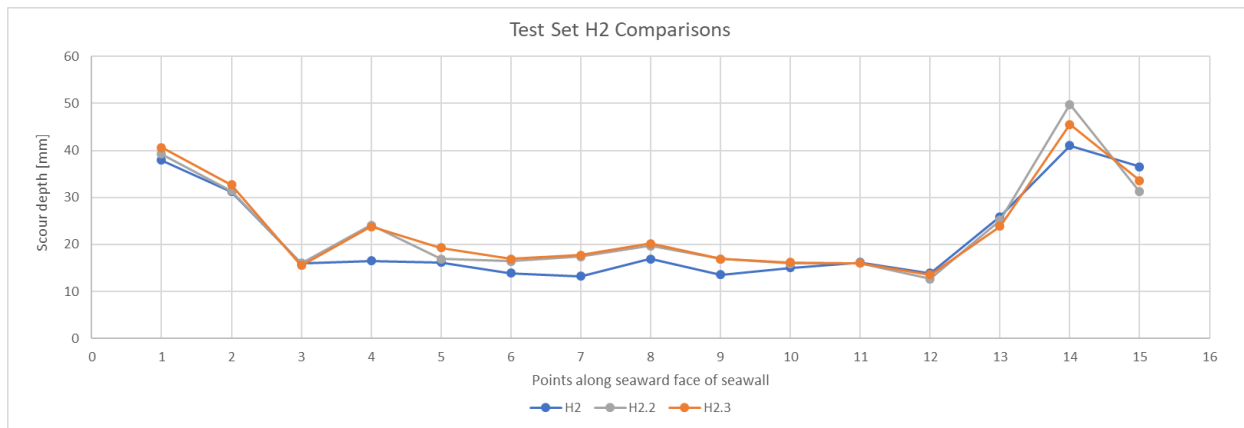
Figure 3-20: Three independent measurements for Test H2

Table 3-7: Summary of average differences between measurements

Test	1st and 2nd readings difference	1st and 3rd readings difference	Average difference
H1	6.5%	10.1%	8.3%
H2	13.4%	14.4%	13.9%

3.11 MODEL SET-UP COMPARISON WITH MALAN (2016)

3.11.1 General

As mentioned in Section 3.7, the basic design of the seawall structure and rubble-mound berm is based on the preceding scour tests conducted by Malan (2016). Therefore, some of this thesis's results can be directly compared to the results of Malan (2016). However, there are several fundamental differences between the two experimental set-ups that have to be considered when comparing the magnitudes of the different scour results. Figure 3-21 and Figure 3-22 shows the two model set-ups:

(i)   Cross-section of structure of Malan's (2016) tests

H_s: 1.364 – 2.031 m

T_p: 7.753 – 8.101 s

Scour measurement: Dowels
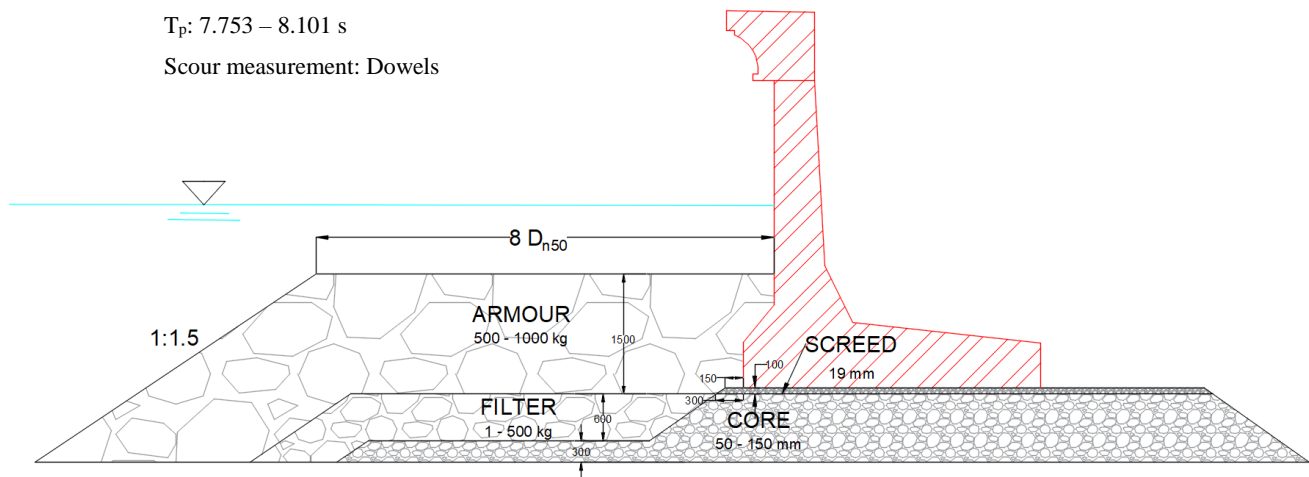
Figure 3-21: Cross-section of structure of Malan's (2016) tests

(ii)   Cross-section of structure of this thesis's tests

H_s: 1.3 m

T_p: 8– 14 s

Scour measurement: Sonar and Dowels
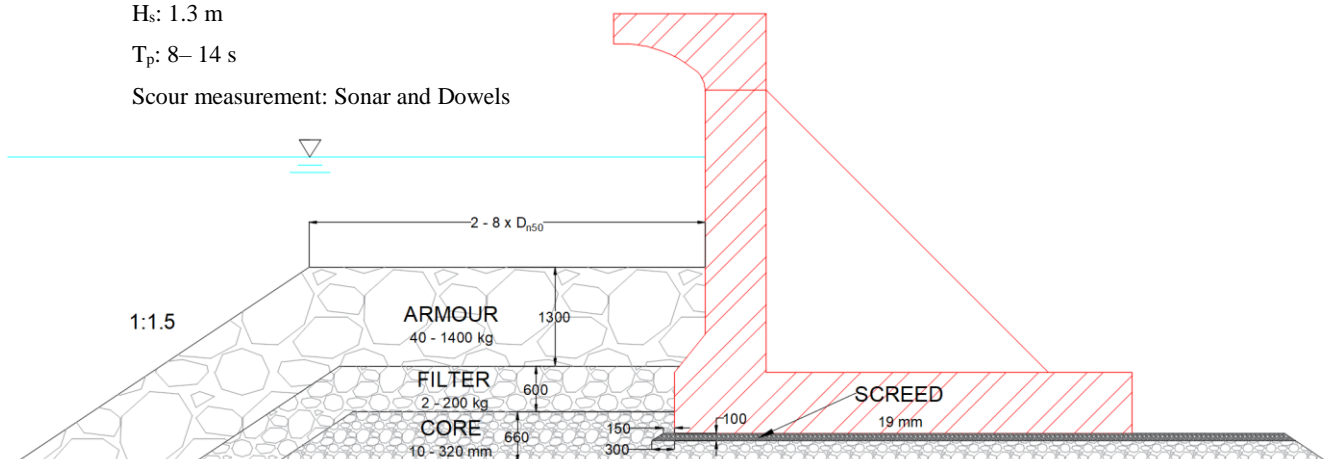
Figure 3-22: Cross-section of structure of this thesis's tests

3.11.2 Differences between the two set-ups

The figures above show that there are clear differences between the two experimental set-ups and therefore it can be expected that the scour results of the two set-ups will differ significantly:

(i) **Wave height**: The range of wave heights that the structures were exposed to, differ with Malan's (2016) H_s range covering larger waves than the H_s range of this thesis. Larger waves generally cause more scour and therefore it is expected that Malan's (2016) tests will result in the worst scour damage.

(ii) **Wave period**: This thesis tests a range of wave periods between 8 and 14 s while Malan (2016) only tested a T_p of around 8s. Therefore, only the 8 s wave period tests of this thesis could be directly compared to Malan's (2016) tests.

(iii) **Berm width**: The same situation applies for the berm width parameter. Malan (2016) only tested a berm width of 8 D_{n50} while this thesis tested a range of 2 to 8 D_{n50} wide berms. Therefore, only the tests with 8Dn50 berm widths could be directly compared to Malan's (2016) tests.

(iv) **Rock grading**: It can be seen in the figures above that Malan used coarser and wider gradings of rock for the respective rubble-mound layers compared to this thesis. It is hypothesised that a coarser and wider rock grading would result in more scour since there is less interlocking and filtering action that can take place between the coarser rubble-mound layers. This hypothesis must be confirmed with this thesis's results.

(v) **Screed toe layout**: The layout of the screed toe structure was adjusted for this thesis with the aid of Malan's (2016) research. The layers over the screed toe adheres to the filter rule mentioned in Section 3.8.1. in this thesis, while Malan's (2016) layout does not. Therefore, it is expected that the screed layer will be protected more effectively in this thesis and therefore less scour is expected with this set-up, compared to Malan's (2016) set-up.

(vi) **Scour measurements**: Malan (2016) only used the dowel method for measuring scour underneath the seawall while both the dowel and sonar method was used in this thesis. It is expected that dowel measurements will show deeper (or more extensive) scour damage since dowel measurements are intrusive as mentioned in Section 3.10. Dowel measurements are also not constant and objective since the force used to probe underneath the base of the seawall is not consistent. The sonar measurements are therefore expected to be more accurate and possibly showing less scour damage.

3.12   TEST SET-UP ROUTINE AND TEST PLAN

3.12.1   Test Set-up Routine

The following step-by-step routine was developed to set up and conduct each of the tests as consistent and time-efficient as possible:

1. Slowly fill flume from both ends without disturbing screed layer with flow past seawall to either side.
2. Set wave-maker paddle to "HOME" position while filling.
3. Ensure design water level has been reached. Drain if necessary.
4. Calibrate probes.
5. Rezero probes.
6. Set Dynamic Wave Absorption System gain.
7. Input test parameters into wave-maker and probe software.
8. Take "BEFORE" photographs of berm for stability tests (Jarvis, 2018).
9. Start wave-maker. Start probe sampling 30 seconds afterwards.
10. Run test for specified test durations for different wave periods.
11. Make qualitative visual observations of overtopping as well as scour process in screed layer against the glass boundaries of the flume.
12. When test finishes, check recorded probe data while waiting for water to still.
13. Take "AFTER" photographs for stability tests (Jarvis, 2018).
14. Drain flume until working space in front of structure is dry.
15. Deconstruct berm partially.
16. Take scour measurements with ultrasound and dowels.
17. Reconstruct berm and refill flume for further stability tests.
18. Drain flume partially again and deconstruct foundation and berm entirely after all stability tests.
19. Reconstruct foundation and fresh screed layer.
20. Place wall and silicon to glass. When all the wave period sets for one berm has been completed, shift the wall one berm width unit forward with placement so a new berm width can be tested.
21. Reconstruct berm and leave silicon to dry overnight.

3.12.2 **Test Plan**

The experimental scour tests were conducted in sets that were numbered alphabetically. Each set had a different berm set-up and most of the sets consisted of varying wave periods. The order of test sets was determined by the most effective use of material, ease of construction and the influence that the preceding test results had on the following tests. The test sets were ordered as follows:

Test set A: Scour development

Test set B: 6 D_{n50} wide berm

Test set C: 8 D_{n50} wide berm

Test set D: 4 D_{n50} wide berm

Test set E: 3 D_{n50} wide berm

Test set F: 2 D_{n50} wide berm

Test set G: Screed thickness

Test set H: Verification of recommended berms

The detail of each test is described in Table 3-8. The tests were conducted accordingly and the results are given and analysed in Chapter 4.

Table 3-8: Test plan layout [prototype values]

Test nr	Test code	Berm width	Input T_p[s]	Duration [waves]	Screed thickness [mm]	Input H_s [m]
1	A-500W	$6D_{n50}$	8	500	100	1.3
2	A1-1000W	$6D_{n50}$	8	500	100	1.3
3	A1-1500W	$6D_{n50}$	8	500	100	1.3
4	A1-2000W	$6D_{n50}$	8	500	100	1.3
5	A1-3000W	$6D_{n50}$	8	1000	100	1.3
6	A2-1000W	$6D_{n50}$	8	1000	100	1.3
7	A2-2000W	$6D_{n50}$	8	2000	100	1.3
8	A2-3000W	$6D_{n50}$	8	3000	100	1.3
9	B1-8S6D	$6D_{n50}$	8	Equilibrium*	100	1.3
10	B2-10S6D	$6D_{n50}$	10	Equilibrium	100	1.3
11	B3-12S6D	$6D_{n50}$	12	Equilibrium	100	1.3
12	B4-14S6D	$6D_{n50}$	14	Equilibrium	100	1.3
13	C1-8S8D	$8D_{n50}$	8	Equilibrium	100	1.3
14	C2-10S8D	$8D_{n50}$	10	Equilibrium	100	1.3
15	C3-12S8D	$8D_{n50}$	12	Equilibrium	100	1.3
16	C4-14S8D	$8D_{n50}$	14	Equilibrium	100	1.3
17	D1-8S4D	$4D_{n50}$	8	Equilibrium	100	1.3
18	D2-10S4D	$4D_{n50}$	10	Equilibrium	100	1.3
19	D3-12S4D	$4D_{n50}$	12	Equilibrium	100	1.3
20	D4-14S4D	$4D_{n50}$	14	Equilibrium	100	1.3
21	E1-8S3D	$3D_{n50}$	8	Equilibrium	100	1.3
22	E2-10S3D	$3D_{n50}$	10	Equilibrium	100	1.3
23	E3-12S3D	$3D_{n50}$	12	Equilibrium	100	1.3
24	E4-14S3D	$3D_{n50}$	14	Equilibrium	100	1.3
25	F1-8S2D	$2D_{n50}$	8	Equilibrium	100	1.3
26	F2-10S2D	$2D_{n50}$	10	Equilibrium	100	1.3
27	F3-12S2D	$2D_{n50}$	12	Equilibrium	100	1.3
28	F4-14S2D	$2D_{n50}$	14	Equilibrium	100	1.3
29	G1-200T	Chosen berm**	Chosen period**	Equilibrium	200	1.3
30	G2-300T	Chosen berm	Chosen period	Equilibrium	300	1.3
31	H1-TBC**	Chosen berm	Chosen period	Equilibrium	100	1.3
32	H2-TBC	Chosen berm	Chosen period	Equilibrium	100	1.3

The number of waves required to reach equilibrium in the scour process must first be determined by Test Set A. The enhancement factor used to generate the JONSWAP irregular waves remain constant at 3.3.

** TBC = To Be Confirmed. The recommended berm width that has to be verified in Test Set H together with the appropriate wave period, must first be determined by the preceding test sets.

4. RESULTS AND ANALYSIS

4.1 VISUAL OBSERVATION

4.1.1 Wave Breaking

The berm and seawall structure were visually observed and filmed during testing to determine the overall physical behaviour of the entire rubble-mound structure under different wave conditions. The bathymetry was designed to induce plunging breaking, or almost plunging breaking, at the location of the berm toe. Spilling and plunging breaking was observed at this location during the calibration process without the structure, as described in Section 3.9. However, it was observed that once the structure was built in place, the reflected waves that occurred, prevented any waves from breaking in front of the berm. The waves only broke against the seawall itself as shown in Figure 4-1.

Figure 4-1: Front view of waves breaking against the seawall

4.1.2 Wave Periods

During the shorter wave period tests, i.e. 8 and 10 second tests, a rapid change in wave direction and celerity occurred due to the short waves that frequently crash against the seawall and reflected waves that are generated seaward again. The rapid wave breaking and change of wave direction caused a faster and deeper drawback of the water level on the berm (see Figure 4-2), which resulted in more damage to the armour rocks and deeper penetration of energy into the screed layer, which seemed to have caused deeper scour.
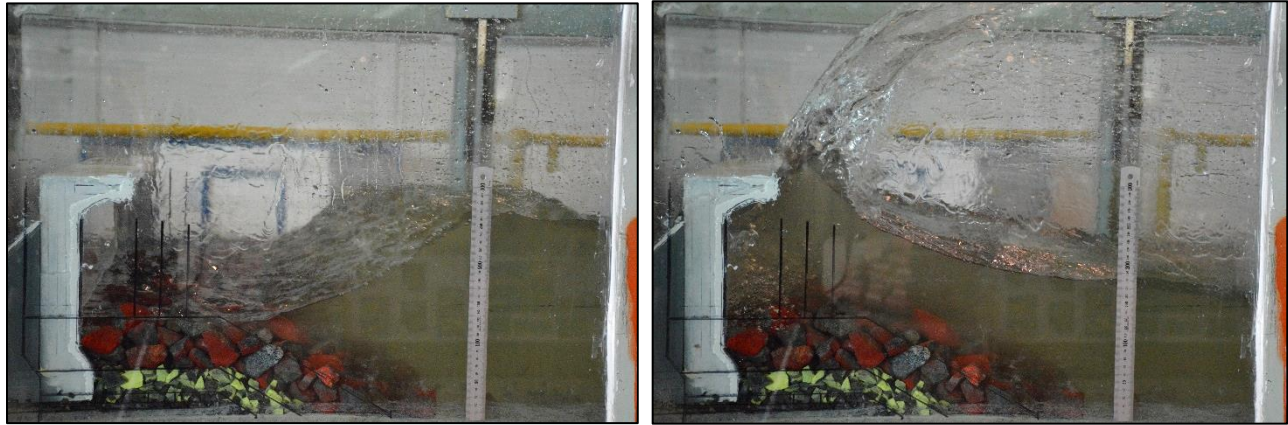
Figure 4-2: Short wave period test (a) deep drawback   (b) and large splash off seawall recurve

Slower transitions between incident and reflected waves occurred during the longer 12 and 14 second wave period tests. Therefore, reflected waves were generated off the seawall without as much interference from the incident waves and could clearly be distinguished from the incident waves as it moved in the opposite direction up the flume. From visual inspection it was suspected that most of the wave energy is reflected back and does not penetrate the berm so deep into the screed layer and therefore less scour was expected. This is in contrast from what was hypothesised in Section 3.2.3 that a longer wave period generates a wave with a higher celerity and orbital velocities and would therefore cause more scour. Figure 4-3 shows the shallower drawback and smaller back splash for the longer wave period tests.
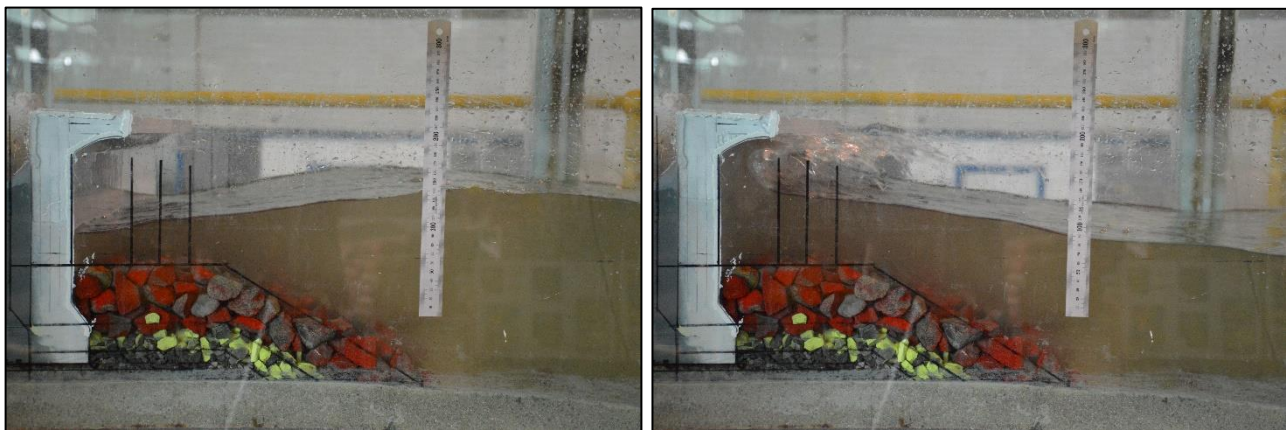
Figure 4-3: Long wave period tes t(a) shallow drawback   (b) and smaller splash off seawall recurve

4.1.3   **Berm Width**

The reflection coefficient is a good indication of the energy that is absorbed by the berm and seawall and the energy that is reflected back off the structure. The width of the berm had a significant effect on the reflection coefficient since a wider berm absorbed more of the wave energy from breaking against the wall and therefore the reflected waves were smaller. The screed layer was protected by the wider berm since the wave energy did not penetrate as far into the berm structure and therefore less scour was expected, which is consistent with the hypothesis in Section 3.2.3. Figure 4-5 shows how the waves break differently against the berm due to the different berm widths.

4.1.4   **Overtopping and Splashing**

The splashing and overtopping over the seawall structure were also significantly influenced by the varying wave periods and berm widths. The shorter wave periods caused the incident and reflected waves to occasionally superimpose to create much larger waves that crashed against the seawall and cause significant splashing. However, the majority of the splashing was thrown back seaward by the recurve seawall. The minority of the splashing spilled over the seawall as green water. The longer wave periods caused the waves to approach the seawall more gradually. The incident and reflected waves were far enough apart so that superimposing waves did not occur at the seawall as often. Therefore, less splashing but more overtopping occurred as the wave spilled over seawall crest as green water, as shown in Figure 4-4.
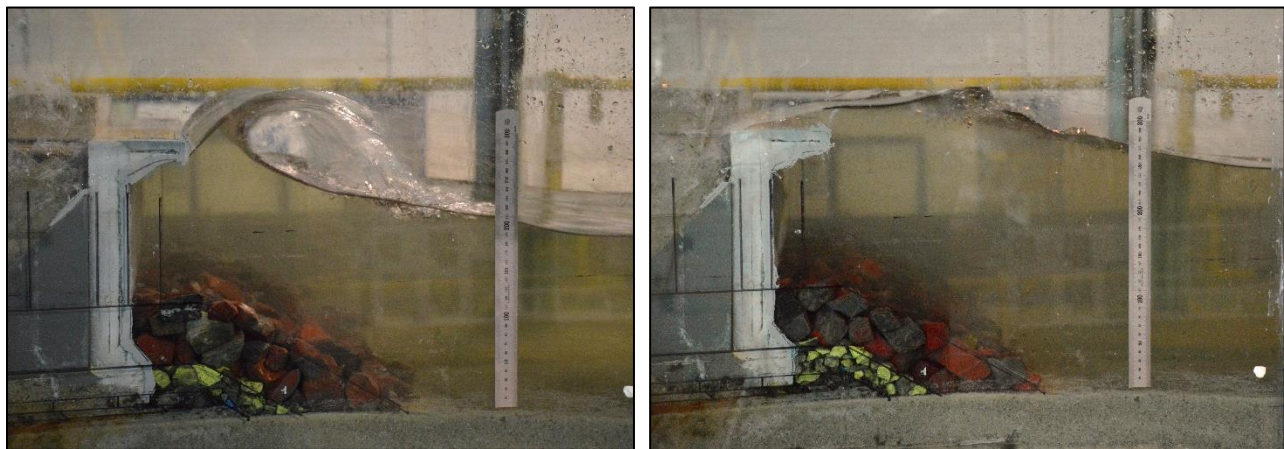
Figure 4-4: (a) Short wave period splashing   *(b) and long wave period overtopping*

The berm width also had an effect on the splashing and overtopping: a wider berm absorbed more of the wave energy and therefore less wave energy could be transferred to overtopping and splashing with the wider berm set-up. This observation is shown in Figure 4-5 where a (a) $6D_{n50}$ and (b) $3D_{n50}$ berm are compared.
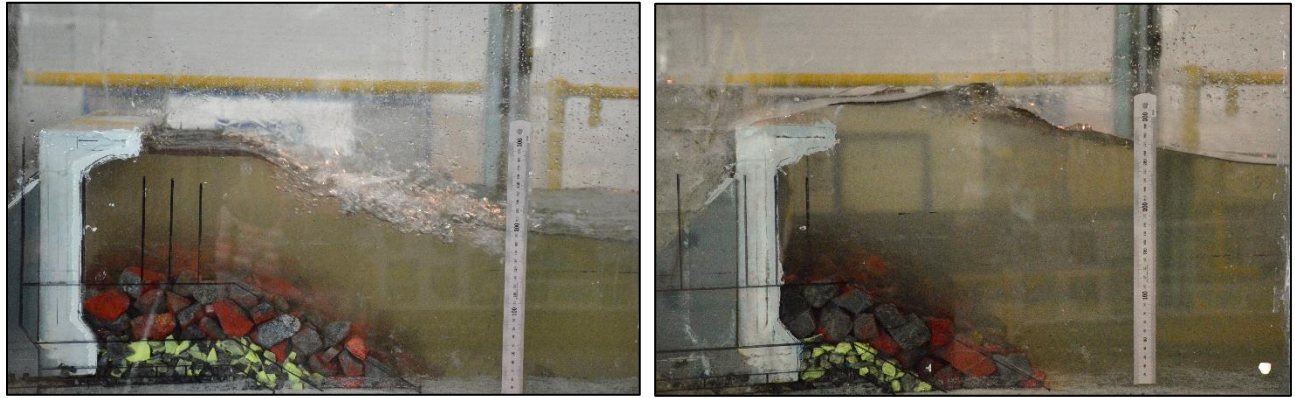
Figure 4-5: (a) 6D$_{n50}$ wide berm with less overtopping   *(b) and 3D$_{n50}$ wide berm with more overtopping*

4.2   RAW DATA ANALYSIS

4.2.1 Dowels and Sonar Measurements

An example of the raw data as it is acquired from the ultrasound measurements (referred to as "sonar") and the dowels (referred to as "5mm" and "10mm") is shown in Figure 4-6. The codename of the test is shown in the title of the graph and includes the period "10S" which refers to 10 seconds and the berm width "4D" which refers to 4 D_{n50}. The 15 data points of each type of measurement refer to the 75 cm length along the seaward face of the seawall that was divided into 5 cm intervals.
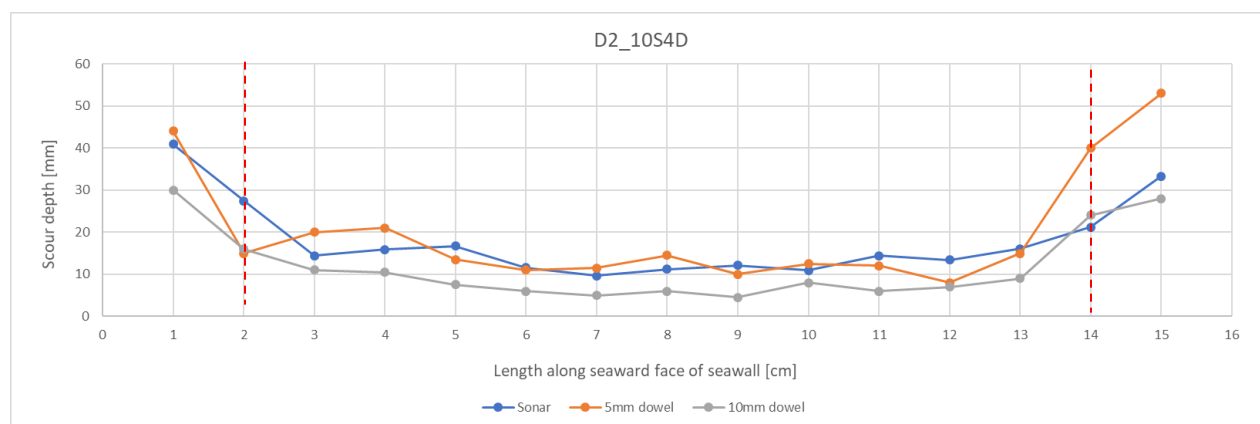
Figure 4-6: Raw data analysis of scour depth along the seaward face of seawall with boundary effects [model dimensions]

It can be observed that there were boundary effects within 10 cm (2m in prototype) off the sides of the flume since the scour depth is significantly more at Points 1 and 2 and Points 14 and 15. This is due to water that passes around the corners of the seawall and pulls more screed material through, since the seawall cannot be perfectly sealed off. Therefore, the four outer data points are influenced by wall effects and have to be omitted with data analysis as shown with the dashed red lines in Figure 4-6.

More examples of raw data measurements on different test set-ups with varying wave periods and berm widths are shown in Figure 4-8, Figure 4-7 and Figure 4-9. The same boundary effects can be observed in all the experiments, which confirm that the two outer readings on both sides have to be omitted as being model effects.
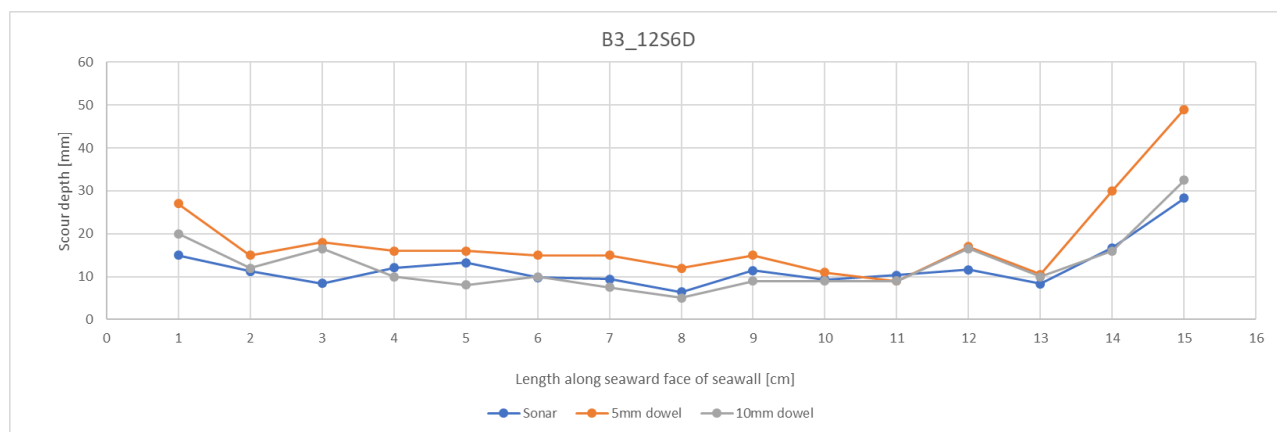
Figure 4-8: Raw data of Test B3 showing boundary effects [model dimensions]
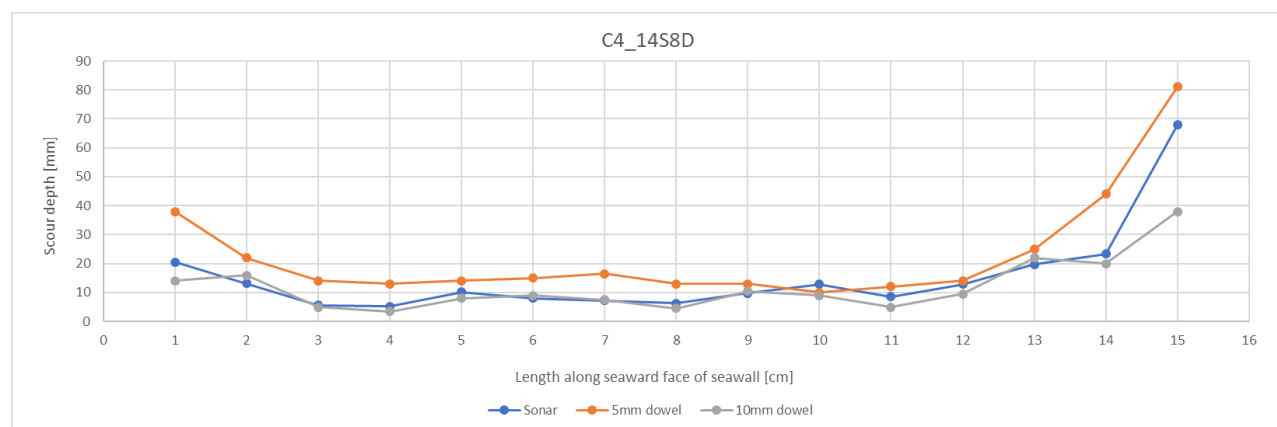
Figure 4-7: Raw data of Test C4 showing boundary effects [model dimensions]
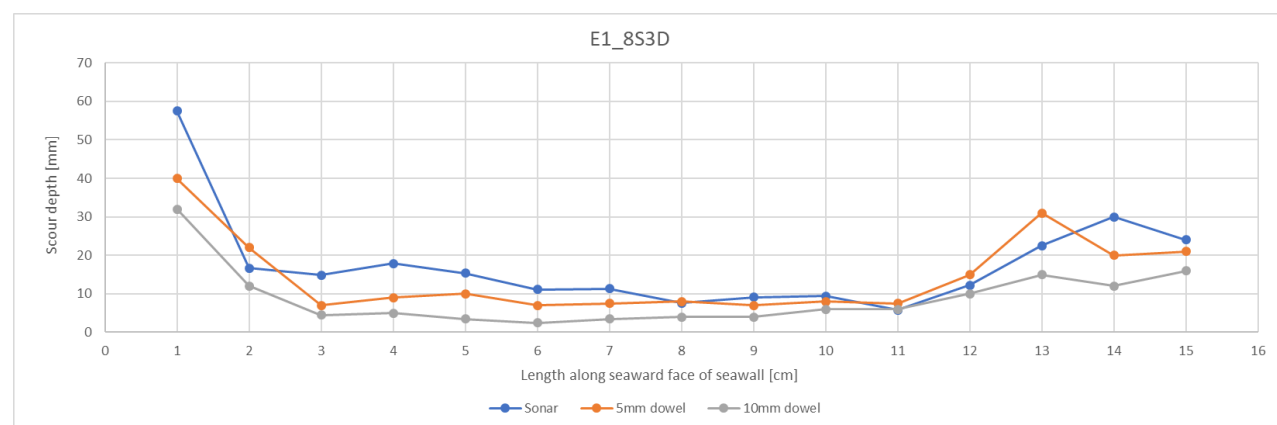
Figure 4-9: Raw data of Test E1 showing boundary effects [model dimensions]

4.2.2 Statistical Analysis for Boundary Effects

The data was statistically analysed as well in order to determine whether omitting the two outer data points on each side would be sufficient to remove boundary effects or if more data must be omitted. The average scour depth between Point 7 and 9 was determined for sample tests, as well as the standard deviation. More data points were added consecutively on each side, from Point 6 to 10, then Point 5 to 11, Point 4 to 12, Point 3 to 13, Point 2 to 14 and eventually including all the points from Point 1 to 15. This was done to determine at which point the data points start differing significantly. The statistical analysis of Test D2_10S4D shown in Figure 4-10:
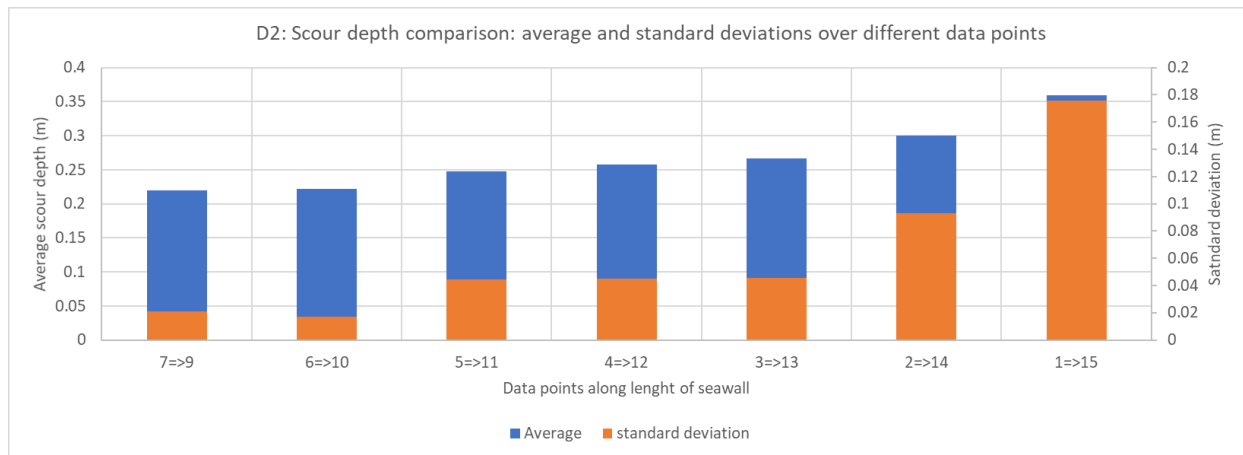
Figure 4-10: Statistical analysis of Test D2 over different data point segments

It can be seen that the average and the standard deviation increases significantly from the point segment from "Point 3 to 13" to "Point 2 to 14". This means that the boundary effects are significant up to Point 2 and Point 14 and decrease as the analysis move more to the centre of the seawall length. Figure 4-11, Figure 4-12 and Figure 4-13 confirm this pattern with the three alternative test results.
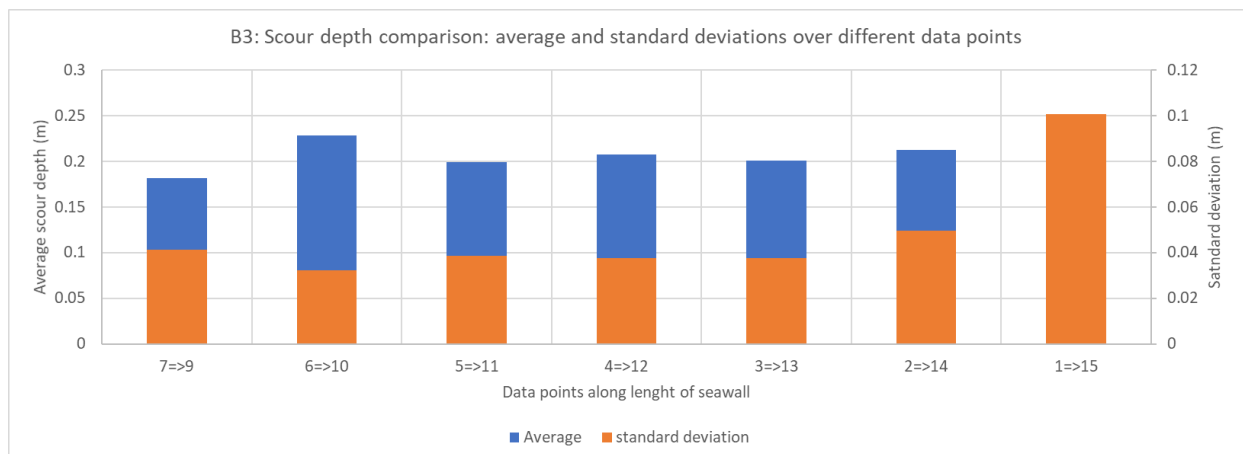
Figure 4-11: Statistical analysis of Test B3 over different data point segments
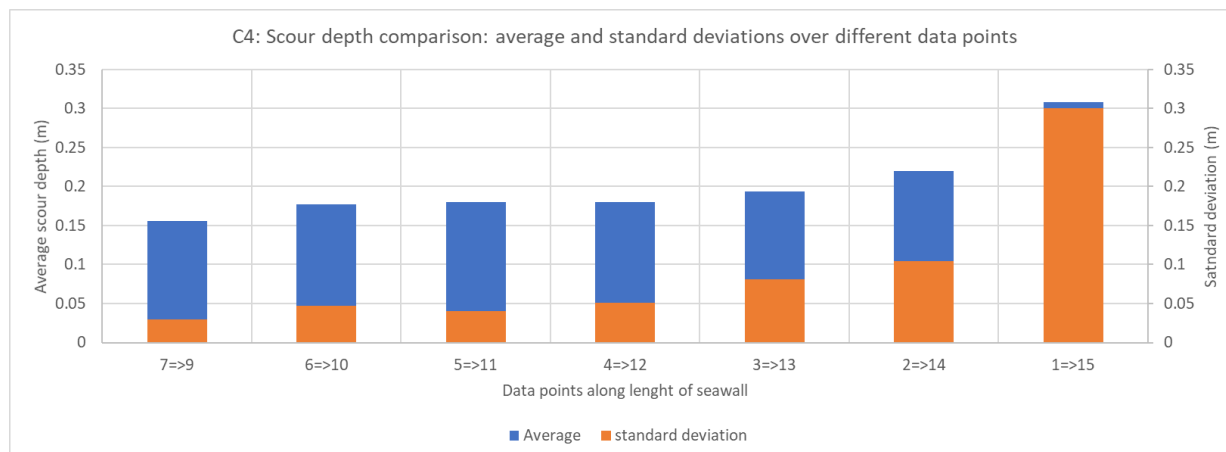
Figure 4-12: Statistical analysis of Test C4 over different data point segments
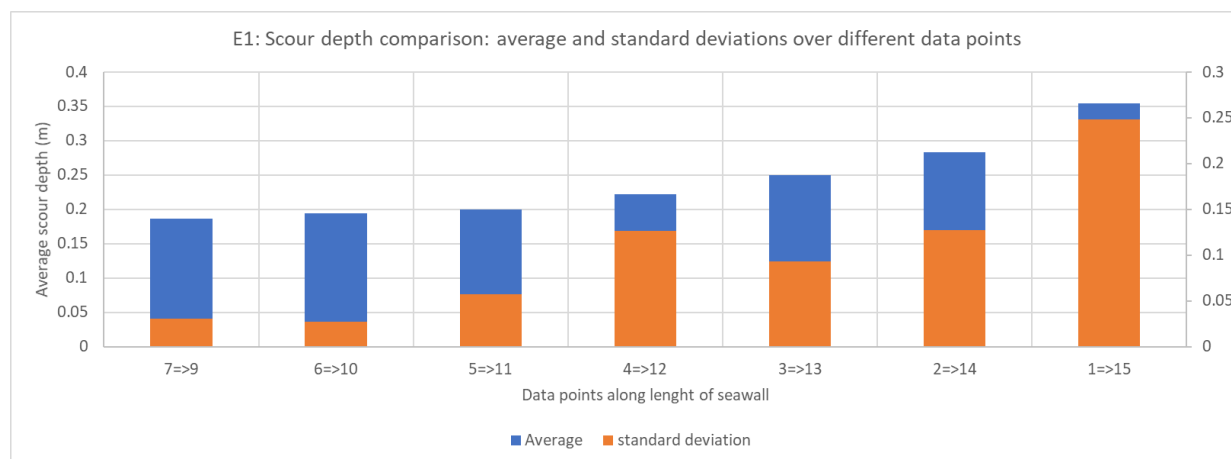
Figure 4-13: Statistical analysis of Test E1 over different data point segments

The general observation is that the data between Point 3 and 13 is not significantly influenced by boundary effects and therefore it is confirmed that the two outer data points on each side of the seawall, that is 13,3% on each side, should be omitted from the data analysis to exclude boundary effects. Therefore, the recommendation for future experimental set-ups would be to omit data of at least 13.3% of the total seawall length on each side in order to exclude boundary effects from influencing the data inaccurately.

4.2.3 **Simplification of Raw Data**

The graphs in Figure 4-6 to Figure 4-9 show that the small 5 mm dowels penetrate deeper into the screed layer while the larger 10 mm dowels cannot probe as deeply underneath the seawall because of the wider diameter. The sonar measurements correlate relatively well with the two different dowel measurements as it can be observed that

the sonar measurements tend to fall between the small dowel readings and the large dowel readings. Therefore, it was considered to compare and check the correlation between the sonar measurements and an average of the small and large dowel measurements.

An average of the two dowel measurements was therefore used to compare with the sonar measurements in order to determine whether the sonar measurements yield trustworthy results. Figure 4-14 shows the simplified graph that will be analysed.
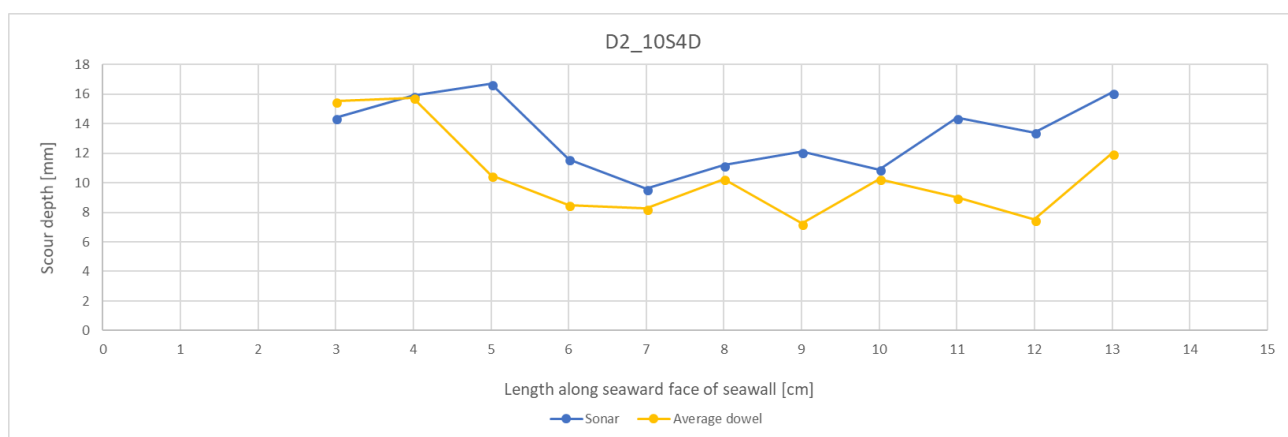
Figure 4-14: Raw data with sonar and average dowel measurements and boundary data points omitted [model dimensions]

The dowel measurements were taken to be consistent with the preceding scour tests and so that the sonar measurements could be compared to a ballpark value. However, since the sonar measurements match the general pattern of the dowel measurements, it was decided to only use the sonar measurements in further analysis. This is because the sonar measurements are believed to be more accurate since it is a non-intrusive method and not dependent on the varying force with which the dowels are pushed underneath the seawall base. More examples that confirm the correlating pattern of the sonar and the average dowel measurements are shown in Figure 4-15, Figure 4-16 and Figure 4-17.
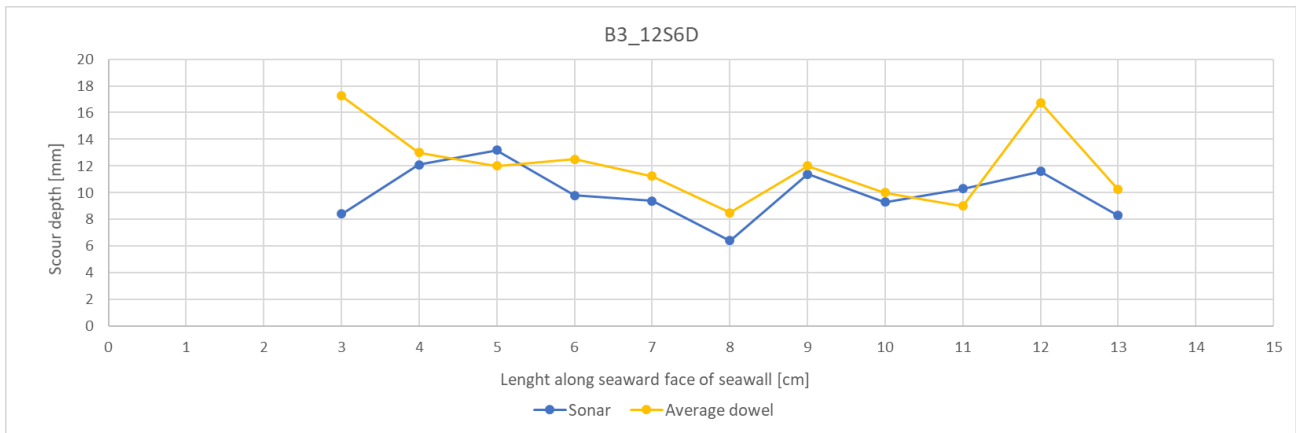
Figure 4-15: Raw data of Test B3 comparing sonar and average dowel measurements [model dimensions]
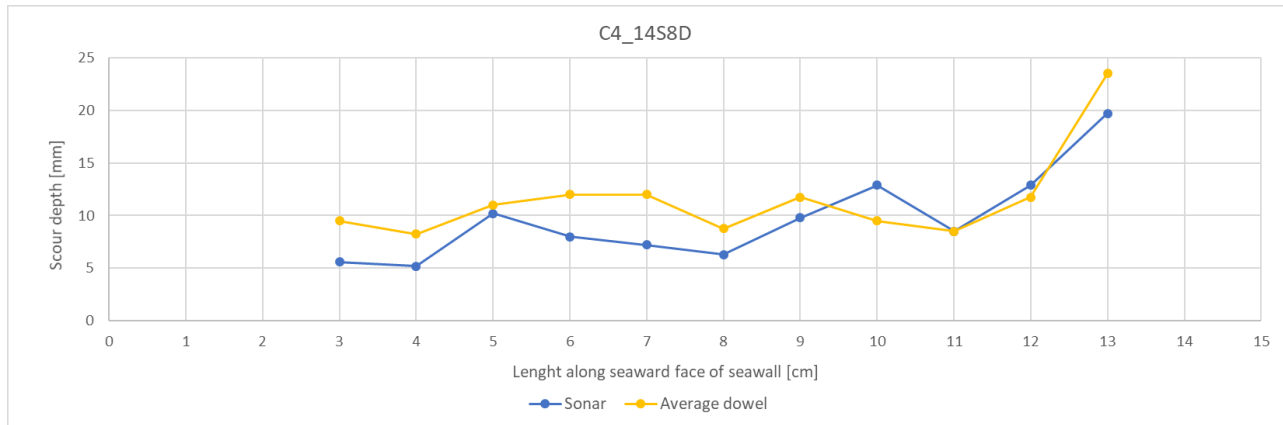
Figure 4-16: Raw data of Test C4 comparing sonar and average dowel measurements [model dimensions]
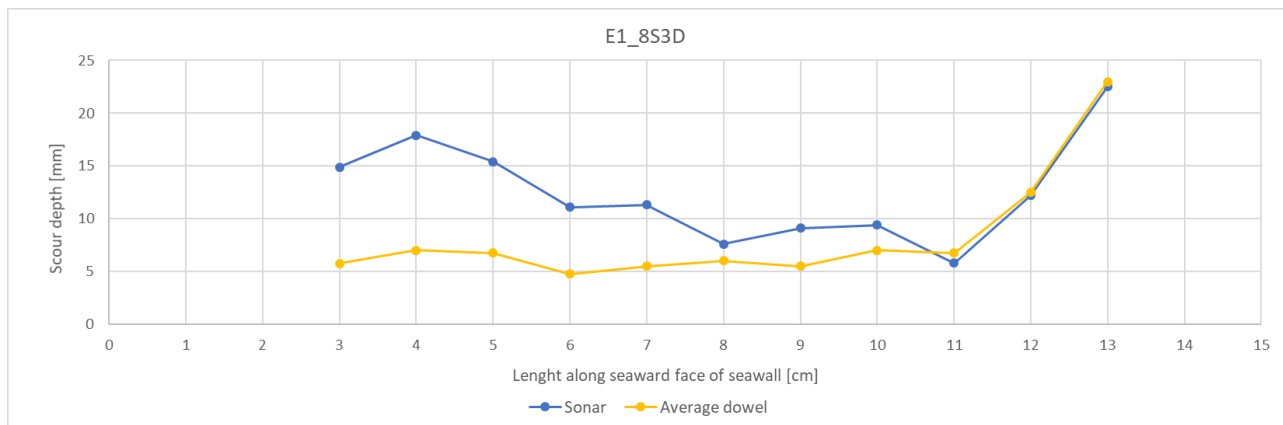
Figure 4-17: Raw data of Test E1 comparing sonar and average dowel measurements [model dimensions]

Figure 4-18 shows how the sonar measurements of the 15 scour depth points are integrated in order to obtain an average area throughout the whole length of the seawall. The depth measured at each data point is multiplied with the width that each data point covers (which is 5 cm in the model and 1 m in prototype) and then these areas are added to obtain the total scoured area over the length of the model seawall.
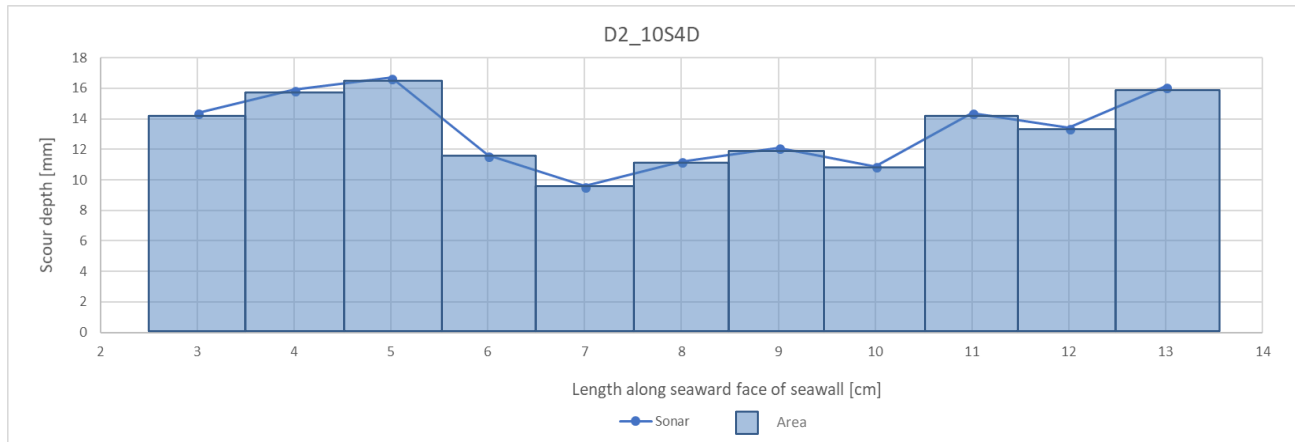
Figure 4-18: Integration of sonar measurements of scour depths of Test D2 [model dimensions]

Figure 4-19, Figure 4-20 and Figure 4-21 show how the integration process was applied to all the tests mentioned above as examples.
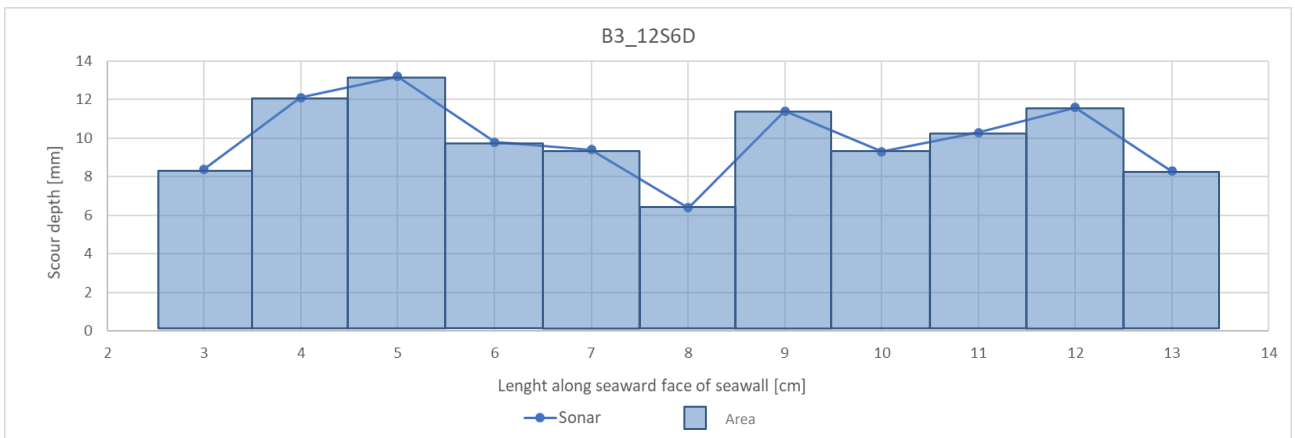
Figure 4-19: Integration of sonar measurements of scour depths of Test B3 [model dimensions]
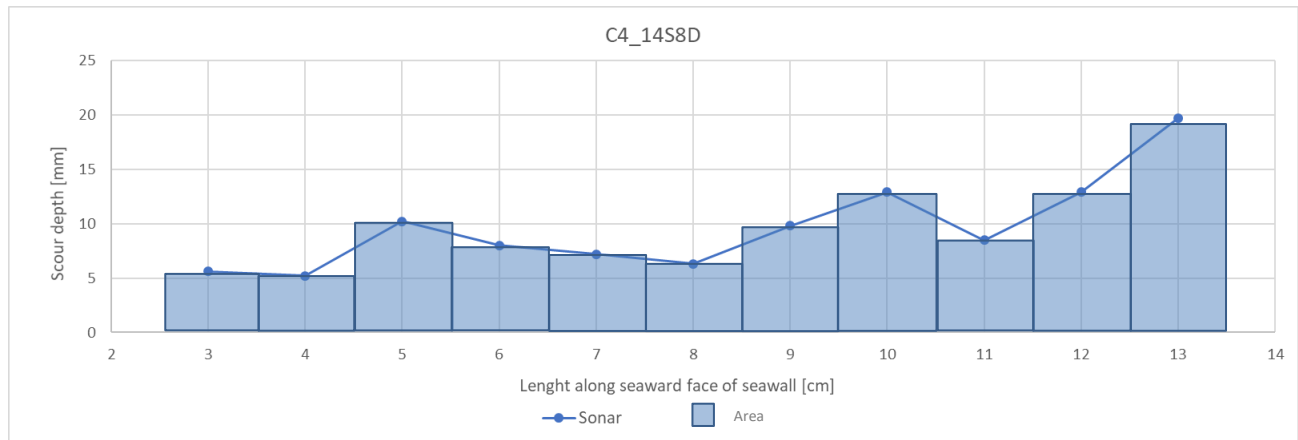
Figure 4-20: Integration of sonar measurements of scour depths of Test C4 [model dimensions]
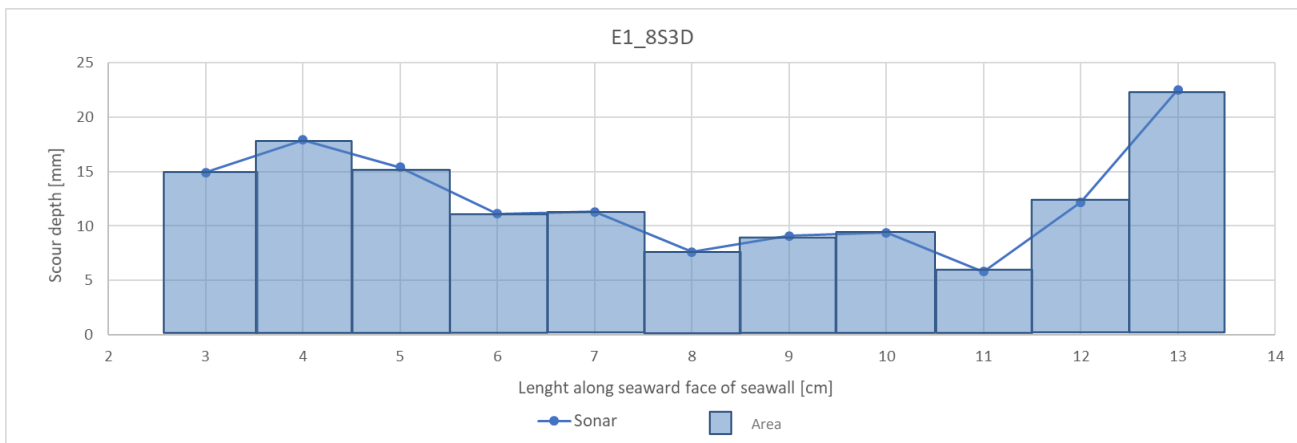
Figure 4-21: Integration of sonar measurements of scour depths of Test E1 [model dimensions]

The average area of scour damage of each test can be obtained in the same manner so the different scour tests can be directly compared to each other. The complete set of raw data is shown in Appendix D.

4.3   BERM TEST SETS

4.3.1 General

The test sets that are described in Section 3.12.2, are analysed and discussed separately before the test sets are compared to each other so that a berm size could be recommended and verified. The following graphs are in prototype dimensions while the model measurements are shown in Appendix D.

4.3.2   Test Set A: Scour Development

As mentioned in Section 2.3.3, the scour process develops and scour increases over time, but reaches an equilibrium at a certain stage. The point of equilibrium is reached within a certain duration of the test, in other words a specific number of waves that the structure had to be exposed to. It was important to first determine the number of waves that has to elapse for the scour process to reach equilibrium, so the consequent tests could be conducted with exposure to that specific number of waves. Two sets of scour development tests were conducted with a constant peak wave period of 8 seconds and berm width of 6 D_{n50}.

A1 tests were conducted as continuous scour damage tests. This means that the structure was exposed to 500 waves, then scour measurements were taken and then the structure was exposed to another 500 waves before a 1000-wave measurement was taken and so forth. The structure was not entirely rebuilt after every reading. The berm was only partially deconstructed to take scour measurements and was then repacked. The measurements are shown in Figure 4-22 and the average scour area of the tests are shown in Figure 4-23 in increasing number of waves.
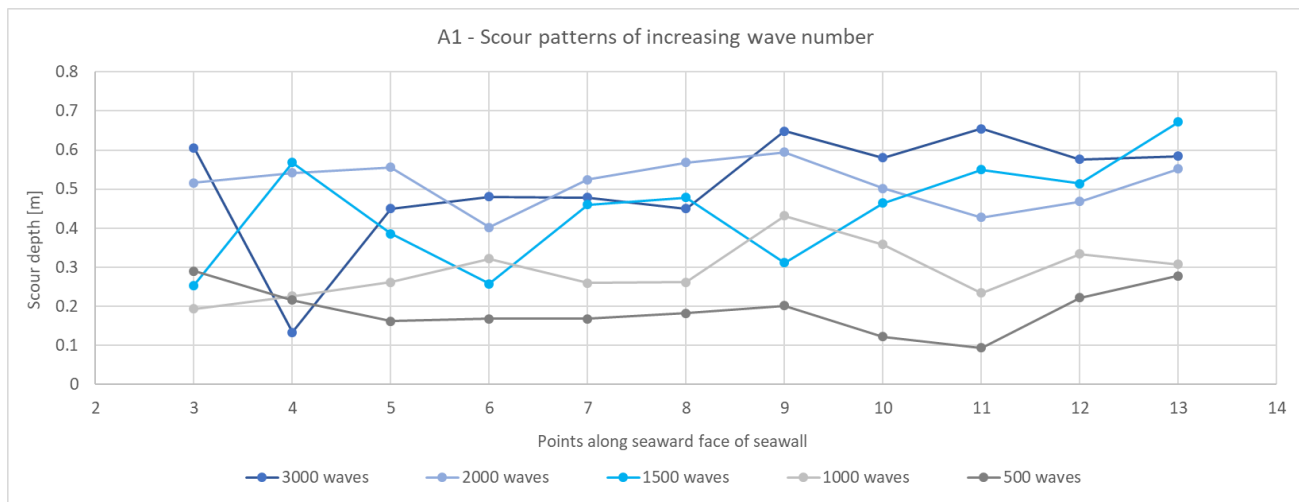
Figure 4-22: A1 test results of the scour patterns of increasing wave exposure
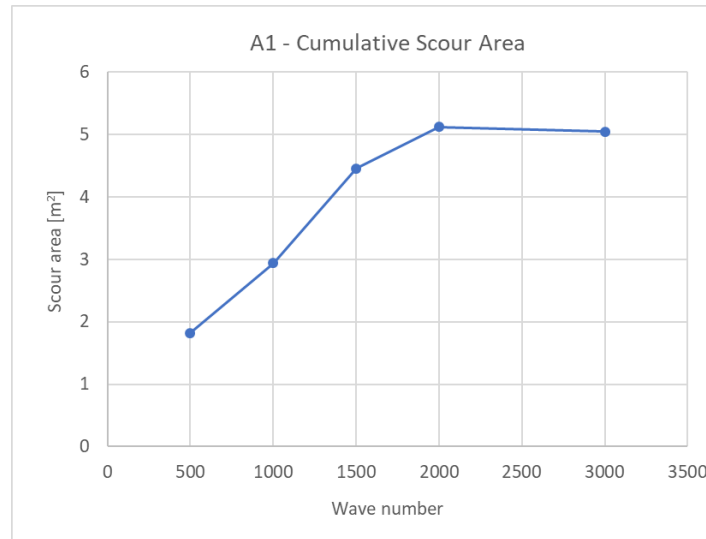
Figure 4-23: Cumulative scour area for increasing number of waves for Test A1

The cumulative scour area for the increasing number of waves is shown in Figure 4-23 and it inclines to a logarithmic curve. It can be observed that the scour equilibrium was reached at 2000 waves. However, with the partial deconstruction and repacking of the berm layers, the screed layer was particularly disturbed by the manual handling and so the scour damage measurements showed extensive damage. It was decided to redo the scour development tests so manual handling could be mitigated.

The A2 test set was conducted differently. After each test's scour measurements were taken, the whole structure was rebuilt. During Test A2_500, the structure was exposed to 500 waves before scour measurements were taken and then the structure was rebuilt. Then Test A2_1000 was conducted where the new structure was exposed to 1000 waves and so forth. This method of continuous testing mitigates manual handling of the screed material since it is only disturbed when taking measurements before it is rebuilt entirely. The results of the A2 tests are shown in Figure 4-24 and Figure 4-25. Due to time limitations and since a trend was already forming, it was not necessary to conduct an A2 test with 1500 waves.
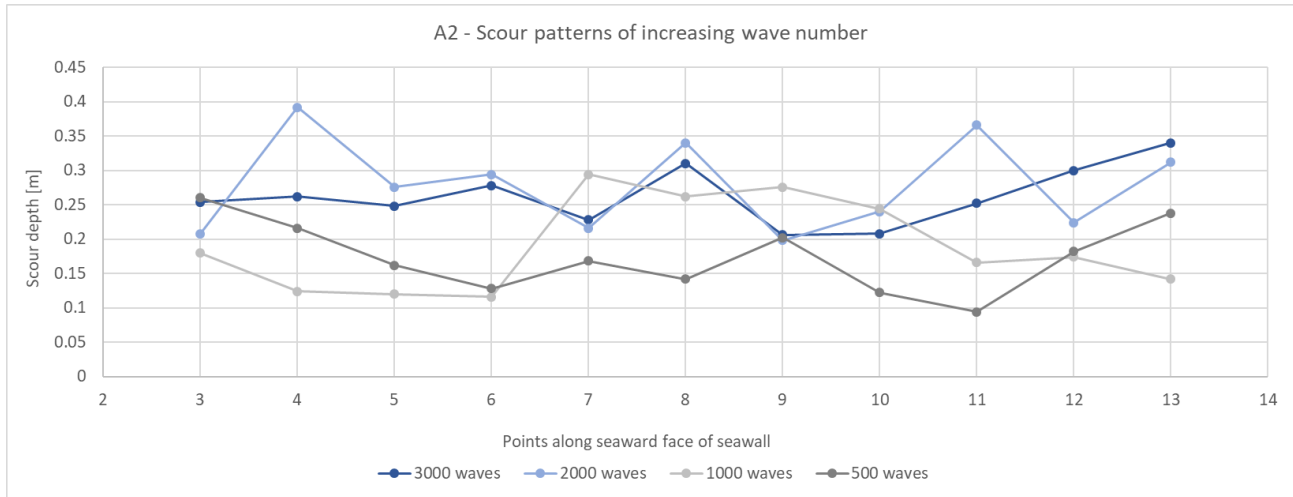
Figure 4-24: A2 test results of the scour patterns of increasing wave exposure
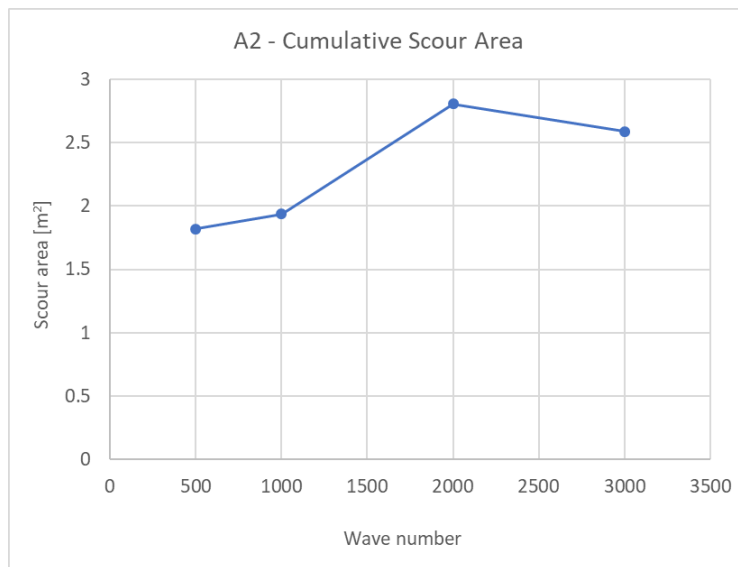
Figure 4-25: Cumulative scour area for increasing number of waves for Test A2

The cumulative scoured area for the A2 test set is relatively smaller than that of the A1 test set, as shown in Figure 4-25. However, it can be seen that the scour process also reaches equilibrium at 2000 waves with the A2 test set since the cumulative scoured area peaks at 2000 waves and plateaus to 3000 waves.

Figure 4-26 compares the cumulative scour area results of the two tests directly as well as the results of Malan's (2016) wave number tests. It is clear that more extensive scour damage occurred during Test A1 due to the disruptive action of dismantling and reconstruction the berm for scour measurements. However, both tests A1 and A2 show that scour process reached equilibrium after the structure was exposed to 2000 waves. Malan's (2016)

wave number tests show significantly more scour due to a different set-up and data acquisition method, but the scour process also reached equilibrium at 2000 waves. Therefore, in order to ensure that scour equilibrium is reached in all the following tests, 2000 waves were used.
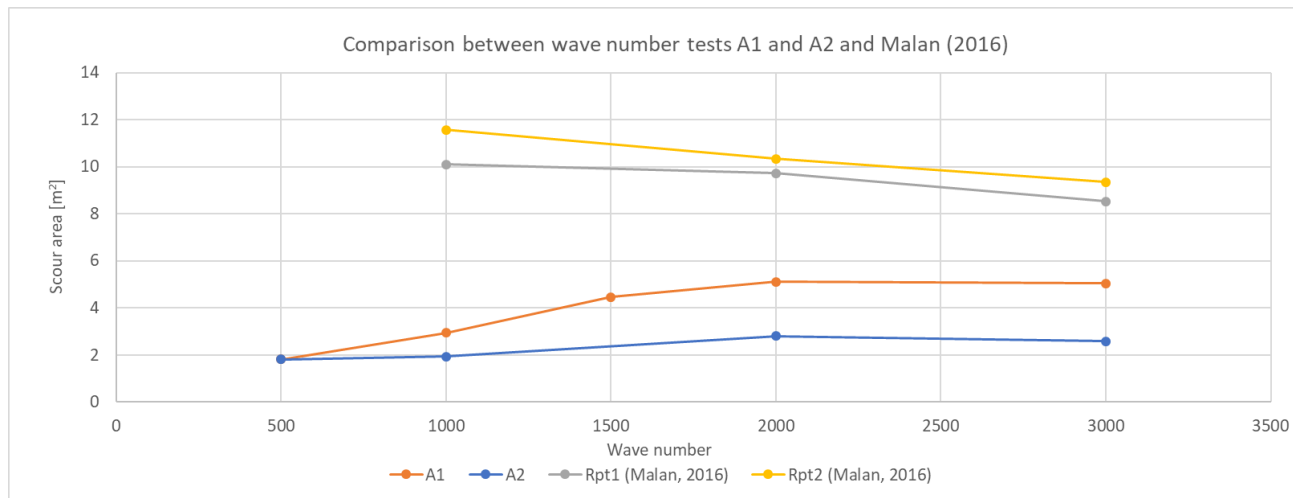
Figure 4-26: Comparison of wave number tests A1, A2 and Malan 2016

4.3.3 Test Set B: 6D$_{n50}$ Berm Width

The first berm width was 6 times the width of the median armour stone diameter and therefore the B test sets are referred to as the 6D$_{n50}$ tests. The sonar measurements of scour under the varying wave period conditions along the seaward face of the seawall are shown in Figure 4-27 and the average scour area for the varying periods is shown in Figure 4-28.
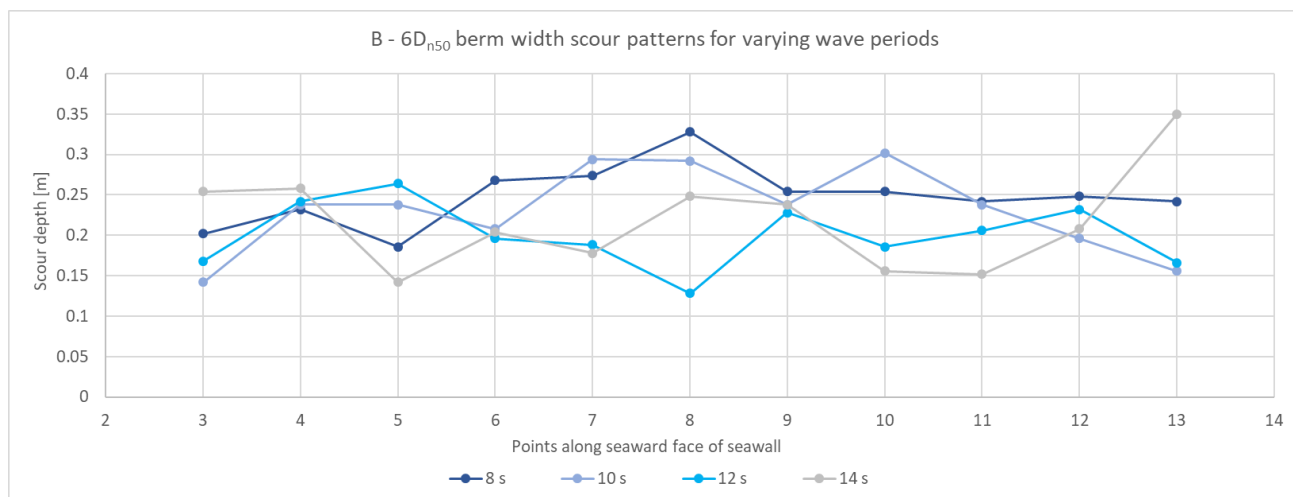
Figure 4-27: B tests scour patterns underneath the seawall

Figure 4-27 shows the different scour patterns for each of the peak wave period tests that were conducted on the $6D_{n50}$ wide berm. As mentioned in Section 4.2, the four outer data points were omitted from the data analysis so the wall effects do not influence the results. It can be seen that the scour patterns in the screed layer along the face of the seawall is not consistent with each different peak wave period test. Data points 7 to 9 can be seen as the most accurate data since these points are furthest from the wall edges so wall effects are minimal and scour damage would be closest to representing a prototype case. In Test set B, data points 7 to 9 also seem to be where maximum scour occurs. However, this trend is not visible throughout all the other test sets. This can be due to the wall effects that reach further than the four outer data points. In conclusion, the location of the data points (save the boundary data points) along the face of the seawall does not have a significant effect on the scour damage in the screed layer. However, the peak wave period does have an effect, as also discussed below.
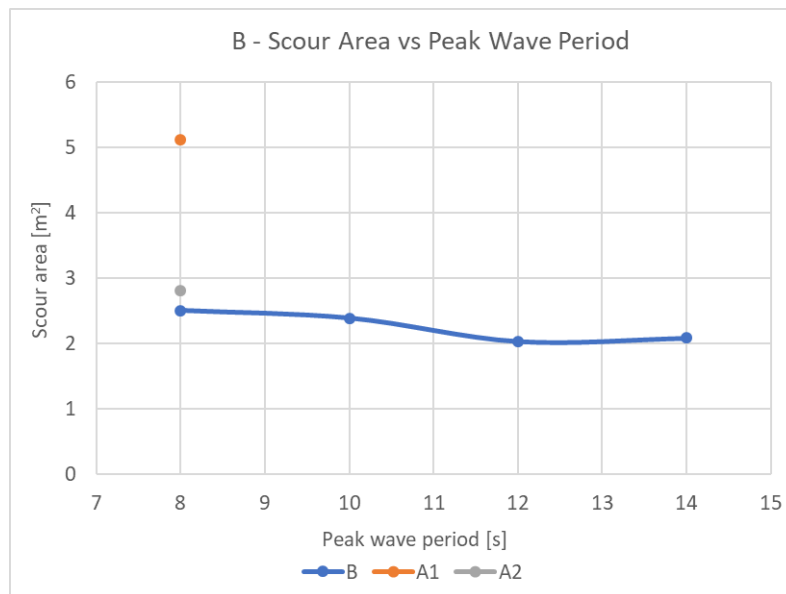
Figure 4-28: Test set B average scour area under seawall for varying peak periods

A slight trend can be observed from the graphs above. The shorter the wave period, the more scour occurs. This is in direct contrast to what was hypothesised in Section 3.2.3. It was originally anticipated that a longer wave period would result in more scour since the wave celerity is directly proportional to the wave period and a higher wave celerity was expected to cause more scour damage. However, as mentioned in the visual observations in Section 4.1.2, the wave energy of the shorter wave periods seemed to actually penetrate deeper into the screed layer. This is confirmed with the integrated scour areas of the varying wave periods shown in Figure 4-28.

Relevant test results from Tests A1 and A2 are also displayed in Figure 4-28. These tests are relevant because the berm width of Test set A was also $6D_{n50}$ wide and the peak wave period was 8 s. Therefore, the average scour

areas of the 8 s peak wave period tests could be directly compared with each other in order to determine repeatability of the experimental set-up. A very simple statistical analysis was conducted on the three data points of average scour area in the screed layer under a $6D_{n50}$ wide berm exposed to 2000 waves with an 8s peak wave period.

Table 4-1: Simplified statistical analysis of scour tests with $6D_{n50}$ wide berm and T_p of 8 s

Test	Scour area [m^2]	Average [m^2]	Population standard deviation [m^2]
A1_2000W	5.118	With A1: 3.477	With A1: 1.166
A2_2000W	2.806	Without A1: 2.657	Without A1: 0.149
B1_8S6D	2.508		

Test A1's results increased the average and standard deviation significantly and should actually be seen as an outlier because of the test method that was not acceptable, as mentioned in Section 4.3.2. Therefore, the statistical analysis was also done without A1 so the average scour area and standard deviation is smaller and supports the repeatability of the experimental set-up. However, more tests should preferably be conducted to confirm the repeatability, as discussed in the recommendations in Section 5.4.

4.3.4   Test Set C: $8D_{n50}$ Berm Width

The next test set was conducted on a berm with a width of 8 times the median armour stone diameter, $8D_{n50}$. This is the berm width that the preceding scour tests by Malan (2016) were conducted on so the magnitude of scour pattern of the 8 second wave period test (8s8D) can technically be compared to the results of Malan (2016) since it is the closest match to the preceding test set-up. The test set results are shown in Figure 4-29 and Figure 4-30 and the comparison with Malan's (2016) tests is shown in Figure 4-31 and Figure 4-32.
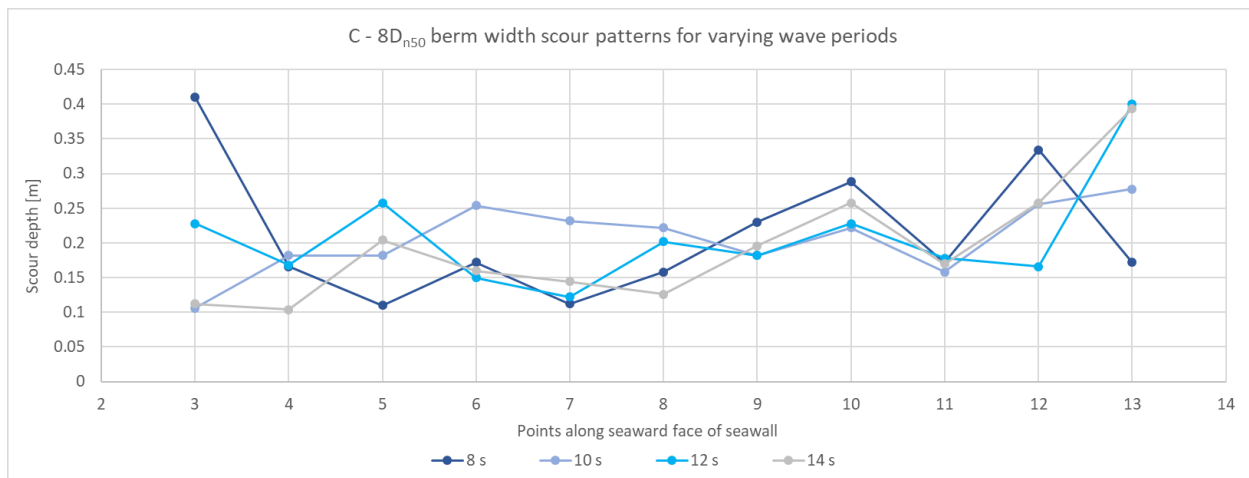
Figure 4-29: C tests scour patterns underneath the seawall
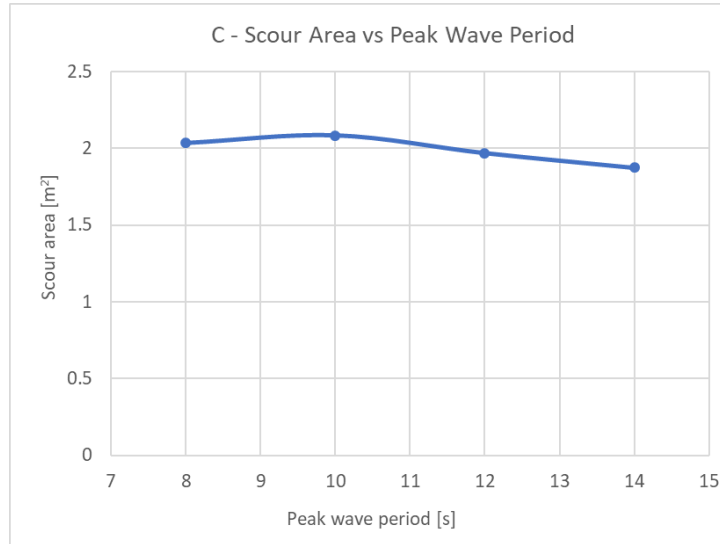
Figure 4-30: Test set C average scour area under seawall for varying peak periods

The same general slight trend can be observed with the $8D_{n50}$ tests as with the $6D_{n50}$ test: the shorter the wave period, the more the scour damage. However, the trend is not as distinct since the scour areas of the different wave period tests do not vary much. The 8 s test actually yielded slightly less scour than the 10 s test, but this could be accounted to construction inconsistencies.
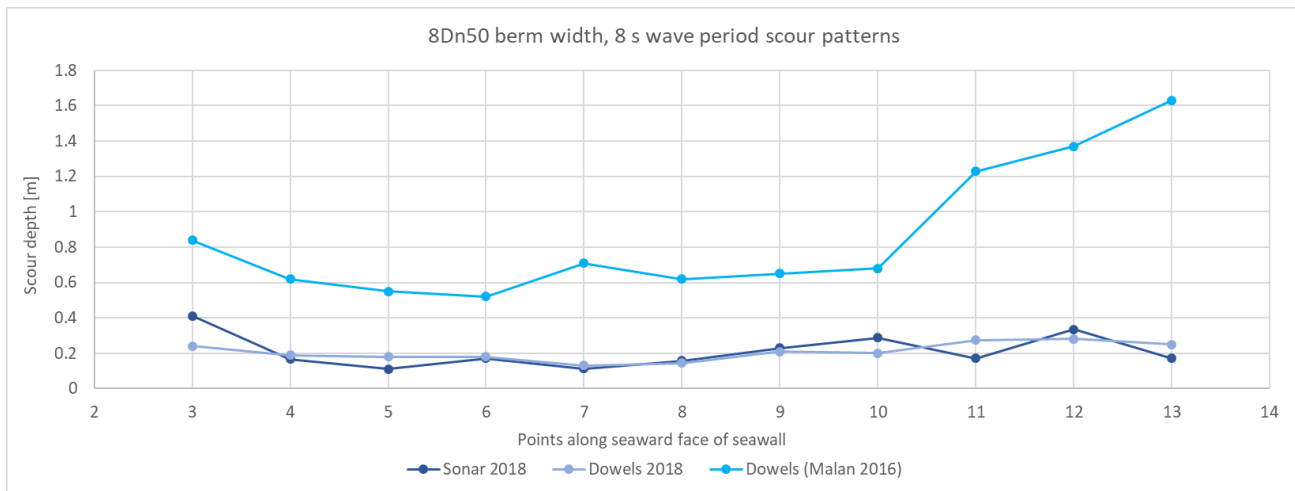
Figure 4-31: Comparison of scour patterns of 2016 and 2018 8S8D tests
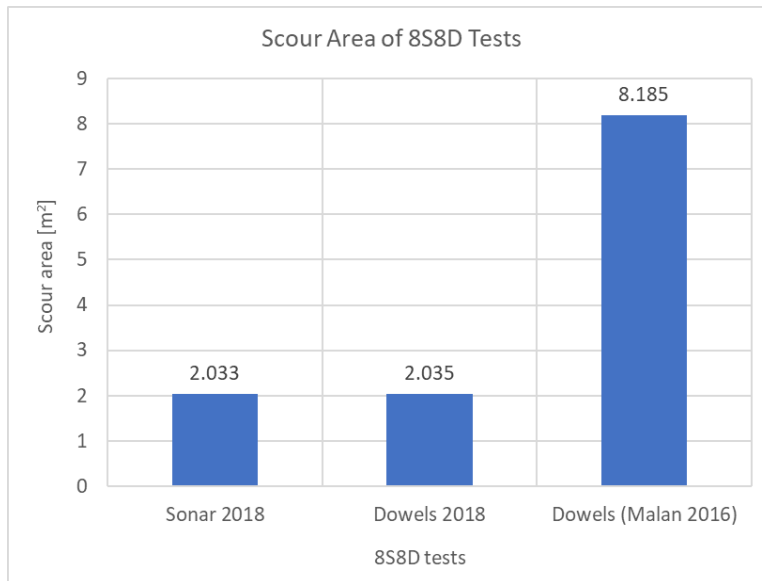
Figure 4-32: Comparison of average scour area of 2016 and 2018 8S8D tests

It is interesting to note the big difference in the 2016 and 2018 test results in Figure 4-32. The resulting average scour area of the 2016 tests, measured with dowels, is significantly more than the 2018 scour area, which is confirmed with both the dowel measurements and sonar measurements. The biggest differences between the two test set-ups were that the wave height for the 2016 8S8D test was measured at 1.46 m, while the 2018 8S8D test wave height was 1.27 m. The rock gradings for the 2016 test were also larger than the 2018 rock gradings. This is interesting since it would be expected that a larger rock grading would provide more protection for the screed layer against wave attack and scour. However, the smaller rock grading from the 2018 test yielded less scour than the 2016 test.

4.3.5   Test Set D: $4D_{n50}$ Berm Width

The seawall was shifted forward or backward during each new test set's construction, according to the next berm width that was to be tested, thus the front of the berm toe remained in the same location in the wave flume. After the widest $8D_{n50}$ tests, the wall was placed forward to construct a berm with a width of 4 times the median rock armour diameter. The results of the $4D_{n50}$ tests are shown in Figure 4-33 and Figure 4-34.
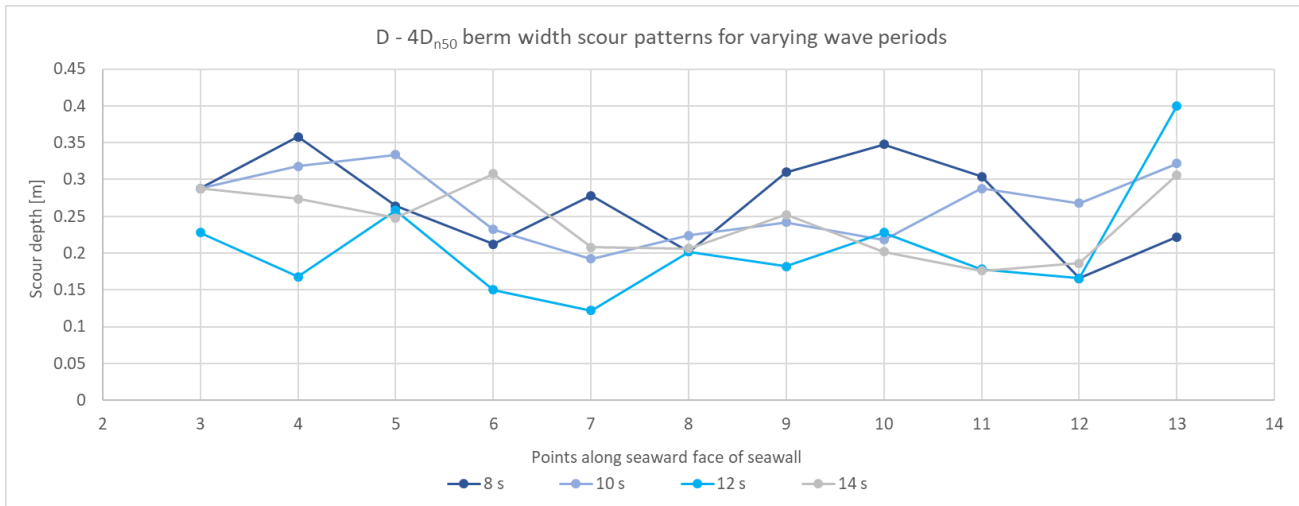
Figure 4-33: D tests scour patterns underneath the seawall
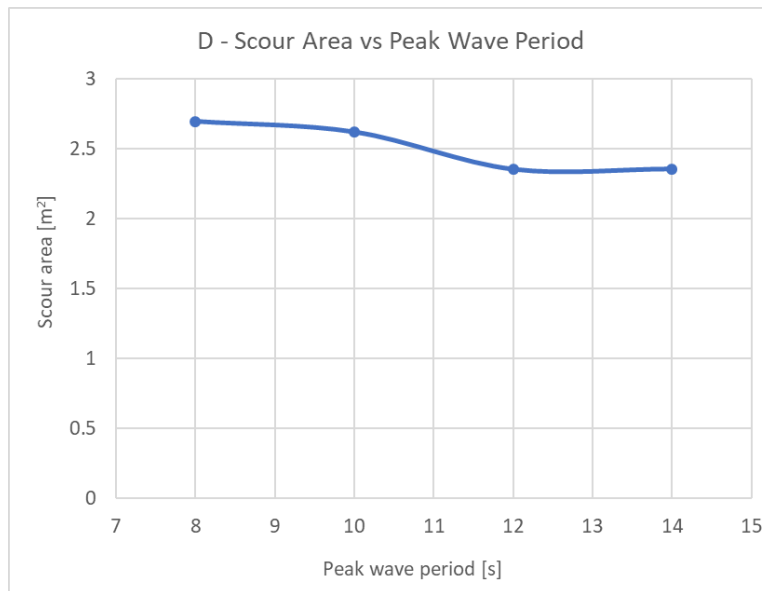
Figure 4-34: Test set D average scour area under seawall for varying peak wave periods

Once again, it can be observed in Figure 4-34 that the shorter wave periods created more scour underneath the seawall. The two shorter wave period tests seem to result in the same general extent of scour, while a significant decrease in scour can be observed between the 10 s and 12 s wave period tests. The scour extent of the two longer wave period tests are generally the same.

4.3.6   Test Set E: 3D$_{n50}$ Berm Width

According to design standards, a berm width of 3 times the median armour stone diameter is the minimum width that the berm can still effectively protect the toe of a marine structure like a vertical seawall (CIRIA, 2007b). The 3D$_{n50}$ test set put this design standard to the test in terms of scour and berm stability (see Jarvis, 2018) and the scour results are shown in Figure 4-36.
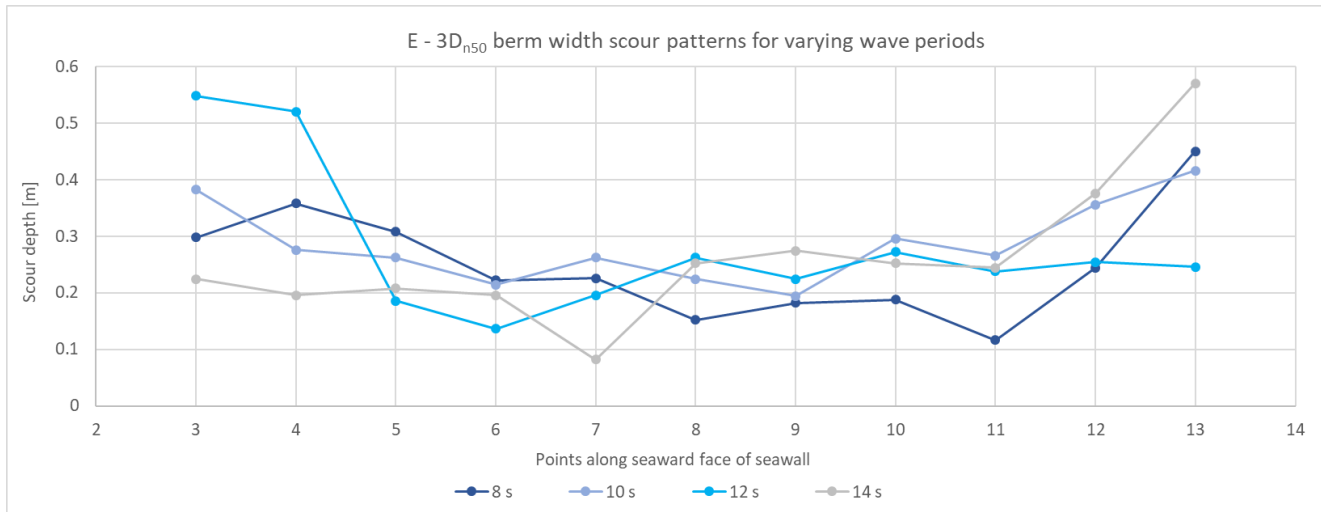
Figure 4-36: E tests scour patterns underneath the seawall
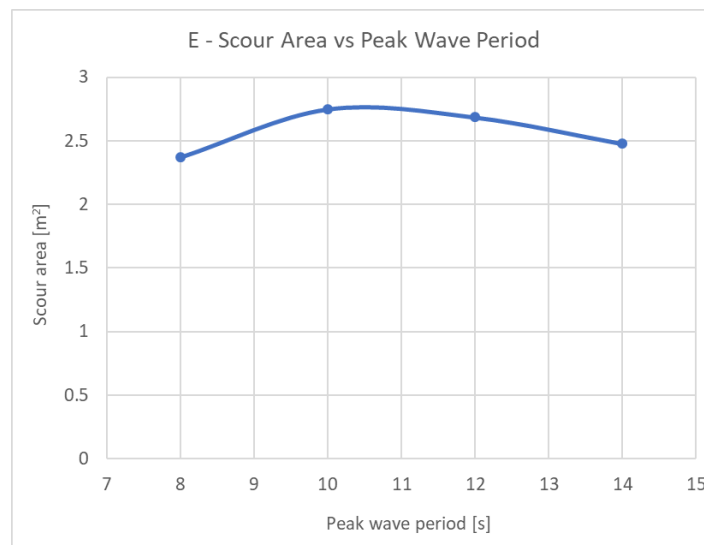
Figure 4-35: Test set E average scour area under seawall for varying peak wave periods

The resulting scour patterns did not precisely follow the general trend that was observed in the preceding test sets. Test E1 (*T$_p$* of 8 s) yielded much less scour than anticipated when the preceding tests were considered. The other wave periods seemed to follow the general trend again. Therefore, it was suspected that the construction process

of Test E1 was not consistent with the other tests. However, due to time limitations, the 8S3D test could not be redone. If the faulty test is not considered, the trend of shorter wave periods that yield more scour, is still applicable.

4.3.7 Test Set F: $2D_{n50}$ Berm Width

As mentioned in Section 4.3.6 above, the minimum design standard for an effective berm width is $3D_{n50}$. The objective of the $2D_{n50}$ test set is to prove that this design standard should be followed, since it was expected that the $2D_{n50}$ tests would show significant scour. The results are shown in Figure 4-37.
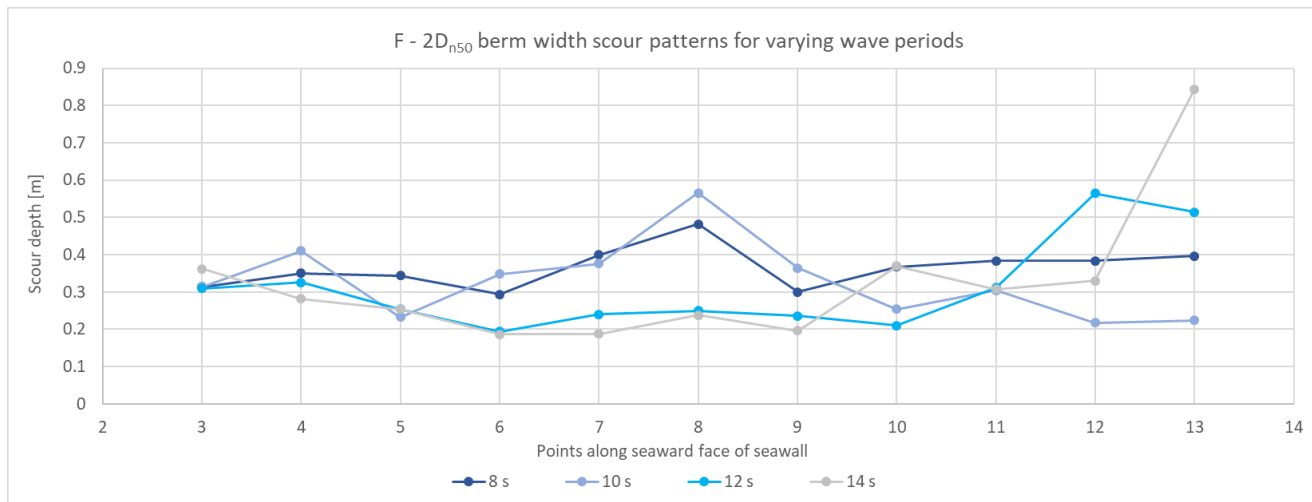
Figure 4-37: F tests scour patterns underneath the seawall
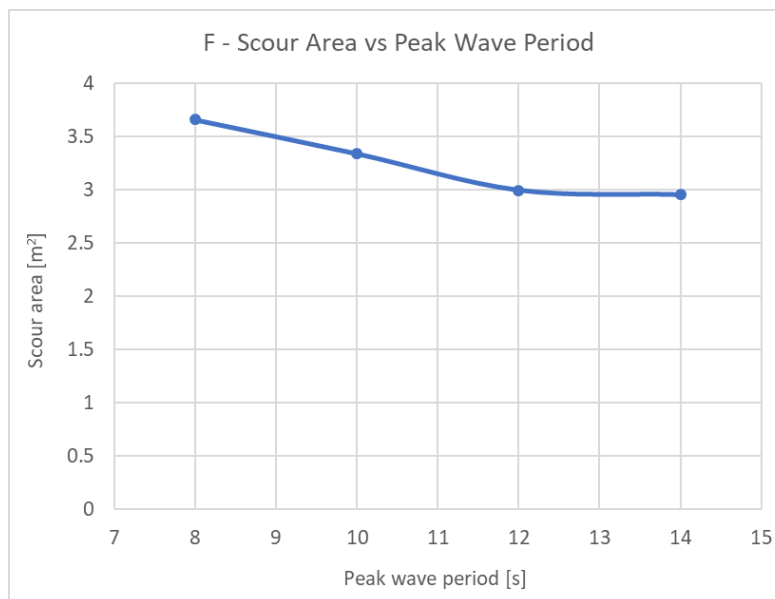
Figure 4-38: Test set F average scour area under seawall for varying peak wave periods

It is clear that the extent of scour is significantly more than all the preceding tests. This proves that the design standard of a minimum berm width of $3D_{n50}$, should be followed. A narrower berm in front of the seawall allows too much scour to occur underneath the vertical seawall. The trend that a shorter wave period results in more scour can also be observed with the $2D_{n50}$ tests.

A summary of all the different berm width tests B to F is discussed in Section 4.3.8 below.

4.3.8   Berm Width Tests Summary and Recommendations

The above-mentioned tests can be summarised in comparison with the respective reflective coefficients in Figure 4-39 as well as a direct comparison between berm widths in Figure 4-40.
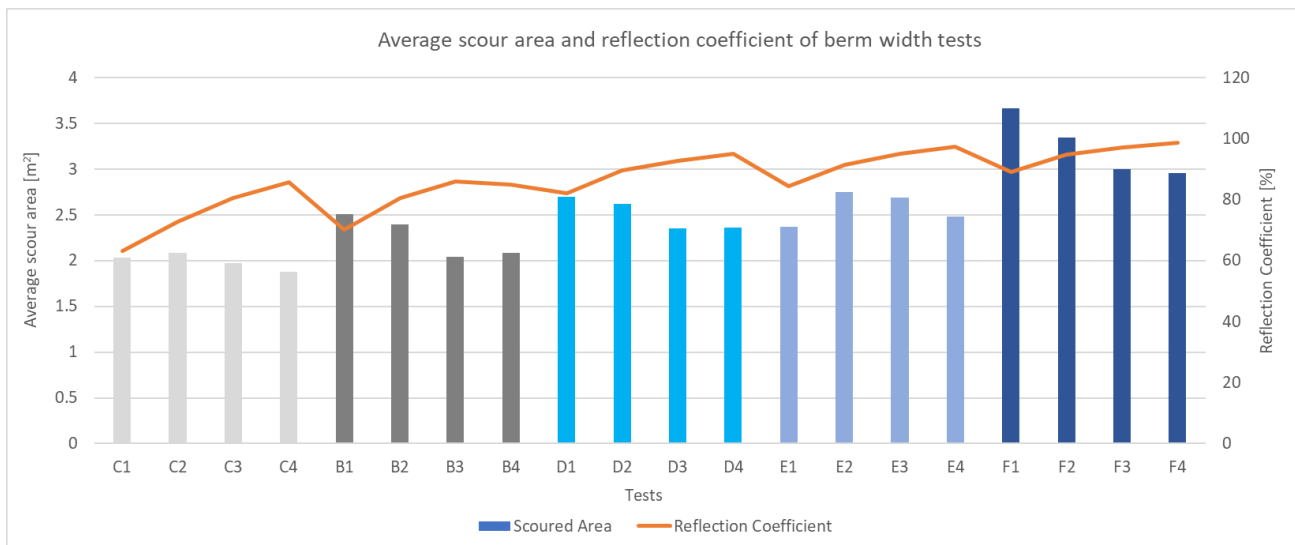
Figure 4-39: Summary of berm width tests B to F in comparison with reflection coefficients
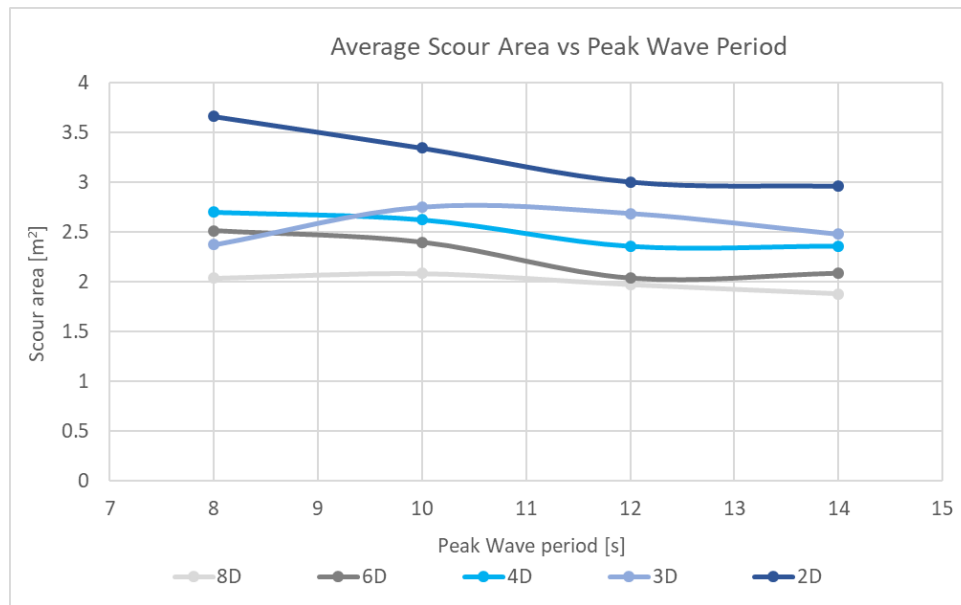
Figure 4-40: Summary of average scour areas of berm width tests B to F

The objective of this thesis is to create an effective standard design for a rubble-mound berm and foundation for a vertical seawall. Part of this standard design is to determine an optimal berm width. The above-mentioned tests were used to recommend a berm width according to its performance in terms of scour and reflection mitigation, armour unit stability (determined by Jarvis, 2018), overtopping (only qualitative visual observations), economical and construction considerations.

The scour damage was determined by the above-mentioned scour measurements and the armour unit stability was determined by Jarvis (2018) which will be discussed in Section 4.7. The reflection coefficients of the berm and seawall structure were obtained from the wave probe outputs and are shown in Figure 4-39. Overtopping was determined by visual inspection, since the open-system set-up did not allow for specific overtopping measurements. The construction considerations were judged according to the author's personal experience of constructing the model and the economic considerations were made based on the volume of rock required to construct each berm width.

According to the above-mentioned results, the berm width did not have as significant an influence on the scour than had been expected. Therefore, it was decided to consider either a $3D_{n50}$ or $4D_{n50}$ berm as the standard recommended design since these berm widths showed stable scour results. According to standard design codes, berm widths should be limited to a minimum of $3D_{n50}$ wide (CIRIA, 2007b) and this is confirmed by the $2D_{n50}$ results that show extensive scour and an unstable berm. Therefore, a $2D_{n50}$ berm is not considered a recommended

berm width. On the other hand, wider berms like the $6D_{n50}$ and $8D_{n50}$ berms shows slightly more stability and less scour but require much more material and construction expenses. Therefore, the $3D_{n50}$ and $4D_{n50}$ berms would provide an optimised and balanced design between scour protection, stability and economical factors. The $3D_{n50}$ and $4D_{n50}$ berms were compared according to the above-mentioned criteria in Table 4-2.

Table 4-2: Criteria for berm width recommendation between $3D_{n50}$ and $4D_{n50}$

Criterion	Preferred Berm Width	Explanation
Scour protection	$4D_{n50}$	Scour area is 1.3% less than $3D_{n50}$ berm, but the small difference is due to inconsistent 8S3D test. In general, the scour damage is less for $4D_{n50}$ than $3D_{n50}$ berm.
Armour stability	$4D_{n50}$	According to Jarvis (2018), the armour unit stability of the $4D_{n50}$ was significantly better than the $3D_{n50}$ berm. This is due to more space for rocks to settle before rolling down the berm slope. Refer to Section 4.7 for more detail.
Wave reflection	$4D_{n50}$	Wave reflection has an adverse effect on activities on the seaward side of a reflective structure, like vessel movement. The reflection coefficients for the $4D_{n50}$ tests were generally lower than the $3D_{n50}$ tests, due to the wave energy absorption that occurs on the berm.
Overtopping	$4D_{n50}$	A wider berm absorbs more wave energy so less energy is transferred as overtopping, as mentioned in Section 4.1.4. Therefore, a $4D_{n50}$ berm should be used to minimise overtopping.
Construction	$4D_{n50}$	Constructability is easier with a wider berm since larger tolerances are acceptable during placement and the wider berm relative to the slope allows for easier placement and settlement of armour rocks.
Economic	$3D_{n50}$	A narrower berm results in less material and less time required for construction so the capital costs for $3D_{n50}$ berm would be less. However, as mentioned in the "scour" and "stability" criteria, $3D_{n50}$ berm is less stable than $4D_{n50}$ berm so maintenance cost may cause $3D_{n50}$ berm to eventually become less economical.

The evaluation criteria suggest that a $4D_{n50}$ wide berm should be recommended as the ideal standard berm width that is both effective in preventing damage but still remains economical in terms of construction and maintenance. Therefore, the screed layer thickness tests (Test set G) were conducted on $4D_{n50}$ berms. The verification tests (Test set H) verified both the $4D_{n50}$ berm and the $3D_{n50}$ berm results as a final check that the extent of scour damage remains relatively consistent and the $4D_{n50}$ berm performs better in scour protection.

4.4   SCREED LAYER THICKNESS: TEST SET G:

The thickness of the screed layer forms part of the standard design that this thesis is attempting to determine. Screed thickness tests were conducted by Malan (2016) and were repeated in order to determine what minimum screed thickness would result in the least amount of scour but will still be thick enough to smooth out core irregularities in order to create a level bed for the concrete seawall L-element to be placed on. As mentioned above, the screed layer thickness tests were conducted on the recommended berm width of $4D_{n50}$ and the peak wave period was set to 10 seconds as this is a typical wave period found along the South African coastline. The results of the tests of the three screed layer thicknesses (100mm, 200mm and 300mm prototype) are shown in Figure 4-41 and Figure 4-42.
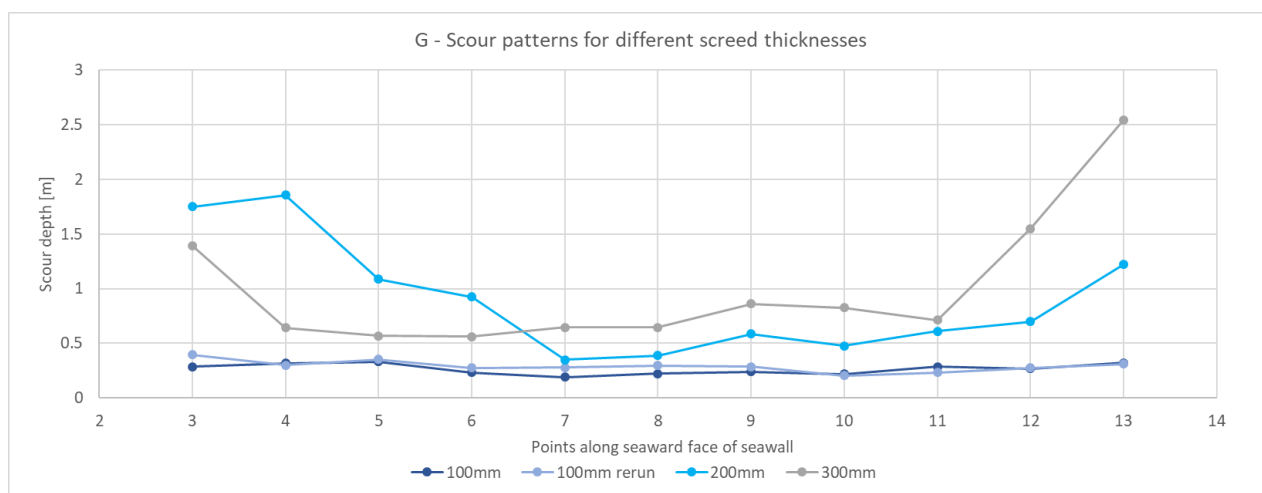
Figure 4-41: G tests scour patterns underneath the seawall with varying screed layer thicknesses

Figure 4-42: Test set G average scour area under seawall for varying screed layer thicknesses

Figure 4-41 and Figure 4-42 show a clear correlation between the screed layer thickness and the scour damage: the thicker the screed layer, the more extensive the scour damage. This is because the screed layer material consists of the smallest particle sizes in the rock berm and thus offers the least amount of resistance against the wave energy that causes washout of granular material. The thicker the screed layer, the greater area of fine particles is exposed to wave energy hence more scour damage can be expected. Therefore, a minimum screed layer thickness is recommended for an optimal rubble-mound berm design. However, the screed layer must still have sufficient thickness to cover the unevenness of the coarser core layer in order to provide a level surface to place the concrete wall element. A minimum screed layer of thickness of 100 mm is recommended.

The results of the screed layer thickness tests could partially be compared to Malan's (2016) tests even though Malan (2016) only tested 100mm and 200mm screed layer thicknesses and with an $8D_{n50}$ wide berm instead of $4D_{n50}$ and different wave conditions (8 s period instead of 10 s and 1.5 m heights instead of 1.3 m). The comparisons are shown in Figure 4-43.
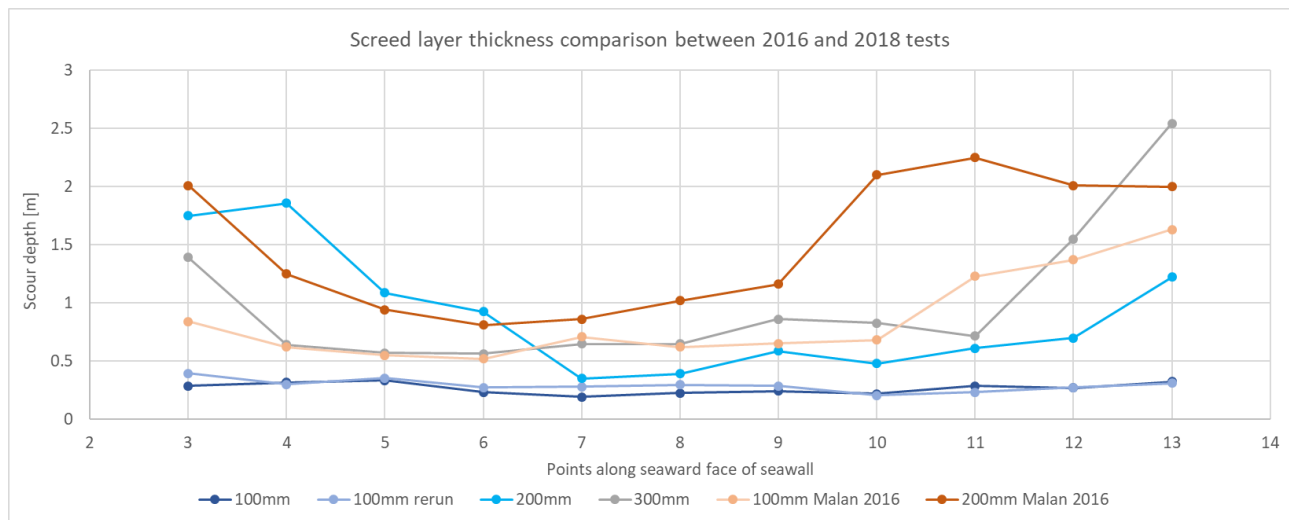
Figure 4-43: Comparison of scour pattern of 2016 and 2018 screed layer thickness tests
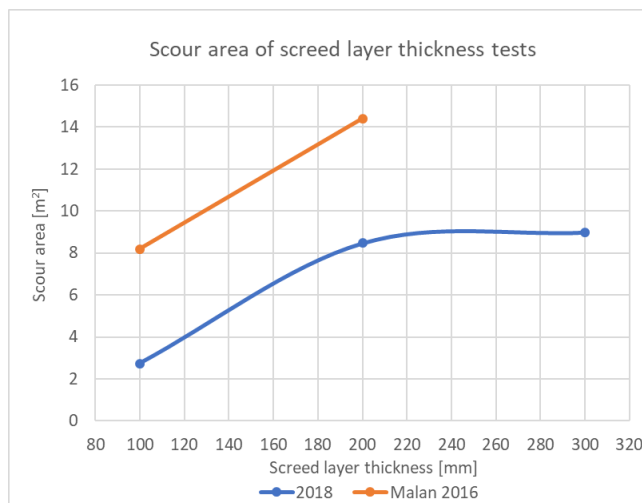
Figure 4-44: Comparison of average scour area of 2016 and 2018 screed layer thickness tests

Since the 2018 screed layer thickness test set-up differs so much from the 2016 tests, the values should not be compared directly but a general trend can be observed from both test set-ups: the thicker the screed layer, the more scour occurred. This observation correlates with the hypothesis stated in Section 3.2.3 that a thicker screed layer exposes more fine material to wave energy penetration and is therefore generally more susceptible to scour.

The significant decrease in scour from Malan's (2016) tests to this thesis, as seen in the whole of Section 4.3 as well, proves the hypotheses set forth in Section 3.11 that the smaller wave heights, finer and narrower rock gradings and alternative screed toe layout resulted in less scour.

4.5   VERIFICATION OF RECOMMENDED BERMS: TEST SET H

The two berm widths that were considered for recommendation in Section 4.3.8, were verified with one additional test each. The number of verification tests was limited to one for each berm width due to time constrictions at the facility. Test H1 was conducted with the same set-up as Test Set G: a berm width of $4D_{n50}$ and a peak wave period of 10 seconds. The alternative $3D_{n50}$ berm width was verified with Test H2. The wave period for Test H2 was 12 seconds so the verification tests included both 10 second and 12 second wave periods, which are characteristic of the South African coastline.

Test H1 results in Figure 4-45 and Figure 4-46 show that the scour damage is slightly more than the original 10S4D test (Test D2). Figure 4-46 shows that there is a 9% variance in scour area. This variance can be attributed to

construction differences like the placement of the rocks of the berm that cannot be exactly the same for two different tests.
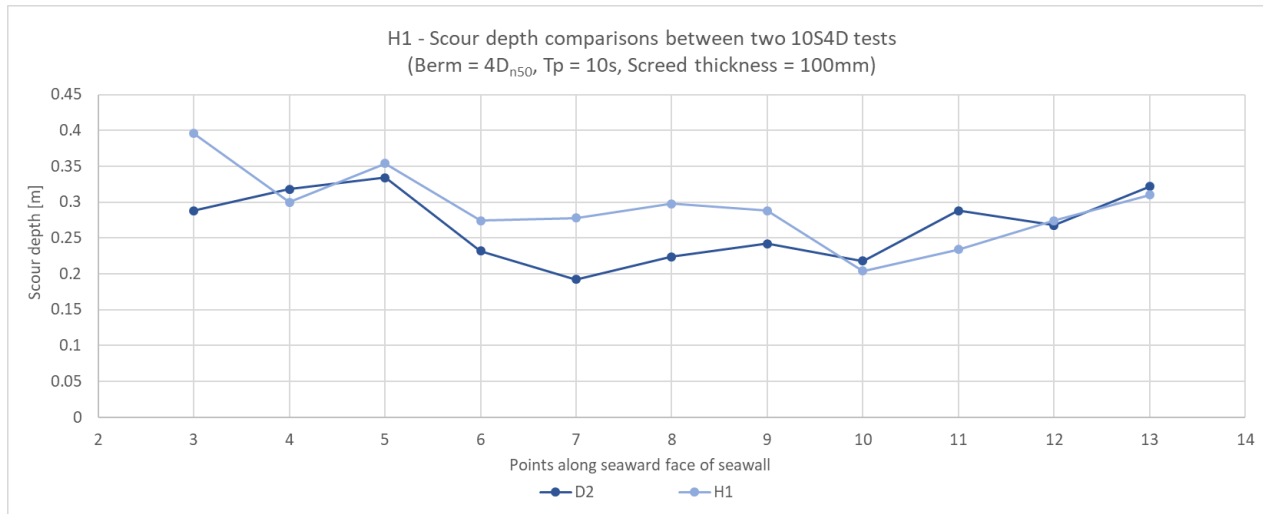
Figure 4-45: Test H1 scour patterns compared to Test D2
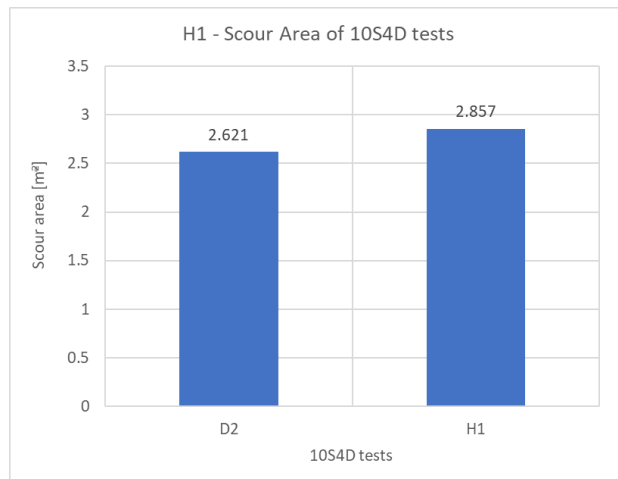
Figure 4-46: Average scour area of two 10S4D tests

Test H2 resulted in significantly more scour but as mentioned in Section 4.3.6, Test Set E resulted in lower scour readings than expected and therefore the verification test H2 was all the more necessary. There is 16% variance between Test E3 and Test H2, as shown in Figure 4-48. This can once again be attributed to construction inconsistencies.
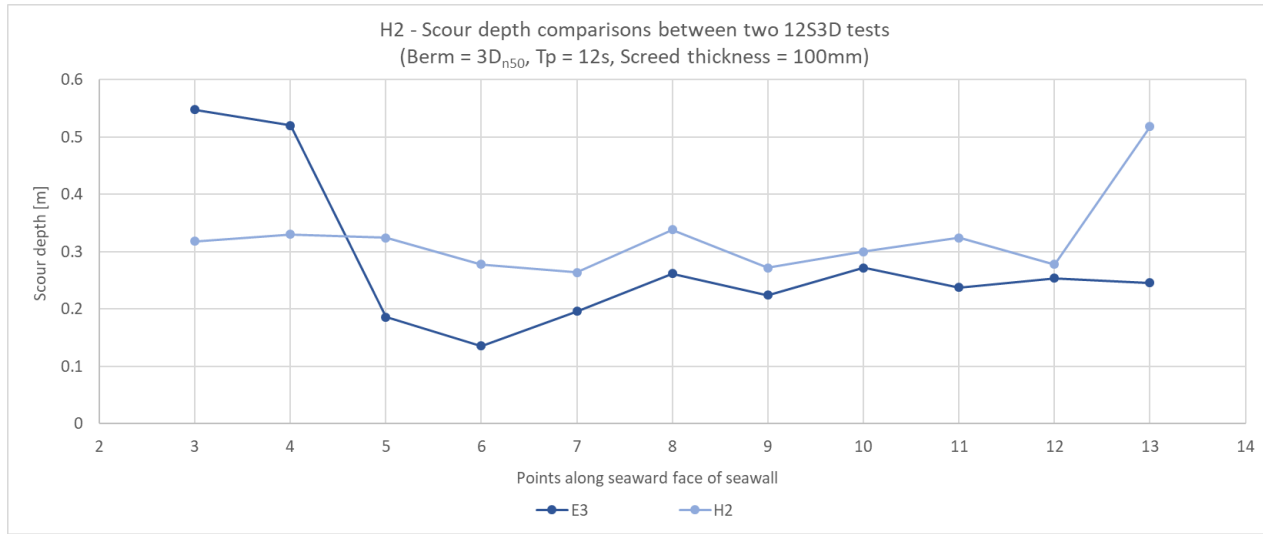
Figure 4-48: Test H2 scour patterns compared to Test E3
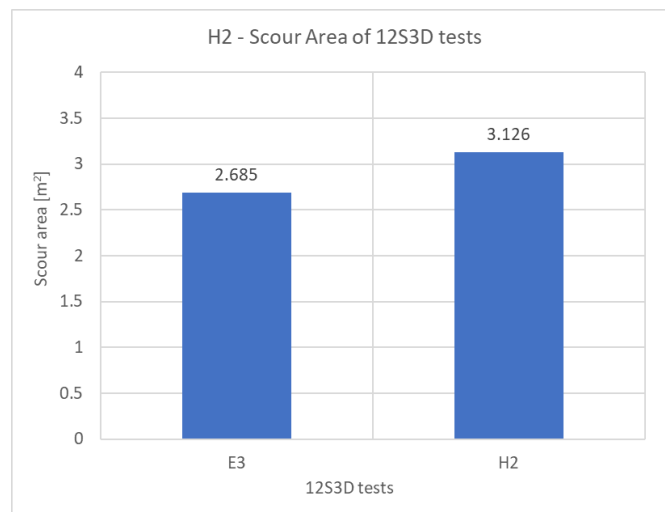
Figure 4-47: Average scour area of two 12S3D tests

However, Figure 4-49 shows that both 12S3D tests resulted in more scour than the 10S4D tests, even though the $3D_{n50}$ berms were exposed to a longer wave period, which generally results in less scour as discussed earlier. This indicates that the berm width in front of the seawall has a significant effect on the extent of scour that occurs underneath the seawall. Therefore, the verification tests confirm that a rubble-mound berm width of $4D_{n50}$ should be recommended as a standard design to protect the seawall against wave attack and scour damage.
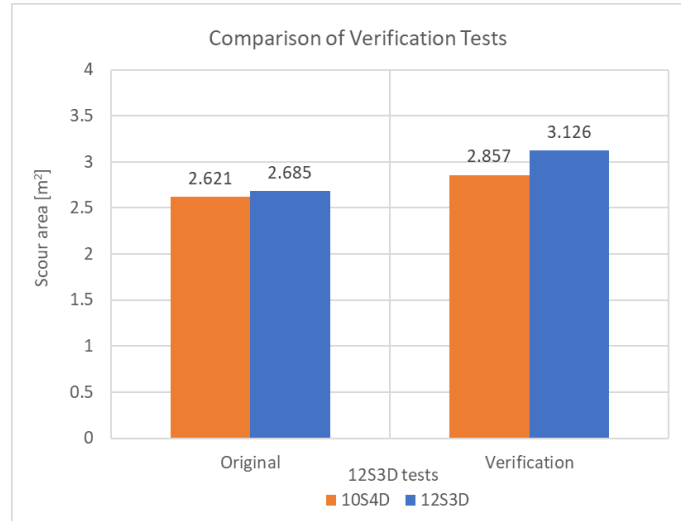
Figure 4-49: Comparison between 10S4D (Berm=4D$_{n50}$) and 12S3D (Berm=3D$_{n50}$) tests

4.6 SCOUR PREDICTION WITH DIMENSIONAL ANALYSIS

4.6.1 Dimensionless Parameters

It was attempted to use the experimental data to develop equations for predicting scour damage as a function of the wave conditions that a marine structure is exposed to, as well as the dimensions of the marine structure's berm. Data from test sets B to F were used to develop the equations. Test sets A, G and H did not specifically investigate the effect of the berm width on the scour damage and therefore the results were not included in the dimensional analysis. The independent variables for the experimental set-up were the wave period and the berm width. The wave periods can be converted to wavelengths, with dimensions in meters. Therefore, a dimensionless independent variable could be created:

$$L_0/B \qquad\qquad (4\text{-}1)$$

The dependent variable for the experimental set-up was the scour that developed underneath the seawall structure due to the wave attack and resulting currents from the wave-maker. This variable can either be represented in the horizontal scour depth (S_D) that was directly measured with the wooden dowels and sonar, or the scour can be represented as an average horizontal scour area (S_A) that was integrated from the measured scour depth data points.

However, the single horizontal scour depth (S_D) that is used to represent a specific test set-up, should be carefully considered so that it is an accurate representation of the entire seawall length of that test set-up. The top 5% of the

scour depths that were acquired from a test set-up was considered, but this would not be an accurate representation since the deepest scour points are usually found on the edges of the seawall due to boundary effects even though the outer two data points on each edge were omitted in the data analysis. Furthermore, if a single data point shows significant scour damage, but the neighbouring data points do not show such deep horizontal scour, that single point (1 m in prototype) is not expected to cause structural failure since L-wall elements are generally wider than 1 m. The remaining option for a single representative horizontal scour depth for an entire test set-up, was the average scour depth over the whole seawall length.

The dependent variable has to be dimensionless as mentioned with the independent variable. A parameter that can be used with the scour depth and area is supposed to remain constant throughout the different experimental set-ups, and that is the significant wave height (H_S) at the structure. However, only the deep-water wave heights (H_0) were recorded since the shallow-water probe set-up was removed during testing to provide sufficient space for scour data acquisition and construction (see Section 3.9). The incident and reflected waves were also so closely grouped at the face of the structure that it was difficult to distinguish and measure accurately. Therefore, the shallow-water wave heights were assumed to remain constant at 1.3 m. The independent dimensionless parameter can then either be one of four options and all four where investigated:

$$\left. S_A \middle/ H_0{}^2 \right. \tag{4-2}$$

$$\left. S_D \middle/ H_0 \right. \tag{4-3}$$

$$\left. S_A \middle/ H_S{}^2 \right. \tag{4-4}$$

$$\left. S_D \middle/ H_S \right. \tag{4-5}$$

The equations that were generated from the data, can only be accurately applied on variables that fall within the specific ranges that were tested. Table 4-3 shows the different variables and in what ranges these variables must lie for the generated equations to be applicable.

Table 4-3: Applicable ranges for test variables

Variable	Applicable range [prototype]
Significant wave height, H_0 and H_s	1.013 – 1.307 m
Peak wave period, T_p	7.758 – 14.335 s
Water depth at toe	4 m
Scour depth	0 – 1.73 m

4.6.2   Scour Prediction with Trend Lines

The deep-water wave height was initially used as part of the dependent variable with both the horizontal scour area and horizontal scour depth. The resulting graphs that were acquired from the dimensionless parameters, are shown in Figure 4-50:
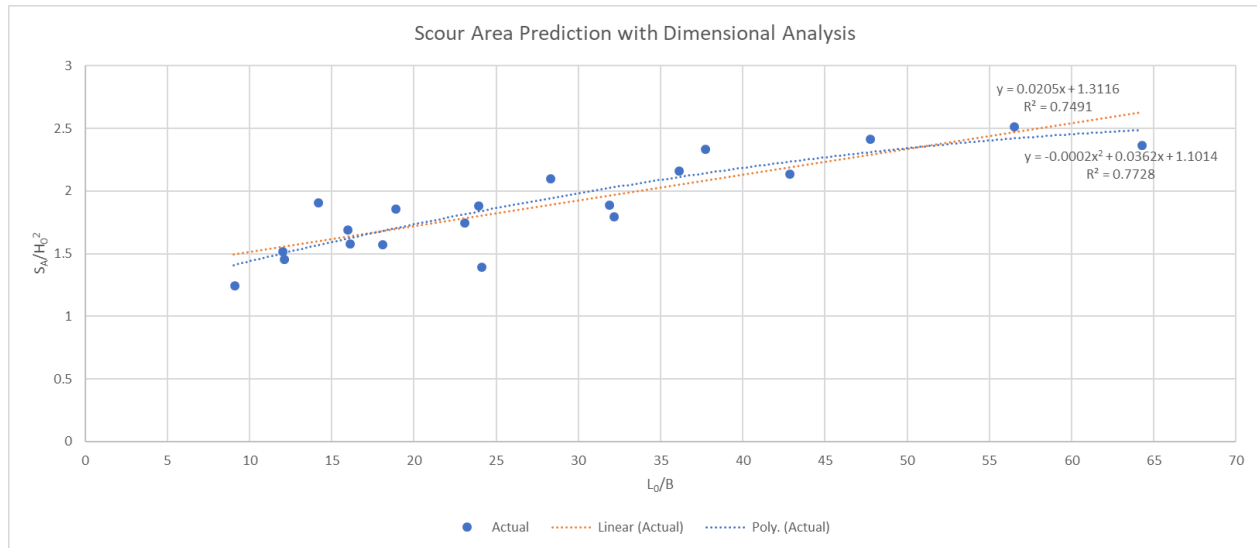
Figure 4-50: Trend lines for average scour area and deep-water wave heights

A linear and polynomial trend line could be developed with regression and the coefficient of determination, or R-squared, shows a relatively significant correlation, 0.749 and 0.773. The equations are as follows:

Linear:
$$\left. S_A \middle/ H_0{}^2 \right. = 0.0205 \cdot \left. L_0 \middle/ B \right. + 1.3116 \qquad R^2 = 0.749 \qquad (4\text{-}6)$$

Polynomial:
$$\left. S_A \middle/ H_0{}^2 \right. = -0.0002 \cdot \left(\left. L_0 \middle/ B \right. \right)^2 + 0.0362 \cdot \left. L_0 \middle/ B \right. + 1.1014 \qquad R^2 = 0.773 \qquad (4\text{-}7)$$

The deep-water wave height was then used with the average horizontal scour depth as a dimensionless dependent variable and the resulting graph and trend lines are shown in Figure 4-51.
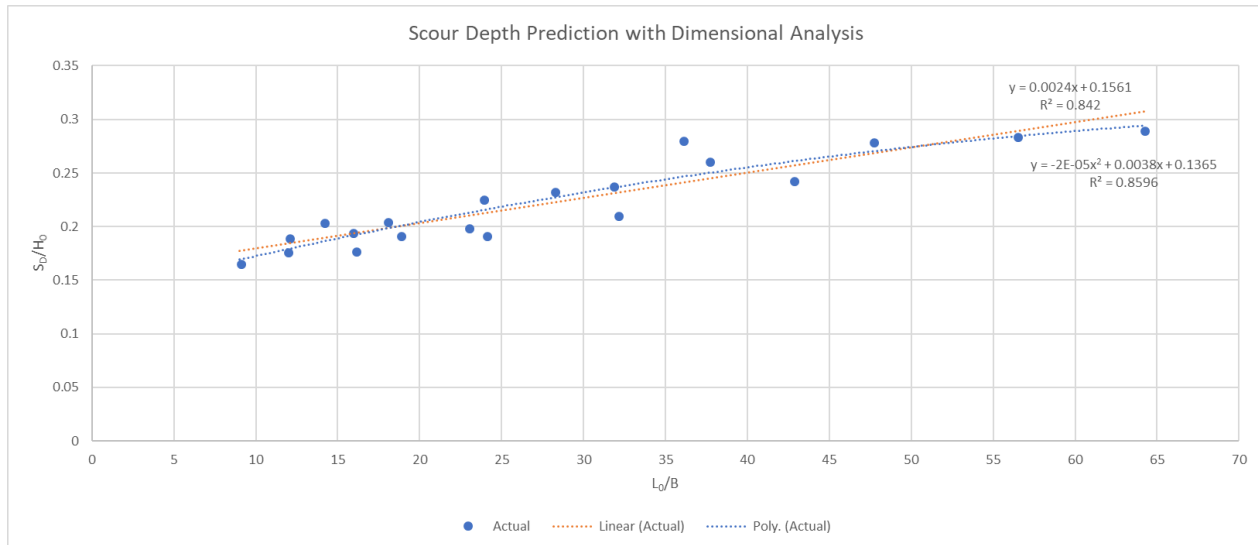
Figure 4-51: Trend lines for average scour depth and deep-water wave heights

The coefficient of determination for the scour depth trend lines showed a better correlation of 0.842 and 0.86 as opposed to that of the scour area trend lines mentioned above. The linear and polynomial equations for the horizontal scour depth parameters are as follows:

Linear:
$$\frac{S_D}{H_0} = 0.0024 \cdot \frac{L_0}{B} + 0.1561 \qquad R^2 = 0.842 \qquad (4\text{-}8)$$

Polynomial:
$$\frac{S_D}{H_0} = -0.00002 \cdot \left(\frac{L_0}{B}\right)^2 + 0.0038 \cdot \frac{L_0}{B} + 0.1365 \qquad R^2 = 0.86 \qquad (4\text{-}9)$$

The same graphs and trend lines were produced, but this time only with the significant shallow-water wave height that was assumed to remain constant at 1.3 m at the toe of the structure. This assumption had to be made since the shallow-water incident significant wave height could not be measured. Therefore, the most conservative assumption is that the wave height remains constant at 1.3 m so the effect of the wave period (expressed as wavelength) and berm width on the extent of scour can be represented clearly.

The trend of the horizontal scour area that develops as a function of the shallow-water wave height, wavelength and berm width, is shown in Figure 4-52.
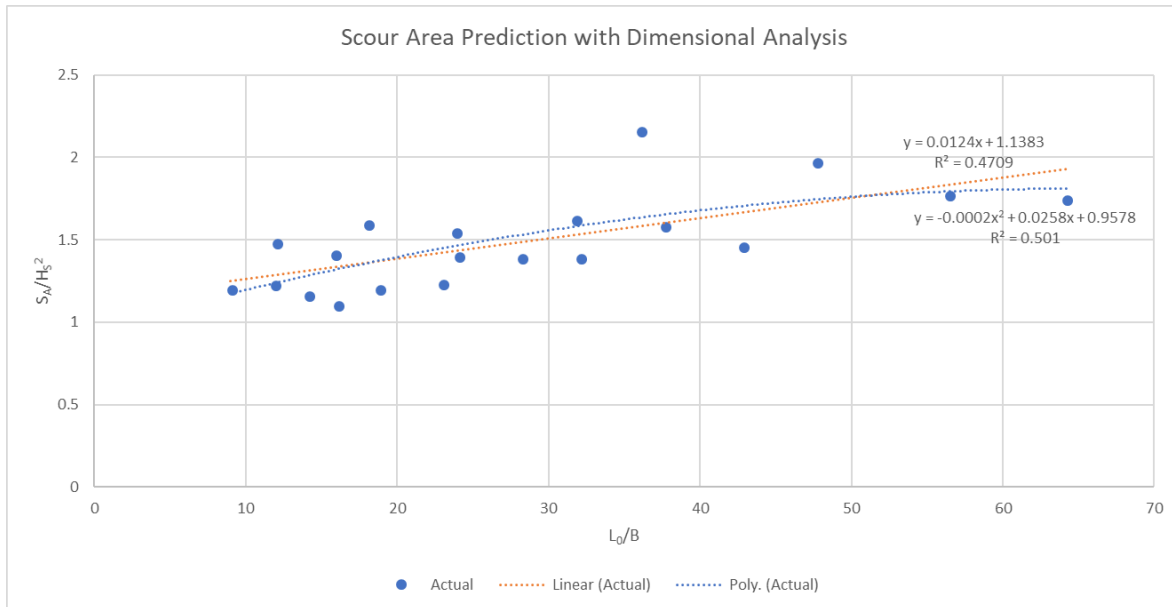
Figure 4-52: Trend lines for average scour area and shallow-water wave heights

The correlations with the predicted regression trend lines are significantly weaker with the dependent variable that includes the shallow-water wave height. It can be seen by the lower coefficients of determination, 0.471 and 0.501. R^2 is too low so that the predicted trend lines are actually not recommended to be used to predict scour damage in terms of the shallow-water wave height, wavelength and berm width. The equations for the trend lines are shown below:

Linear:
$$S_A/_{H_s^2} = 0.0124 \cdot L_0/_B + 1.3183 \qquad\qquad R^2 = 0.471 \qquad (4\text{-}10)$$

Polynomial:
$$S_A/_{H_s^2} = -0.0002 \cdot \left(L_0/_B\right)^2 + 0.0258 \cdot L_0/_B + 0.9578 \qquad R^2 = 0.501 \qquad (4\text{-}11)$$

Lastly, the graph and trend lines for the average horizontal scour depths and shallow-water wave heights are shown in Figure 4-53.
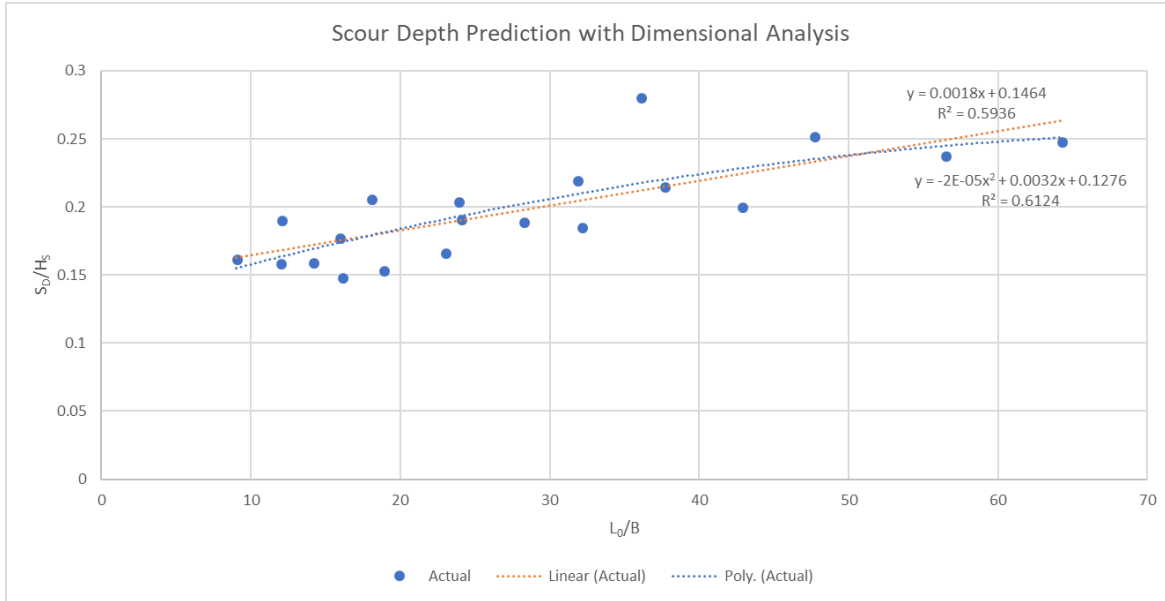
Figure 4-53: Trend lines for average scour depth and shallow-water wave heights

Once again, the trend lines' correlations are better with the average horizontal scour depth than with the scour area shown above, but the correlations are also not as significant with the shallow-water wave heights as with the deep-water wave heights. The equations for the linear and polynomial trend lines are shown below with corresponding R^2 values:

Linear: $$\left. S_D \middle/ H_s \right. = 0.0018 \cdot \left. L_0 \middle/ B \right. + 0.1464 \qquad R^2 = 0.594 \qquad (4\text{-}12)$$

Polynomial: $$\left. S_D \middle/ H_s \right. = -0.00002 \cdot \left(\left. L_0 \middle/ B \right. \right)^2 + 0.0032 \cdot \left. L_0 \middle/ B \right. + 0.1276 \qquad R^2 = 0.612 \qquad (4\text{-}13)$$

115

4.6.3   **Conclusion on Scour Prediction**

A significant correlation can be observed with the dependent dimensionless parameter S_A/H_0 and an even stronger correlation for S_D/H_0. However, the strong correlations might be due to the fact that the deep-water wave heights are influenced by the different wave periods and consequently the wavelengths that reflect differently from the vertical seawall structure. The wavelengths are also found in the independent parameter L_0/B and therefore it can be the reason for the strong correlation.

Thus, it would technically be more accurate to use the shallow-water wave heights in the dependent parameter since the wave-maker was calibrated to constantly produce 1.3 m shallow-water waves for all the different wave periods. However, this only refers to the incident shallow-water waves. The high reflection coefficient of the vertical seawall results in significant reflected waves which make the incident shallow-water waves difficult to measure. It can only be assumed that the shallow-water incident waves are 1.3 m high.

The correlation with the dependent dimensionless parameter S_A/H_S and S_D/H_S is much weaker than the correlations with the deep-water wave heights but it is technically more accurate. Therefore, it can be concluded that there is a correlation between the extent of scour and the wave period (wavelength), berm width and wave height, but it is not as significant. More tests have to be conducted and better methods of data acquisition are required to find a strong correlation.

In conclusion, the equation that is recommended for predicting scour in terms of berm width and wavelength, is Equation (4-7), since scour area is a more accurate representation of the scour damage that occurred than average scour depth. The polynomial equation also had a higher coefficient of determination ($R^2 = 0.773$) than the linear equation in Equation (4-6) ($R^2 = 0.749$). However, Equation (4-7) uses the deep-water wave height, while the shallow-water wave height at the toe of the structure would technically be a more accurate representation of the wave height that has an influence on the scour in the screed layer. A shallow-water wave height polynomial equation is suggested in Equation (4-11) but the coefficient of determination is too low ($R^2 = 0.501$) to be recommended as an accurate prediction for scour. This is due to the fact that the shallow-water wave height could not be measured during testing. It is recommended to design a method to measure the incident shallow-water waves accurately so an equation that includes measured shallow-water wave heights can be used to predict scour.

4.7 ARMOUR ROCK STABILITY BY JARVIS (2018)

4.7.1 **General**

Armour rock stability tests were conducted simultaneously with the scour tests on the same 2D wave flume set-up. The tests were conducted and analysed by Ross Jarvis and the results were provided as a contribution to this thesis.

The stability of the rubble-mound berm's armour rocks was determined with a percentage damage, which is defined as follows:

$$\% \, damage = \frac{Number \, of \, rocks \, moved}{Total \, number \, of \, rocks} \tag{4-14}$$

where the total number of rocks is the number of rocks that are visible from a front view of the rubble- mound berm and the number of rocks moved is the number of rocks that could be visually identified to have moved during exposure to waves during testing. The visual observation was done with a flicker method that entails flicking back and forth between "before" and "after" images taken of the front view of the rubble-mound berm and counting the rocks that moved.

The stability factor, N_s, as defined in Equation (2-1) as well, was used with the critical significant wave height, $H_{s,critical}$, to analyse the test results and determine the influence the berm width has on the armour rock stability:

$$N_s = \frac{H_{s,critical}}{\Delta \, D_{n,50}} \tag{4-15}$$

4.7.2 **Armour Rock Stability with Varying Wave Periods**

Numerous stability tests were conducted with varying wave periods and wave heights. The results on the influence of the wave period on the amour rock stability are shown in Figure 4-54.
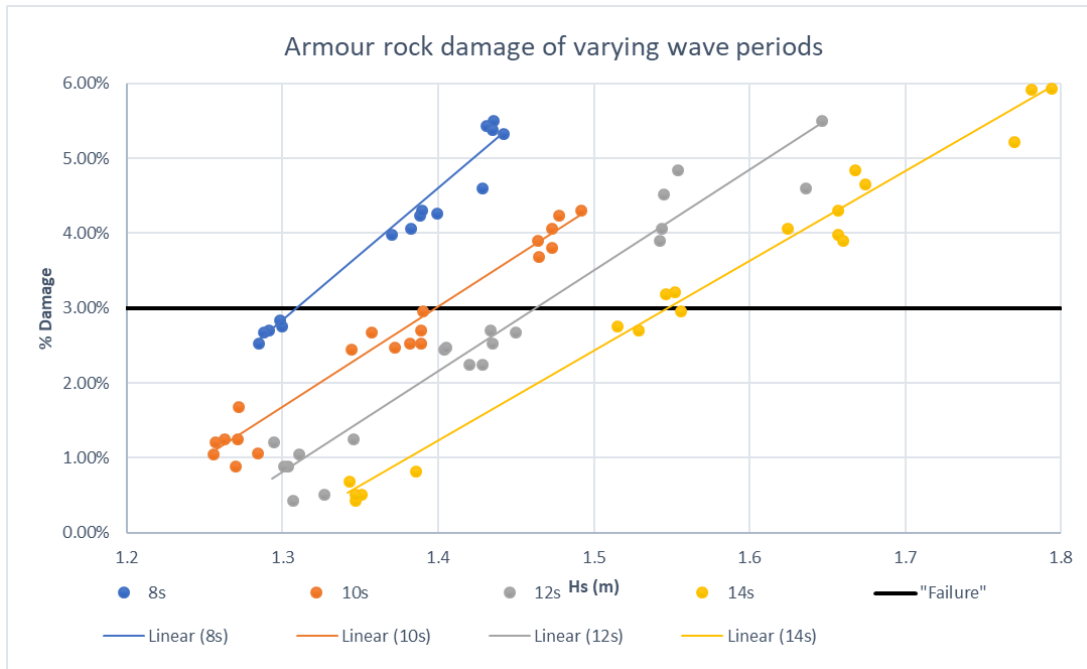
Figure 4-54: Influence of wave periods on armour rock damage (Jarvis, 2018)

It is evident that the wave period has a significant effect on the damage that occurs in the armour rock layer of the berm: smaller wave heights are required to result in the same amount of damage with 8 second waves, compared to the rest. This means that shorter wave periods result in more damage. The reason for this is assumed to be the same as mentioned in Section 4.1.2, where it was observed that shorter waves cause significant interaction between the incident and reflected waves, which result in deeper drawbacks and superimposed breaking waves that cause more damage to the rubble-mound berm, from the armour layer to the screed layer (Jarvis, 2018).

4.7.3 Armour Rock Stability with Varying Berm Widths

The influence of the berm width on the stability of the armour rock layer of the berm was also tested. A higher stability factor, *Ns*, represents a more stable berm set-up. The berm width test results are shown in Figure 4-55.
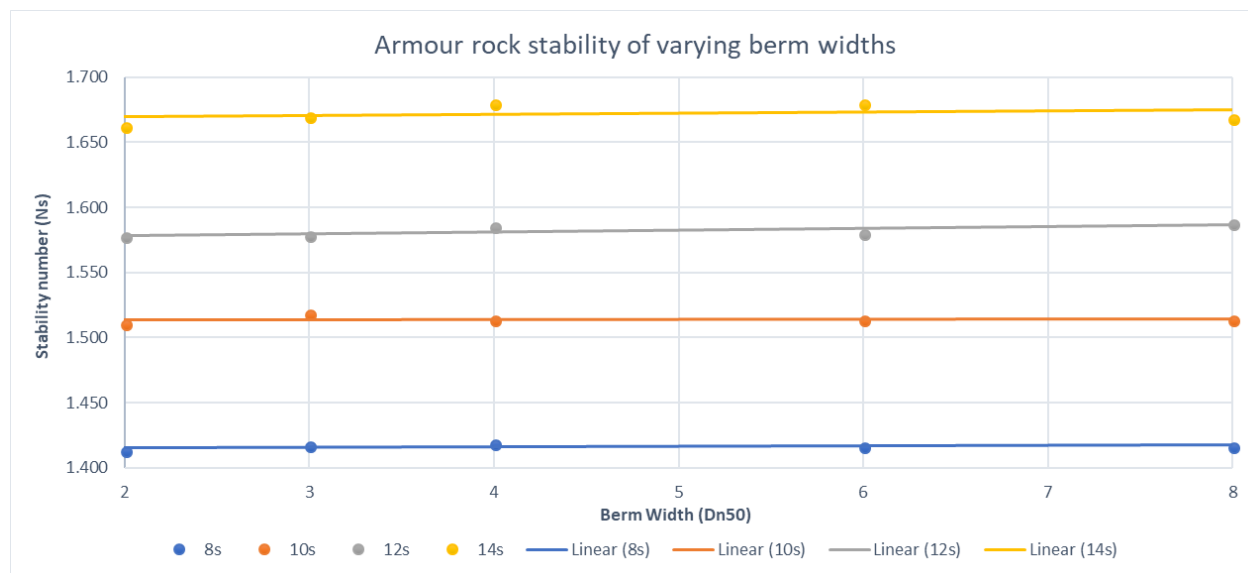
Figure 4-55: Influence of berm width on armour rock stability (Jarvis, 2018)

Once again, it can be seen that the wave period has a significant influence on the armour stability with shorter wave periods that cause more destabilisation than longer wave periods. However, the berm widths did not seem to have as much of an influence on the stability of the armour layer. The stability number for the 8 and 10 second waves remains relatively constant for all the berm widths, from $2D_{n50}$ up to $8D_{n50}$. The 12 and 14 second wave period tests showed a slight increase in stability as the berm widths increased (Jarvis, 2018).

4.7.4 **Relation Between Armour Rock Stability and Scour Damage**

Figure 4-56 shows the correlation between the scour area in the screed layer and the stability number of the armour rock of the berm. The scour areas for the different berm set-ups with varying peak wave periods were measured during Tests B to F that were discussed in Sections 4.3.3 to 4.3.7. The corresponding stability numbers for the armour rocks for each of these tests were determined by Jarvis (2018) and therefore the results of the two different measurements could be directly compared in Figure 4-56.
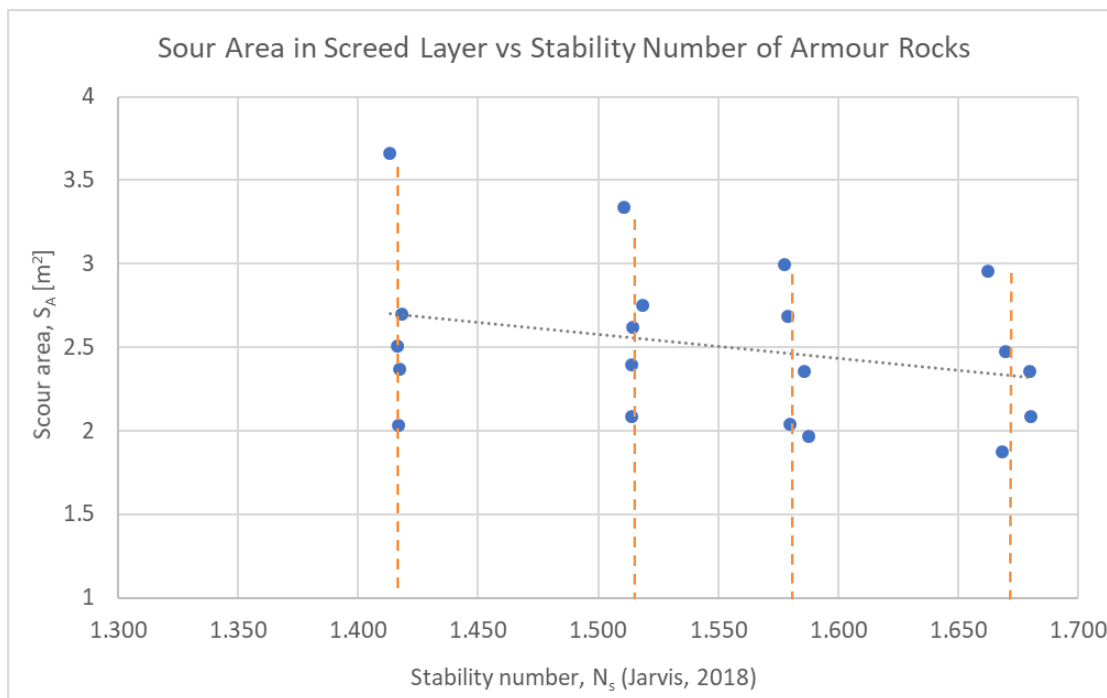
Figure 4-56: Correlation between scour area in screed and stability number in armour rocks

It can be observed that the graph as a whole forms a general scatter plot, but when inspecting the patterns that form within the scatter, it is clear that four distinct lines result which show four values of stability numbers that remain relatively constant throughout five different tests with increasing scour damage (shown in orange). These four lines show the effect of the four different wave periods and the five increasing scour area values show the general effect of the decreasing berm widths. Figure 4-56 also shows a general trend that an increasing stability number results in a decreasing scour area, in other words less scour damage (shown in grey).

The conclusion for the trends shown in Figure 4-56 is that a higher stability number results in less scour damage, which is consistent with the hypothesis stated in Section 3.2.3. This is because a more stable armour rock layer protects the berm structure better against wave attack and therefore less wave energy can penetrate through the berm and wash out the screed material to eventually cause scour.

5. CONCLUSIONS AND RECOMMENDATIONS

5.1 GENERAL

Coastal defences are becoming more and more important as the value of coastal properties increase while the risk of flooding due to sea level rise also increases. Seawalls are hard engineering options to defend the landward side of the coastline against wave attack and flooding. However, the robust structure of seawalls can have an adverse effect on the natural coastal processes like sediment transport and wave breaking and can cause damaging processes like scour to develop underneath the seawall. Scour undermines the stability of seawalls and can eventually cause failure. Therefore, it is vital to investigate the scour process at seawalls in an attempt to understand which parameters govern the process and how seawall structures can be protected against scour.

The objective of this study was firstly to investigate literature on seawalls and how scour develops underneath seawalls. Previous physical model studies were investigated to gain knowledge on experimental set-ups for scour tests in a 2D flume and how scour prediction is done. Physical model tests were then conducted to determine the influence of the wave period, the berm width and the screed layer thickness on scour that developed underneath the model seawall. A relation between the armour rock stability and the scour damage was also investigated. The main objective of the study was to eventually contribute to a design standard for a rubble-mound foundation for a vertical seawall, specifically focusing on the screed layer to be resistant to scour.

5.2 LITERATURE REVIEW CONCLUSIONS

A thorough investigation of literature revealed different designs for seawalls in different coastal environments. Vertical seawalls were found to be specifically susceptible to scour since the reflection coefficient for vertical seawalls is significantly high. Thorough research was done on the development, 2D flume experimental set-ups and the prediction of sand scour at vertical seawalls or breakwaters, specifically by Xie (1981), Sumer and Fredsøe (1997 – 2006) and Burchart and Hughes (2001 – 2012). Hughes (2001) formulated Equation (2-17) that predicts the maximum sand scour that can be expected at vertical structures that are exposed to breaking waves while Xie (1981) developed Equations (2-18) and (2-19) to predict sand scour for non-breaking waves. Sumer and Fredsøe (1997) also conducted numerous experiments on the sand scour process and developed Equation (2-20) to predict scour at the lee-side of a breakwater roundhead, among others. However, insufficient literature was found on

granular scour and the physical modelling and prediction thereof. Therefore, new methods of experimentally testing granular scour had to be developed like the use of sonar technology. Sonar technology can create detailed images of small and submerged surfaces, which is ideal for measuring scour in a thin screed layer underneath the submerged base of a seawall. The gap in coastal research and thus in design guidelines on granular scour further motivated this study to be conducted.

For more detail, refer to the full summary of the literature review in Section 2.9.

5.3 CONCLUSIONS OF PHYSICAL EXPERIMENTS

5.3.1 General

32 scour tests were conducted in a 2D glass wave flume at the CSIR hydraulic laboratory in Stellenbosch. The 32 tests investigated the effect that the number of waves, the peak wave period, berm width and screed layer thickness had on the scour that developed in the screed layer directly underneath the seawall. The tests were conducted simultaneously with armour rock stability tests by Jarvis (2018) so that a correlation between the scour damage and the armour stability could also be investigated.

5.3.2 Scour Measurement: Dowel and Sonar Techniques

There are no standard methods to measure scour, particularly granular scour, underneath the base of a seawall in an experimental set-up. Therefore, new measuring techniques were developed for the acquisition of scour damage data. Malan (2016) developed the "dowel method" which involves that the rock berm in front of the seawall is removed after the wave test finished in order to gain access to the screed layer. Then wooden dowels are used to probe underneath the seawall to measure how deep the dowel can penetrate until the screed layer offers resistance. These depth measurements are taken at 15 points along the face of the seawall to create a profile of the scour pattern that formed during the test. However, this is an intrusive method of measurement and the scour results can be disturbed as the measurements are taken.

An alternative method, the "sonar method", was developed by the author. This encompasses the use of sonar technology to create images of the submerged scoured screed layer where scour depths can be measured from. This method also involves removing the rock berm in front of the seawall to gain access to the screed layer. However, the sonar probe is only placed in front of the toe of the seawall so an image can be taken of the scoured screed layer and does not penetrate or disturb the screed layer as measurements are taken. Thus, the sonar-method

is a non-intrusive method that also gives more objective measurements as opposed to the dowel-method that can be pushed into the screed layer with varying force that could acquire inconsistent scour depth measurements. The consistency of the sonar measurements was also tested, as mentioned in Section 3.10.3, and an average difference of no more than 14% was found between independent measurements of the same test results.

The sonar equipment was also relatively quick and convenient to set up and the software had a user-friendly interface. Therefore, the sonar method was found to be highly effective and accurate to measure granular scour damage in the screed layer underneath a seawall structure in an experimental set-up.

5.3.3 Influence of Wave Period

The influence of the wave period on the scour process in the screed layer was observed in the wave flume. It could be seen that the shorter wave periods (8 s and 10 s) caused a rapid change in direction of orbital velocities of the water particles as the wave broke against the model seawall and induced a reflected wave. The significant interaction between the incident and reflected waves caused extensive drawbacks and superimposed waves that resulted in rapid back and forth movements of screed material so it eventually washed out and caused significant scour. The longer wave periods (12 s and 14 s) did not show such significant interaction between the incident and reflected waves near the seawall and as a result the screed material was not exposed to such rapid changes in orbital velocities and therefore the scour damage was not as extensive.

The visual observation was confirmed by the scour measurements. Both the dowel and sonar measurements indicated that the shorter wave periods caused deeper scour than the longer wave periods, although not by a large extent. This observation is in direct contrast with what was hypothesised in Section 3.2.3: it was expected that since a longer wave period causes higher orbital velocities, the scour damage would also be more extensive due to those higher orbital velocities. However, the effect of the reflected waves was not expected to be as crucial. The interaction between the incident and reflected waves was more significant with shorter wave periods, which resulted in more scour. It must be emphasised, however, that the general effect of the different wave periods on the scour damage was less significant than what was expected.

It is also important to take into account the range of wave periods that were tested. The abovementioned conclusion should preferably only be applied to a peak wave period range of 8 to 14 seconds. The observations made on the effect of the wave period on the scour underneath the seawall are also specifically applicable to a vertical seawall with a high reflection coefficient. Scour underneath marine structures with different reflection coefficients (for example more gradual slopes) might react differently to varying wave periods and therefore it is important to

consider the site-specific conditions and approach each project individually when it comes to marine structure design.

5.3.4 Influence of Berm Width

The effect of the berm width on the scour process in the screed layer could also be partially visually observed and it was evident that a wider berm did not allow the wave energy to penetrate as far into the screed layer and cause scour as a result. The wider the berm, the less screed material was disturbed by the wave attack.

This visual observation was confirmed by the dowel and sonar measurements of scour depths. Figure 4-39 and Figure 4-40 show a summary of all the berm test results where the average scour areas of each of the berm tests are compared. The widest berm ($8D_{n50}$) resulted in the least amount of scour and the narrowest berm ($2D_{n50}$) showed the worst scour damage. This observation confirms the hypothesis in Section 3.2.3 that a wider berm will effectively protect the screed layer against wave attack and will result in less scour. It is also interesting to note that the scour damage of the $2D_{n50}$ berm is significantly more than the $3D_{n50}$ berm, which confirms the recommended minimum berm width of $3D_{n50}$ in *The Rock Manual* (CIRIA, 2007b).

These observations were considered when an optimal berm width was recommended for the verification Test Set H. The wider berm widths of $8D_{n50}$ and $6D_{n50}$ were not considered since these wide berms require much more material and construction costs even though the wide berms did not seem to protect the screed layer against scour damage as effectively as expected. The $2D_{n50}$ wide berm was also not considered due to the significant scour damage that occurred with this berm width, as mentioned above. Table 4-2 evaluates the remaining $3D_{n50}$ and $4D_{n50}$ berm widths according to appropriate criteria for effective berm design: scour protection, armour stability, wave reflection, overtopping, construction and economic factors. The evaluation criteria suggested that the $4D_{n50}$ wide berm would provide the best balance among the above-mentioned factors of berm design.

5.3.5 Influence of Screed Layer Thickness

The screed layer thickness tests revealed that a thicker screed layer results in more scour. The 200 mm prototype screed layer showed much more scour than the 100 mm screed layer and the 300 mm screed layer resulted in even more scour, as seen in Figure 4-41 and Figure 4-42. However, the screed layer thickness tests were only limited to one test for each thickness due to time constraints and therefore these results should be confirmed in case studies by site specific model tests.

The scour depth results confirm the hypothesis that a thicker screed layer will result in more scour since a larger area of smaller, less stable material is exposed to wave attack. However, the screed layer must still be thick enough to level out the irregularities of the core bedding so the seawall element can be placed level as well as to allow for construction tolerances.

5.3.6 Repeatability of Scour Tests

The variable output parameters of the *HR Wallingford* wave-maker, like the peak wave period, T_p and significant wave height H_s, remained constant throughout all the test sets so the repeatability of the waves produced by the wave-maker was satisfactory. The repeatability of the experimental set-up had to be confirmed as well. Test Set H was conducted to verify the test results on the berm widths $3D_{n50}$ and $4D_{n50}$ that were recommended as mentioned in Section 5.3.4. This verification also confirmed the repeatability of the experimental set-up that was used throughout all the test sets. Test H1 verified the results of Test D2, the $4D_{n50}$ wide berm tested with a 10 s peak wave period. The scour area results from Test D2 and Test H1 differed with an average of 9%. Test H2 verified the results of Test E3, with a peak wave period of 12 s and a berm width of $3D_{n50}$. These tests' scour area results differed with 16%, but this higher variance could be due to construction inconsistencies as well. In general, the repeatability of the tests was adequate.

5.3.7 Relation between Reflection Coefficient and Scour

The reflection coefficient, as determined by the wave probe measurements, had the expected correlation with the scour damage in the screed layer: the tests that resulted in a higher reflection coefficient, showed less scour damage. This may be due to the fact that longer wave periods cause higher reflection coefficients and less scour or because a higher reflection coefficient means less wave energy penetrated the rubble-mound berm and foundation and more energy is reflected backwards. Consequently, the screed layer is not as disturbed so the scour damage is less. The reflection coefficient is lower with wider berm structures since more wave energy can be absorbed. Therefore, a wider berm structure is advantageous to acquire a lower reflection coefficient, which is necessary when activities on the seaside of a reflective structure are sensitive to reflected waves, like docking vessels.

5.3.8 Scour Prediction with Dimensional Analysis

Simple dimensional analysis was applied to the test results in order to produce equations to predict the behaviour of scour in the screed layer of a rubble-mound foundation for a vertical seawall. The dimensionless parameters

included either the deep-water or shallow-water wave heights and linear and polynomial trend lines were tested against the test results. The data ranges that these equations are applicable for are shown in Table 5-1:

Table 5-1: Applicable ranges for test variables

Test Variable	Applicable range [prototype]
Significant wave height, H_0 and H_s	1.013 – 1.307 m
Peak wave period, T_p	7.758 – 14.335 s
Water depth at toe	4 m
Scour depth	0 – 1.73 m

The equation that is recommended to be used is Equation (4-7) since the coefficient of determination, R^2, shows the best correlation to the data:

$$S_A/{H_0}^2 = -0.0002 \cdot \left(L_0/B\right)^2 + 0.0362 \cdot L_0/B + 1.1014 \qquad R^2 = 0.773 \qquad (4\text{-}7)$$

However, as mentioned in Section 4.6.3, it is technically more accurate to use the dimensionless parameter that includes the shallow-water significant wave height H_S, as opposed to the deep-water wave height, H_0, since H_S has a more direct effect on the scour damage. However, H_S could not be measured accurately and therefore the equations that include H_S in the dimensionless parameter are not recommended. The dimensionless parameters that include scour area, S_A, are also preferred to those with average scour depth, S_D, since scour area is more representative of the scour damage along the entire face of the seawall than the average scour depth taken across the entire seawall face.

5.3.9 Relation between Armour Rock Stability and Scour

There is a clear relation between the scour damage in the screed layer of the rubble-mound foundation and the stability of the armour layer of the rubble-mound berm: the wave conditions and berm set-up that result in the most scour, also result in a less stable rock armour layer. The destabilised armour rocks most probably also cause more scour damage in the screed layer since the damaged armour layer does not provide sufficient protection for the screed layer against wave energy penetration.

The influence of the wave period on the armour rock stability was evident: shorter wave periods caused more damage and destabilisation compared to longer wave periods. As mentioned in Sections 4.1.2 and 4.7.2, this is due to the more significant interaction between the incident and reflected waves that cause more rapid changes in orbital velocities with shorter wave periods.

The berm width did not seem to have as significant an effect on the armour stability as expected in the hypothesis in Section 3.2.3. The tests with the shorter wave periods show no real improvement in stability as the berm width increases, while the longer wave period tests show minor stability improvement with a wider berm. This is consistent with the observations made with the influence of the berm width on the scour damage in the screed layer: a wider berm resulted in less scour of screed material, but not to such a large extent. Therefore, the rubble-mound berm design can be economically optimised by keeping the berm as narrow as possible without allowing for too much scour or armour layer damage to occur.

5.4 RECOMMENDATIONS

5.4.1 Optimised Rubble-mound Foundation and Berm Design

The main objective of this study was to contribute to a design standard for a rubble-mound berm and foundation of a vertical seawall with specific focus on the screed layer. It was concluded that more scour can be expected at marine structures where shorter wave periods occur as opposed to longer wave periods. Therefore, the site-specific coastal conditions, specifically wave periods, should be taken into consideration when designing scour protection.

The optimal berm width in terms of scour protection, stability, constructability and economical factors, was found to be the $4D_{n50}$ berm as described in Section 4.3.8. The recommended screed layer thickness was the minimum allowable thickness that is used in practice, which is 100 mm in prototype. However, this is also dependent on the core material that is used in the rubble-mound foundation.

The layout of the different rock layers and the screed toe are also important considerations that have to adhere to general filter rules (CIRIA, 2007b). The cross-section of the recommended rubble-mound foundation and berm of an L-wall is shown in Figure 5-1.
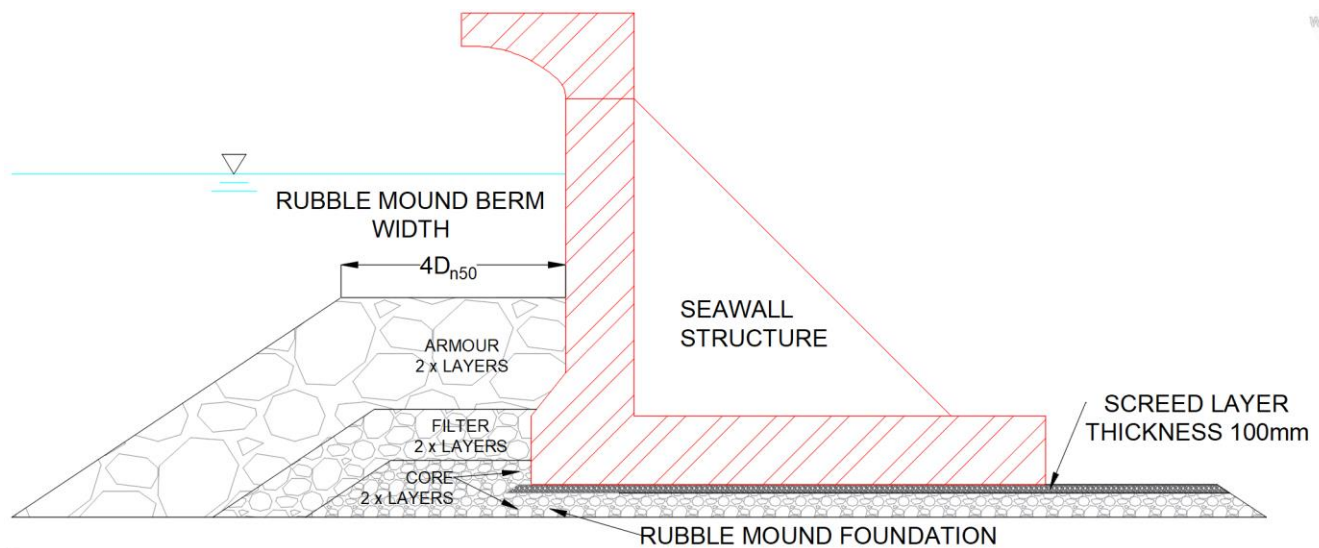
Figure 5-1: Cross-section of recommended rubble-mound berm and foundation for vertical seawall

5.4.2 Recommendations for improved methodology

The methodology for the experimental set-up and execution of the physical model tests was optimised as far as possible and recommendations to improve the methodology are limited to a minimum. However, like most physical model tests, more verification tests are recommended to improve the validity of the results. Due to time limitations, most of the scour tests of this study could only be conducted once and verification tests were limited to the recommended berm structures even though the berm recommendations were based on unconfirmed tests. Yet, the scope of the study also only allowed for the tests that were actually conducted.

It was found that, like the preceding scour tests by Malan (2016), the construction method had a very significant influence on the scour damage that developed underneath the model seawall. The screed layer is specifically sensitive to unevenness and material volume irregularities. The construction method of the core and screed layers may even have a bigger influence on the screed layer's ability to withstand scour than parameters like the berm width. Therefore, it is imperative to keep the construction methodology as constant as possible to be able to compare different experiments, although great care was taken during the experimental tests of this study to remain consistent with the rubble-mound construction.

In terms of data acquisition, shallow water probes would have been very useful to have during testing in order to acquire accurate shallow water wave heights at the toe of the structure. However, the accuracy of the wave height readings would be questionable since the probe set-up would have had to be placed above a shallow-water slope which would result in inconsistent wavelengths and since the interaction between the incident and reflected waves was very evident, incident wave heights would have been difficult to measure.

Data acquisition with sonar technology was very successful during scour depth measurements in the 2D wave flume underneath the model seawall. Clear images could be captured of the scour patterns that formed in the screed layer and relatively accurate measurements could be taken from those images. However, this method can either be developed further or other methods of measuring granular scour can be researched and put to the test.

The boundary effects that can be detected in the scour data must be minimised as far as possible. The seawall was sealed to the glass flume walls on both sides with silicon and it was done as effective as possible. However, boundary effects still had an influence on the data and therefore the data on both edges had to be cropped to acquire an accurate set of data. According to the statistical analysis done in Section 4.2.2, it is recommended that 13,3% on each side (in this case 2 points on each side out of the total of 15 data points) of the entire seawall length's data has to be cropped to acquire an accurate data set that is not influenced by boundary effects.

5.4.3 **Recommendations for Further Research**

The scope of the study only allowed for a limited number of variables to be tested in the physical model scour tests. Malan (2016) varied the construction methods of the screed layer, the screed toe layout and the screed layer thickness. This thesis's variable parameters were peak wave period, berm width and also screed layer thickness to confirm Malan's (2016) findings. A recommendation for further studies would be to vary the wave height and water depth to investigate the effect of these variables on the scour underneath the seawall.

The grading of the rock layers of the berm is another parameter that may have a significant effect on the scour in the screed layer. Different grading sizes and grading widths can therefore be put to the test. The standard filter rules should still be applied where the median dimension of the overlying rock layer should be 10 times the median size of the underlying rock layer.

As mentioned above, time limitations did not allow for extensive verification tests. Therefore, it would be recommended to redo tests identical to this study and to expand the research with verifications or by testing more wave periods, like 16 and 18 seconds, to simulate other South African storm conditions.

Research on further practical application of sonar technology in physical modelling of coastal engineering problems should be encouraged since it is already being used successfully in practice and since medical sonar equipment offers smaller, more manoeuvrable instruments that can be used in a laboratory.

6. REFERENCES

Alexander, M. G. (2016) *Marine Concrete Structures*. Duxford: Woodhead Publishing.

Arneson, L. a. *et al.* (2012) 'Evaluating Scour at Bridges', *U.S. Department of Transportation Federal Highway Administration*, (18), p. 340. Available at: http://www.fhwa.dot.gov/engineering/hydraulics/pubs/hif12003.pdf.

Battjes, J. and Stive, M. (1985) 'Calibration and Verification of a Dissapation Model for Random Breaking Waves', *Journal of Geophysical Research*, 90(C5), pp. 9159–9167.

Bruun, P. (1985) *Design and Construction of Mounds for Breakwaters and Coastal Protection*. Amsterdam: Elsevier Science Publishers B. V.

Burchart, H. and Hughes, S. (2012) *Coastal Engineering Manual (CEM)*. Wahington D. C.: Engineering Manual 1110-2-1100.

Chadwick, A., Morfett, J. and Borthwick, M. (2013) *Hydraulics in Civil and Environmental Engineering*. 5th edn. Danvers: CRC Press.

CIRIA, C. (2007a) 'Chapter 3 Materials', in *The Rock Manual*, pp. 1–14.

CIRIA, C. (2007b) 'Chapter 6 Design of Marine Structures', in *The Rock Manual*, pp. 1–14.

Dean, R. and Dalrymple, R. (2001) *Coastal Processes with Engineering Application*. Cambridge: Cambridge University Press.

Definitions.net (2017) *Hard Engineering*. Available at: http://www.definitions.net/definition/hard engineering. (Accessed: 25 October 2017).

Dolui, G., Chatterjee, S. and Das Chatterjee, N. (2016) 'Geophysical and geochemical alteration of rocks in granitic profiles during intense weathering in southern Purulia district, West Bengal, India', *Modeling Earth Systems and Environment*. Springer International Publishing, 2(3), p. 132. doi: 10.1007/s40808-016-0188-5.

Fowler, J. E. (1992) 'Scour Problems and Methods for Prediction of Maximum Scour at Vertical Seawalls', *Coastal Engineering*, (May).

Fredsøe, J. and Deigaard, R. (1992) *Mechanics of Coastal Sediment Transport*. Singapore: World Scientific Publishing Co. Pte. Ltd.

French, P. (2001) *Coastal defences: Processes, Problems and Solutions*. 1st edn. London: Routledge. Available at: https://books.google.co.za/books?hl=en&lr=&id=zTYGjO91F24C&oi=fnd&pg=PR9&dq= French,+P.W.+ (2001)+Coastal+defences:+Processes,+Problems+and+Solutions.+London:+ Routledge.&ots=bsoHj6dS0J&sig=hMupZD36FThuPNYYdtuPay2Fn3s#v=onepage&q&f=false.

van Gent, M. R. A. and van der Werf, I. M. (2014) 'Toe Stability of Rubble Mound Breakwaters', *Coastal Engineering*, 83, pp. 166–176.

Gislason, K., Fredsøe, J. and Sumer, B. M. (2009) 'Flow under standing waves Part 2 . Scour and deposition in front of breakwaters', *Coastal Engineering*. Elsevier B.V., 56(3), pp. 363–370. doi: 10.1016/j.coastaleng.2008.11.002.

GNS (2018) *Marine Geophysics*. Available at: www.gns.cri.nz (Accessed: 15 August 2018).

Gravesen, H. (2008) 'Rubble Mound Breakwaters', in *MEK DTU: Hydraulic Engineering*, pp. 1–67.

Hoffmans, G. J. (2012) *The influence of turbulence on soil erosion*. Eburon Uitgeverij BV.

Huang, C.-C. (2017) 'Failure mechanisms of steep-faced geosynthetic-reinforced retaining walls subjected to toe scouring', *Marine Georesources & Geotechnology*. Taylor & Francis, 35(8), pp. 1–12. doi: 10.1080/1064119X.2017.1290170.

Hudson, R. Y. *et al.* (1979) 'Coastal Hydraulic Models', *U.S. Army, Corps of Engineers Coastal Engineering Research Centre*, 5.

Hughes, S. A. (1995) *Physical models and laboratory techniques in coastal engineering*. Singapore: World Scientific (Advanced series on ocean engineering ; v. 7).

Hughes, S. A. (2001) 'Design of Maritime Structures: Scour and Scour Protection', in *U.S. Army, Corps of Engineers Coastal Engineering Research Centre*. Mississippi. Available at: http://link.springer.com/10.1007/s40808-016-0188-5.

Jarvis, R. (2018) *Stability Analysis of Varying Berm Widths of a Composite Vertical Seawall*. MEng Thesis Stellenbosch University.

Keulegan, G. (1973) 'Wave Transmission through Rock Structures', *Research Report Research Report H-73-1, US Army Engineer Waterways Experiment Station, Vicksburg, Mississippi.*

Kretschmer, M. M. (2017) 'Effect of the form of the overhang of a recurve seawall to reduce wave overtopping', *MEng Thesis, University of Stellenbosch*, (December).

Liftech Consultants, I. (2013) *Redwood City Wharves*. Available at: http://www.liftech.net/all-galleries/wharf-galleries/redwood-city-wharves-1-2-2013/ (Accessed: 3 February 2018).

Malan, C. T. (2016) 'Scour of the Screed Layer Underneath a Vertical Seawall With a Rubble Mound', *MEng Thesis, University of Stellenbosch*, (December).

Mansard, E. P. D. and Funke, E. R. (1980) 'The Measurement of Incident and Reflected Spectra Using a Least Squares Method', *Coastal Engineering 1980*, pp. 154–172. doi: 10.1061/9780872622647.008.

Van der Meer, J. W. (1993) *Conceptual design of rubble-mound breakwaters*, *Delft Hydraulics no 483*. Delft.

Van der Meer, J. W. (1998) 'Geometrical design of coastal structures', *Seawalls, dikes and revetments*, pp. 1–15.

Le Méhauté, B. (1976) 'Similitude in Coastal Engineering', *Journal of the Waterways, Harbours and Coastal Engineering Division, America Society of Civil Engineers*, 102(WW3), pp. 317–335.

Neelamani, S. and Vedagiri, M. (2002) 'Wave interaction with partially immersed twin vertical barriers', *Ocean Engineering*, 29(2), pp. 215–238.

Pagliara, S., Palermo, M. and Carnacina, I. (2012) 'Live-bed scour downstream of block ramps for low densimetric Froude numbers', *International Journal of Sediment Research*. International Research and Training Centre on Erosion and Sedimentation and the World Association for Sedimentation and Erosion Research, 27(3), pp. 337–350. doi: 10.1016/S1001-6279(12)60039-0.

Pilarczyk, K. W. (2003) 'Hydraulic and Coastal Structures in International Perspective', *Repository.Tudelft.nl*, p. 49. Available at: http://repository.tudelft.nl/view/hydro/uuid:9c8267d4-cdb6-4c53-8045-15afa6294e04/.

Pitkala, L. (1986) 'Retaining Wall made of L-elements as a Quay Structure', *Pianc*, 54.

Rossouw, J., Coetzee, L. W. and Visser, C. J. (1982) 'A South African Wave Climate Study', *Coastal Engineering Proceedings*, pp. 87–107.

Schoonees, J. (2018) 'Personal Communication, Middle East Seawall'. Stellenbosch: University of Stellenbosch.

Schoonees, T. (2014) 'Impermeable recurve seawalls to reduce wave overtopping', *MEng Thesis, University of Stellenbosch*, (April).

SCOPAC (2018) *Research Project: Beach response in front of structures in open coast*, *scopac.uk.org*. Available at: https://www.scopac.org.uk/beach-response.html (Accessed: 12 July 2018).

Sumer, B. and Fredsøe, J. (1997) 'Scour at the round head of a rubble-mound breakwater', *Coastal Engineering*, 29, pp. 231–262.

Sumer, B. M. *et al.* (1994) 'Bed Shear Stress and Scour around Coastal Structures', *Coastal Engineering Proceedings*, 1(24), pp. 1595–1609. doi: https://doi.org/10.9753/icce.v24.%p.

Sumer, B. M. (2006) 'Physical and mathematical modelling of Scour', *Coastal & River Engineering*, pp. 1–18. Available at: http://www.theeuropeanlibrary.org/tel4/record/2000001944196.

Sumer, B. M. and Fredsøe, J. (1997) 'Scour at the head of a vertical-wall breakwater', *Coastal Engineering*, 29(96), pp. 201–230.

Sumer, B. M. and Fredsøe, J. (2000) 'Experimental study of 2D scour and its protection at a rubble-mound breakwater', *Coastal Engineering*, (40), pp. 59–87.

Sumer, B. M., Whitehouse, R. J. S. and Tørum, A. (2001) 'Scour around coastal structures: a summary of recent research', *Coastal Engineering*, 44(2), pp. 153–190. doi: https://doi.org/10.1016/S0378-3839(01)00024-2.

Swart, E. (2016) 'Effect of the overhang length of a recurve seawall in reducing wave overtopping', *MEng Thesis, University of Stellenbosch*, (December).

Van Wageningen, G. (2018) 'Personal Communication, Sonar Technology'. Stellenbosch: Winelands Radiology.

Wallingford, H. R. (2018) 'Wavemakers for physical models Multi-element wavemakers', *Eq-017 R1*, p. 10. Available at: www.hrwallingford.com/equipment.

Warmink, J. and Joustra, R. (2013) 'The design of granular scour protection', *ConcepTueel*, 22(4), pp. 36–39.

Warnock, J. (1950) *Hydraulic Similitude*, *Engineering Hydraulics*. Edited by H. Rouse. New York: John Wiley & Sons.

Wehr, J., Freitag, G. and Köhler, T. (2015) 'Load test on vibro stone columns offshore near Abu Dhabi', in *Deep Foundation Institute Middle East Conference*. Abu Dhabi, pp. 1–7.

Xie, S. L. (1981) *Scouring patterns in front of vertical breakwaters and their influences on the stability of of the foundations of the breakwaters*, *TU Delft*. TU Delft, Faculty of Civil Engineering and Geosciences, Hydraulic Engineering. doi: 10.1016/S0378-3839(96)00024-5.

7. APPENDICES

7.1 APPENDIX A

Irribarren Number

Example of calculation of Irribarren number over bathymetry for different wave periods:

$$L_b = \frac{g\,T^2}{2\pi}\,\tanh(\frac{2\pi\,d}{L_b}) = \frac{9.81 \cdot 8^2}{2\pi}\tanh(\frac{2\pi \cdot 4}{L_b}) \;\therefore\; L_b = 48\,m \tag{7-1}$$

$$\varepsilon_b = \frac{\tan\beta}{\sqrt{H_b/L_b}} = \frac{1/18.6}{\sqrt{1.3/48}} = 0.33 \tag{7-2}$$

Table 7-1: Wave breaker type determination

Wave Period [s]	Wavelength [m]	Irribarren Number	Breaker Type
8	48.0	0.33	Spilling
10	61.0	0.37	Spilling
12	73.8	0.41	Plunging
14	86.5	0.44	Plunging

Wave Transmission

Table 7-2: Parameter scaling for wave transmission

Parameter	Prototype value	Model value
P	0.38	0.38
ΔL	0.1 m	0.005 m
D	0.019 m	9.5×10^{-4} m
h	4 m	0.2 m
H_i	1.5 m	0.075 m
ν	1.0565×10^{-6}	1.00035×10^{-6}

$$P = P_m = P_p \qquad D_m = D_p K \frac{L_m}{L_p}$$
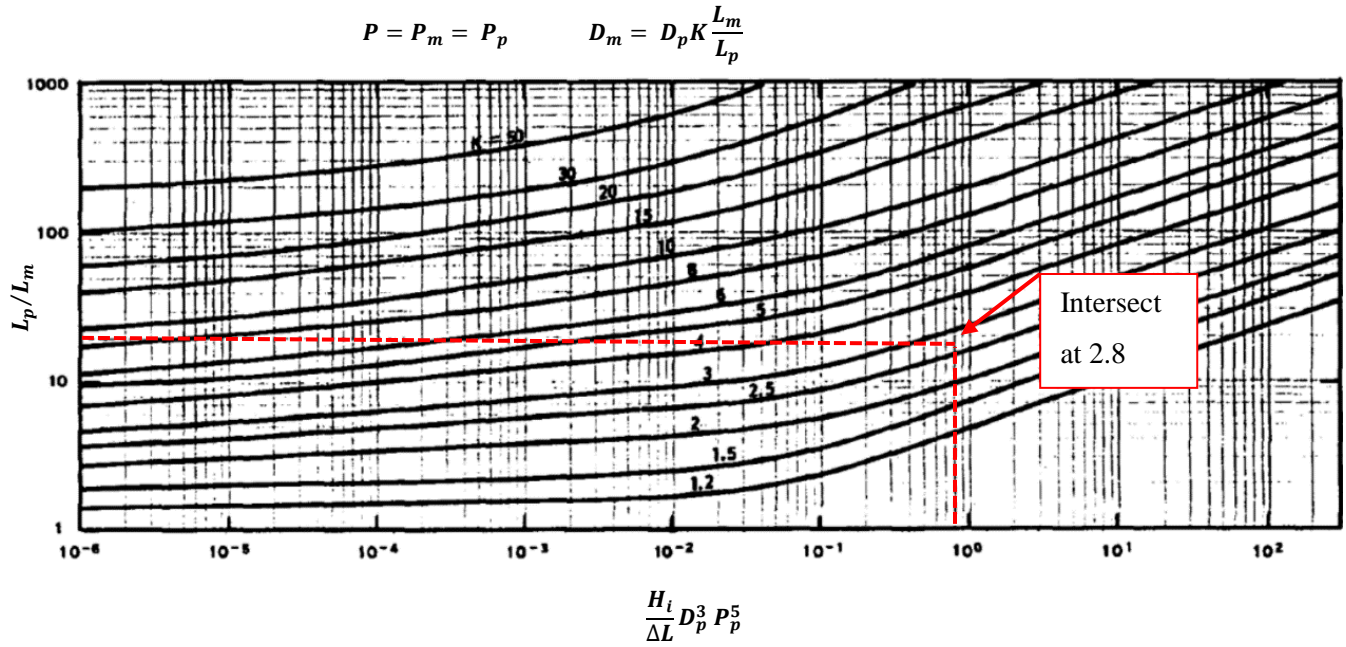
Figure 7-1: Nomogram used for sizing rubble-mound structures for Wave Transmission (Hughes, 1995)

Table 7-3: Wave transmission scaling calculations

T_p [s]	T_m [s]	L_p [m]	L_m [m]	y_p	H_p	$R_{n,p}$	$R_{n,m}$	y_m	D_m	K	Average Keulegan K	Average K with Lé Mehauté
8	1.789	48.006	2.400	12819.1	6.007	7689.082	90.507	3376.967	0.001817	1.913		
10	2.236	60.957	3.048	15610.1	5.802	7810.747	91.939	4147.103	0.001813	1.909	1.907	2.354
12	2.683	73.767	3.688	18471.0	5.695	7876.800	92.716	4929.254	0.001811	1.906	**Final D_m**	
14	3.130	86.497	4.325	21369.0	5.632	7916.660	93.186	5717.909	0.001809	1.905	0.00224	

*p: prototype and m: model

Bathymetry Layout
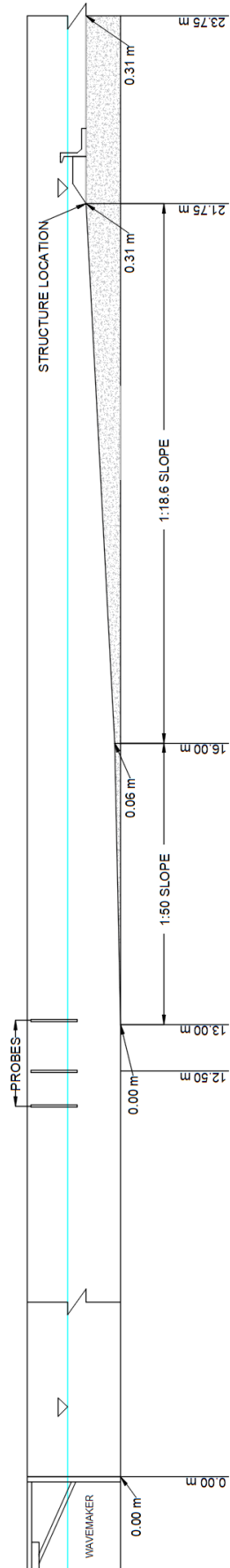
Figure 7-2: Bathymetry layout model dimensions [m]

7.2   APPENDIX B

Rubble-mound Material Gradings
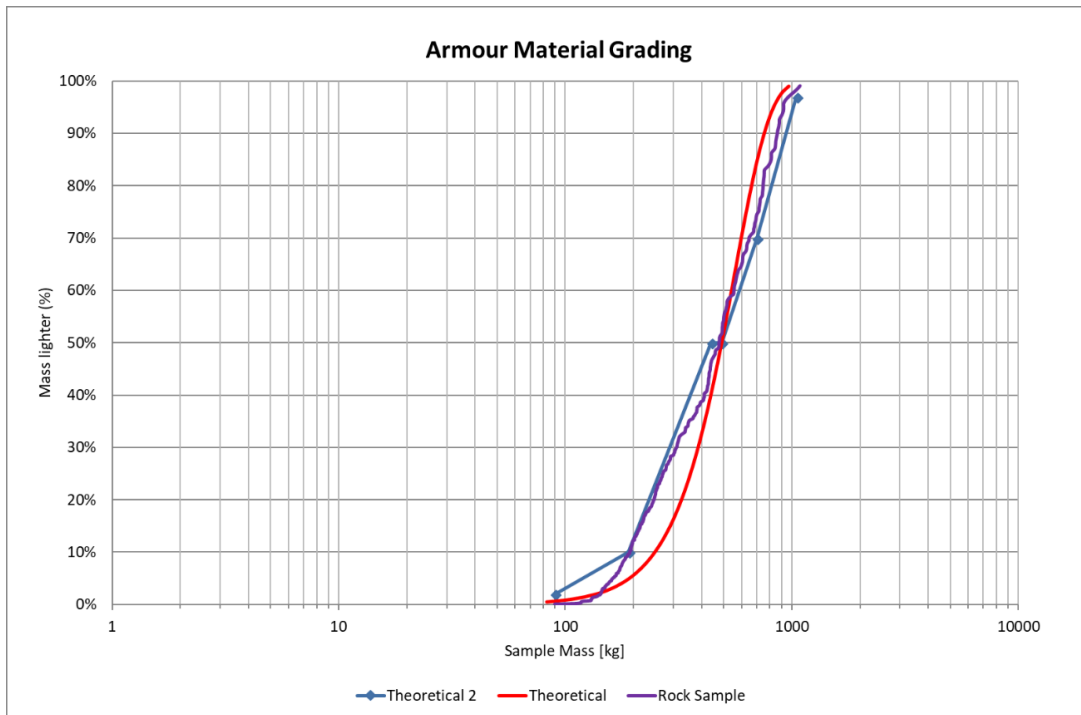
Figure 7-3: Armour material grading curve
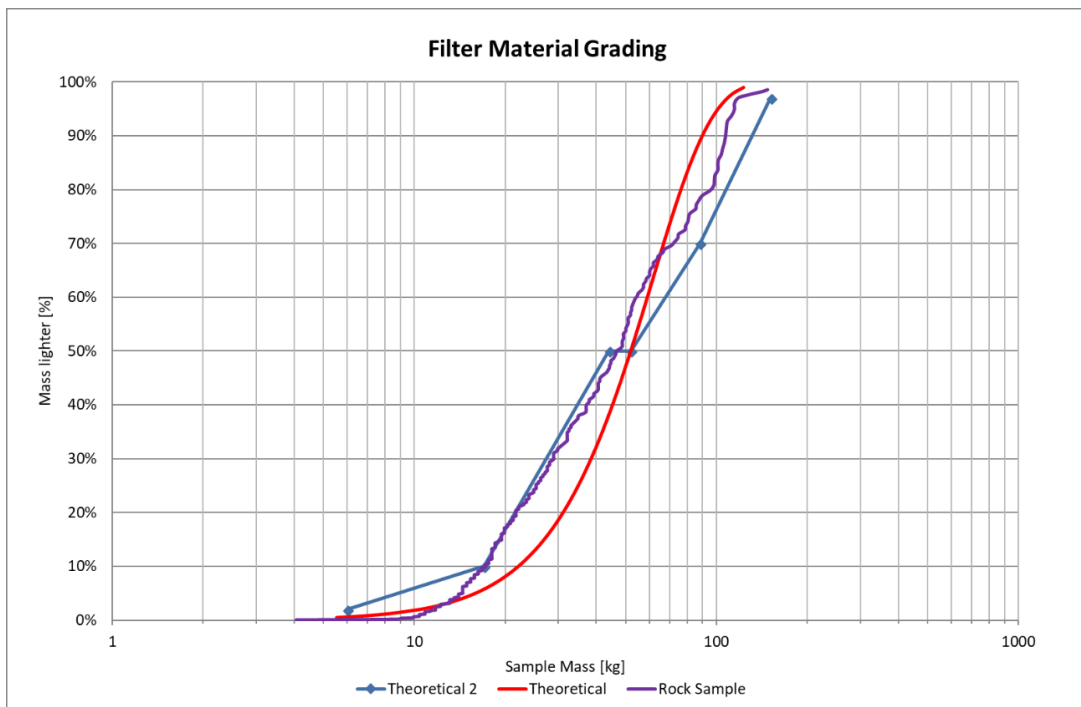
Figure 7-4: Filter material grading curve
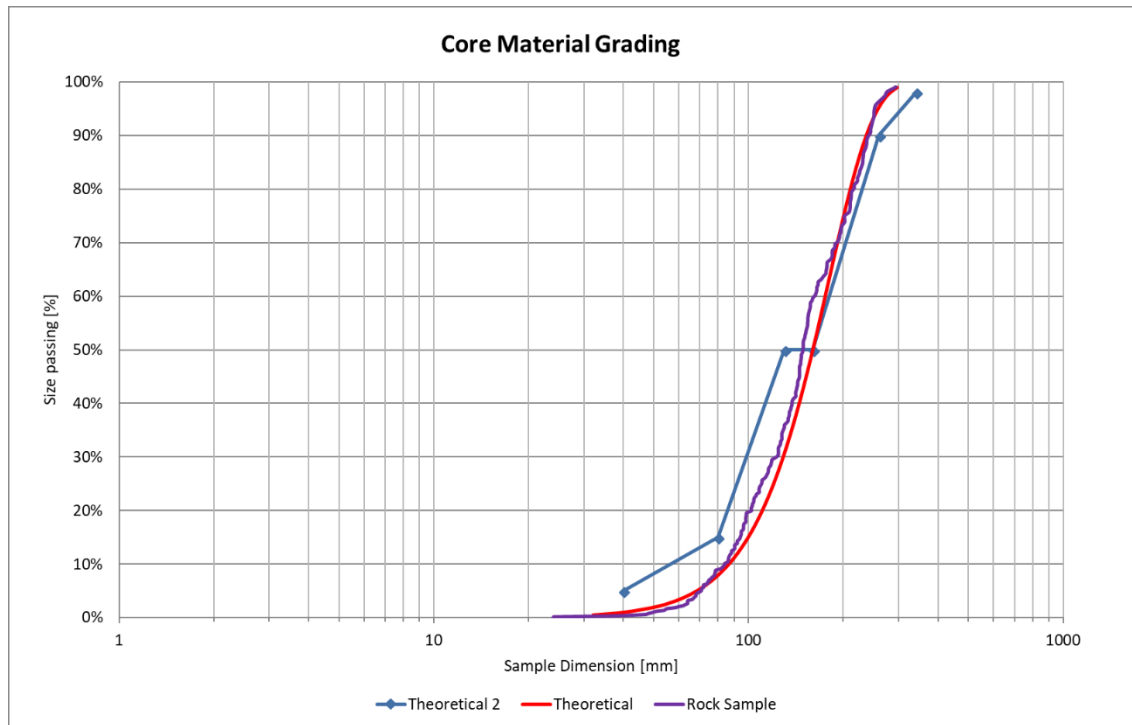
Figure 7-5: Core material grading curve

7.3 APPENDIX C

Bathymetry Construction Process
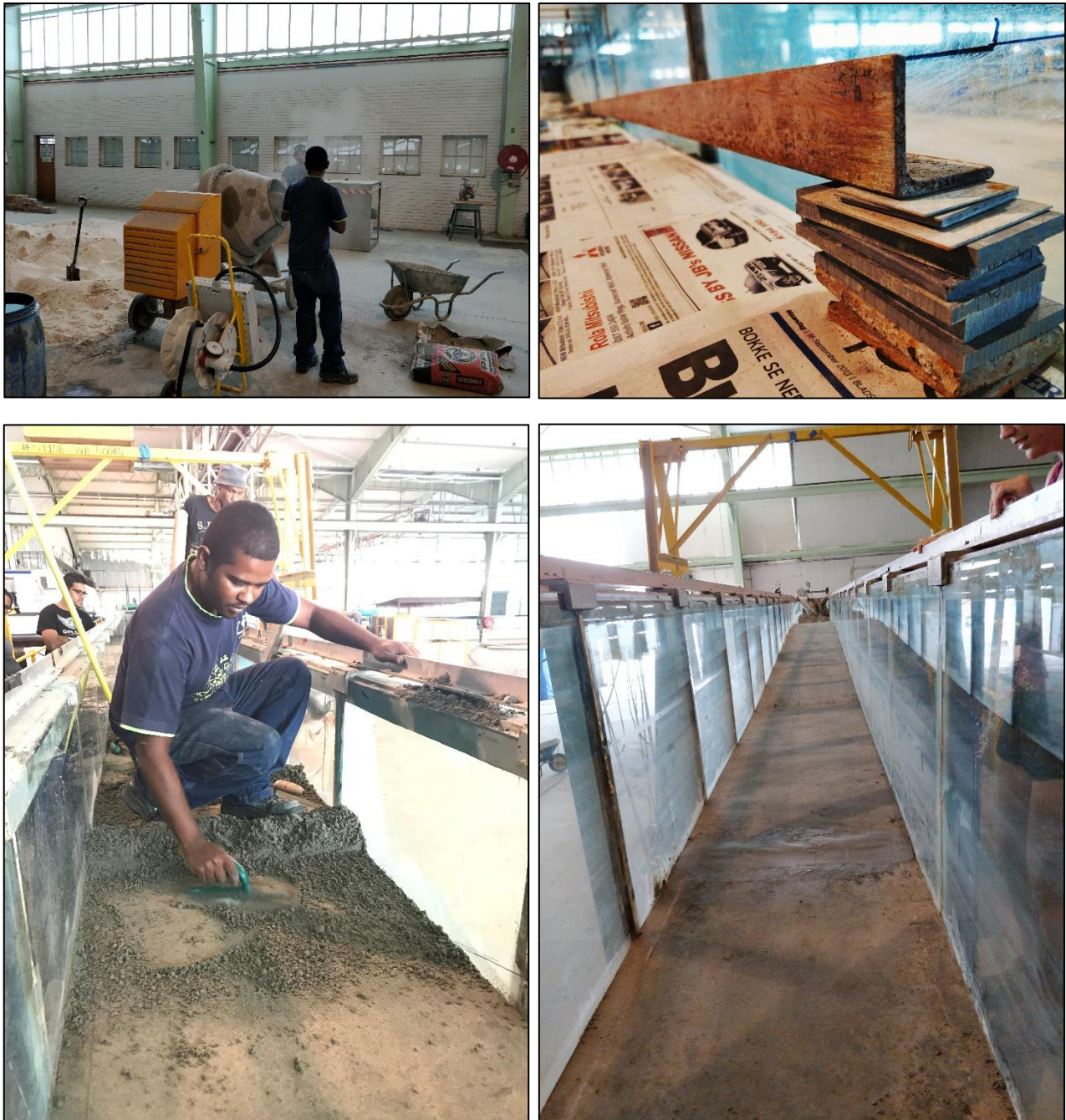
Figure 7-6: Construction process of concrete bathymetry in wave flume

Rubble-mound Foundation and Berm Construction with Sand Screed Layer and Seawall

Figure 7-7: Rubble-mound foundation and berm construction with sand screed layer and seawall placement

Vertical Seawall Structure Model with $6D_{n50}$ Berm in Testing
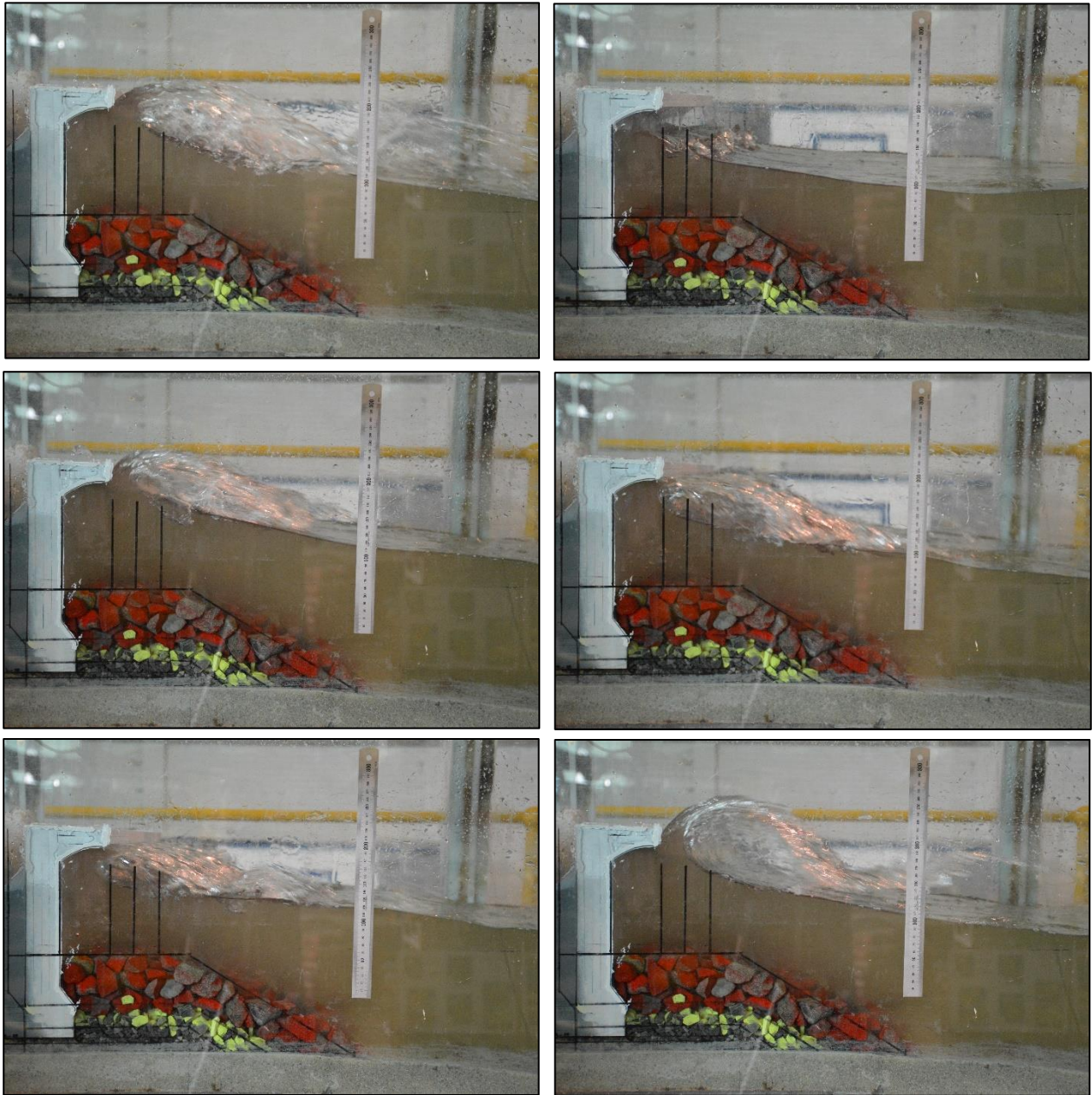
Figure 7-8: Seawall model with $6D_{n50}$ berm in testing

7.4 APPENDIX D

Raw data

Table 7-5: Input values for HR Wallingford wave-maker

Wave Conditions	Wave-maker Software Input Values			
	Wave height [m]	Wave period [s]	Gain	Single JONSWAP cycle duration
1.3M8S	1.3	8	0.97	916
1.3M10S	1.3	10	0.8	1145
1.3M12S	1.3	12	0.66	1374
1.3M14S	1.3	14	0.63	1603

Table 7-4: Raw data measurements of scour for sonar and dowel methods [cm]

TEST SET A1	Method	1	2	3	4	5	6	7	8	9	10	11	12	13	14	15	Area
A1_500W	Sonar	15.6	20	14.5	10.8	8.1	8.4	8.4	9.1	10.1	6.1	4.7	11.1	13.9	15.5	13.5	6147.5
	5mm	16	20.5	24	21	16	15	13	11.5	10	12	4	12	15	15	17	6700
T_p: 7.758	10mm	9	17	11	12	8	5	7	6.5	6	4	1	3	9	10	12	3125
	average	12.5	18.75	17.5	16.5	12	10	10	9	8	8	2.5	7.5	12	12.5	14.5	4912.5
A1_1000W	Sonar	8.7	9	9.7	11.3	13.1	16.1	13	13.1	21.6	17.9	11.7	16.7	15.4	20	15.4	7352.5
	5mm	22	27	24	24	17	23.5	22.5	23	19	16	21	18	25	21	25	10425
T_p: 7.758	10mm	12	25	21	22	17	18	15	13	17	13	13	16	12.5	13.5	16	8037.5
	average	17	26	22.5	23	17	20.75	18.75	18	18	14.5	17	17	18.75	17.25	20.5	9231.25
A1_1500W	Sonar	17.9	18.7	12.7	28.4	19.3	12.9	23	23.9	15.6	23.2	27.5	25.7	33.6	29.2	40.9	11132.5
	5mm	40	29	18	36	18	32	24.5	32	25.5	26	23	20	37	21	28	13225
T_p: 7.758	10mm	21	18	15	25.5	17	19	23	20	19.5	20	14	15	27.5	24	26	9712.5
	average	30.5	23.5	16.5	30.75	17.5	25.5	23.75	26	22.5	23	18.5	17.5	32.25	22.5	27	11468.75
A1_2000W	Sonar	14	18.6	25.8	27.1	27.8	20.1	26.2	28.4	29.7	25.1	21.4	23.4	27.6	29.9	28.3	12795
	5mm	36	38	24	43	30	39	30.5	28	41	28	29	20	28	35.5	30	15725
T_p: 7.758	10mm	26	25	18	26	23	29.5	23	16	27.5	25	19	22	17	23	21	11425
	average	31	31.5	21	34.5	26.5	34.25	26.75	22	34.25	26.5	24	21	22.5	29.25	25.5	13575
A1_3000W	Sonar	16.8	15.6	30.3	6.7	22.5	24	23.9	22.5	32.4	29	32.7	28.8	29.2	30.6	33.6	12612.5
	5mm	43	35	56	42	29	42	30	43	46	34	27	46	32	36	35	19150
T_p: 7.758	10mm	24	23	27	33	21	25	27	20	30	22	21.5	26	23.5	23	31	12537.5
	average	33.5	29	41.5	37.5	25	33.5	28.5	31.5	38	28	24.25	36	27.75	29.5	33	15843.75
TEST SET A2	Method	1	2	3	4	5	6	7	8	9	10	11	12	13	14	15	Area
A2_500W	Sonar	9.8	12.8	13	10.8	8.1	6.4	8.4	7.1	10.1	6.1	4.7	9.1	11.9	13.5	14	4162.5
same as A1	5mm	16	20.5	24	21	16	15	13	11.5	10	12	4	12	15	15	17	6700
T_p: 7.758	10mm	9	17	11	12	8	5	7	6.5	6	4	1	3	9	10	12	3125
	average	12.5	18.75	17.5	16.5	12	10	10	9	8	8	2.5	7.5	12	12.5	14.5	4912.5
A2_1000W	Sonar	17.8	6.2	9	6.2	6	5.8	14.7	13.1	13.8	12.2	8.3	8.7	7.1	11.3	15.2	4842.5
	5mm	17.5	12	15	8	8	7.5	25	21	16	17	22.5	21	14	18.5	16	8025
T_p: 7.758	10mm	14	7	7.5	4.5	5	5	13	16	12	10	8.5	7	4	14	11	4337.5
	average	15.75	9.5	11.25	6.25	6.5	6.25	19	18.5	14	13.5	15.5	14	9	16.25	13.5	6181.25
A2_2000W	Sonar	15.2	11	10.4	19.6	13.8	14.7	10.8	17	9.9	12	18.3	11.2	15.6	16.8	20.7	7015
	5mm	12	14	8	22	13	8.5	10	24	12	23	14	14	19	32	33	7700
T_p: 7.758	10mm	8	5	6.5	8	6	5	8	10	9	8.5	7	9	11	28	17	3962.5
	average	10	9.5	7.25	15	9.5	6.75	9	17	10.5	15.75	10.5	11.5	15	30	25	5831.25
A2_3000W	Sonar	27.1	15	12.7	13.1	12.4	13.9	11.4	15.5	10.3	10.4	12.6	15	17	20.2	25.3	6472.5
	5mm	31	21	15	16	16.5	14.5	11	17	12	11	15	14	23	34	60	7300
T_p: 7.758	10mm	16	9	9.5	10	12	8	9	9.5	6	8	9	10	15	24	23	4687.5
	average	23.5	15	12.25	13	14.25	11.25	10	13.25	9	9.5	12	12	19	29	41.5	5993.75
TEST SET B	Method	1	2	3	4	5	6	7	8	9	10	11	12	13	14	15	Area
B1a_8S6D	Sonar	37.5	24.5	10.1	11.6	9.3	13.4	13.7	16.4	12.7	12.7	12.1	12.4	12.1	10.1	20.3	6270
RC: 71.11	5mm	43	21	38	12	13.5	24	22	40	40	31	45	29	41	55	123	14800
T_p: 7.759	10mm	21	13	12	7.5	13	16	18	24	26	20	24	17	15	29	55	8950
$H_{m0,0}$: 1.307	average	32	17	25	9.75	13.25	20	20	32	33	25.5	34.5	23	28	42	89	11875
B2_10S6D	Sonar	14.7	10.4	7.1	11.9	11.9	10.4	14.7	14.6	11.9	15.1	11.9	9.8	7.8	12.2	23	5982.5
RC: 80.38	5mm	29	19	7	16	15	15	23	21	15	18.5	15	25	11	13	60	8625
T_p: 10.068	10mm	13	7	6	11	12	9	14	12	13	12	7	12	4	10	31	5350
$H_{m0,0}$: 1.186	average	21	13	6.5	13.5	13.5	12	18.5	16.5	14	15.25	11	18.5	7.5	11.5	45.5	6987.5
B3_12S6D	Sonar	15	11.2	8.4	12.1	13.2	9.8	9.4	6.4	11.4	9.3	10.3	11.6	8.3	16.7	28.3	5092.5
RC: 85.93	5mm	27	15	18	16	16	15	15	12	15	11	9	17	10.5	30	49	7012.5
T_p: 11.831	10mm	20	12	16.5	10	8	10	7.5	5	9	9	9	16.5	10	16	32.5	4862.5
$H_{m0,0}$: 1.044	average	23.5	13.5	17.25	13	12	12.5	11.25	8.5	12	10	9	16.75	10.25	23	40.75	5937.5
B4_14S6D	Sonar	26.3	11.6	12.7	12.9	7.1	10.2	8.9	12.4	11.9	7.8	7.6	10.4	17.5	19.4	26.8	5215
RC: 84.91	5mm	61	22.5	13	16	11	10	7	9	11.5	10	9	15	55	124	117	6625
T_p: 14.335	10mm	33	12	10	17	9	7	4	4.5	8	6	4	11	25	32	32	4400
$H_{m0,0}$: 1.089	average	47	17.25	11.5	16.5	10	8.5	5.5	6.75	9.75	8	6.5	13	40	78	74.5	5512.5

TEST SET C	Method	1	2	3	4	5	6	7	8	9	10	11	12	13	14	15	Area
C1_8S8D	Sonar	20.5	25.7	20.5	8.3	5.5	8.6	5.6	7.9	11.5	14.4	8.6	16.7	8.6	22.9	32.9	5082.5
RC: 63.17	5mm	24	35	14	11	11	10.5	9	9.5	12	12	17	16	15	45	40	6125
T_p: 7.758	10mm	15	15	10	8	7	7.5	4	5	9	8	10.5	12	10	22	32	4050
$H_{m0,0}$: 1.273	average	19.5	25	12	9.5	9	9	6.5	7.25	10.5	10	13.75	14	12.5	33.5	36	5087.5
C2_10S8D	Sonar	53.5	11.4	5.3	9.1	9.1	12.7	11.6	11.1	9.1	11.1	7.9	12.8	13.9	16.9	32.9	5205
RC: 72.75	5mm	18	12	13	22	11	19	15	15	10	10	11.5	23	29	46	41	7875
T_p: 10.068	10mm	10	7	5	9	6.5	10	7	9	7	7	6	9	17	24	30	4075
$H_{m0,0}$: 1.167	average	14	9.5	9	15.5	8.75	14.5	11	12	8.5	8.5	8.75	16	23	35	35.5	5975
C3_12S8D	Sonar	25.4	12.1	11.4	8.4	12.9	7.5	6.1	10.1	9.1	11.4	8.9	8.3	20	64.7	73.8	4920
RC: 80.54	5mm	26	21	13	14	17	10	12	16	12	14	12	15	22	78	88	6975
T_p: 11.831	10mm	19	9	10	11	8	9	11	6	8	7	5	11	16	45	59	4450
$H_{m0,0}$: 1.013	average	22.5	15	11.5	12.5	12.5	9.5	11.5	11	10	10.5	8.5	13	19	61.5	73.5	5712.5
C4_14S8D	Sonar	20.5	13.1	5.6	5.2	10.2	8	7.2	6.3	9.8	12.9	8.5	12.9	19.7	23.3	67.9	4682.5
RC: 85.75	5mm	38	22	14	13	14	15	16.5	13	13	10	12	14	25	44	81	7000
T_p: 13.398	10mm	14	16	5	3.5	8	9	7.5	4.5	10.5	9	5	9.5	22	20	38	4000
$H_{m0,0}$: 1.086	average	26	19	9.5	8.25	11	12	12	8.75	11.75	9.5	8.5	11.75	23.5	32	59.5	5500

TEST SET D	Method	1	2	3	4	5	6	7	8	9	10	11	12	13	14	15	Area
D1_8S4D	Sonar	18.8	20.2	14.4	17.9	13.2	10.6	13.9	10.1	15.5	17.4	15.2	8.3	11.1	31.2	33.7	6742.5
RC: 82.13	5mm	51	18	16	12	9.5	9	10	12	11	14	13.5	11	17	27	57.5	5925
T_p: 7.758	10mm	12	10	9.5	8	6	3	3.5	8	4	7	7.5	6	9	15	32	3112.5
$H_{m0,0}$: 1.306	average	31.5	14	12.75	10	7.75	6	6.75	10	7.5	10.5	10.5	8.5	13	21	44.75	4518.75
D2_10S4D	Sonar	40.9	27.4	14.4	15.9	16.7	11.6	9.6	11.2	12.1	10.9	14.4	13.4	16.1	21.2	33.3	6552.5
RC: 89.62	5mm	44	15	20	21	13.5	11	11.5	14.5	10	12.5	12	8	15	40	53	6575
T_p: 10.068	10mm	30	16	11	10.5	7.5	6	5	6	4.5	8	6	7	9	24	28	3525
$H_{m0,0}$: 1.177	average	37	15.5	15.5	15.75	10.5	8.5	8.25	10.25	7.25	10.25	9	7.5	12	32	40.5	5050
D3_12S4D	Sonar	64.2	19.2	11.9	10.9	11.4	13.1	10.7	13.1	11.9	8.9	9.6	10.5	23.4	33.8	79.4	5887.5
RC: 92.78	5mm	64	27	13.5	11	10	7.5	5.5	10	11	6	8	14	17.5	77.5	70	4925
T_p: 11.831	10mm	45	27	11.5	6.5	8	7.5	5	9	7	6	3	6.5	15	39	41	3587.5
$H_{m0,0}$: 1.056	average	54.5	27	12.5	8.75	9	7.5	5.5	9.5	9	6	5.5	10.25	16.25	58.25	55.5	4256.25
D4_14S4D	Sonar	74.9	24.5	14.4	13.7	12.4	15.4	10.4	10.3	12.6	10.1	8.8	9.3	15.3	52.7	74.4	5892.5
RC: 95.11	5mm	74	24	30	16	19	19	34	12	17	11	9	14	17	77	79.5	8725
T_p: 13.398	10mm	43	22	8.5	10	13	13.5	11	8	7	5	5.5	9	12	45	29	4612.5
$H_{m0,0}$: 1.142	average	58.5	23	19.25	13	16	16.25	22.5	10	12	8	7.25	11.5	14.5	61	54.25	6668.75

TEST SET E	Method	1	2	3	4	5	6	7	8	9	10	11	12	13	14	15	Area
E1_8S3D	Sonar	57.5	16.7	14.9	17.9	15.4	11.1	11.3	7.6	9.1	9.4	5.8	12.2	22.5	30	24	5925
RC: 84.28	5mm	40	22	7	9	10	7	7.5	8	7	8	7.5	15	31	20	21	4900
T_p: 7.758	10mm	32	12	4.5	5	3.5	2.5	3.5	4	4	6	6	10	15	12	16	2712.5
$H_{m0,0}$: 1.300	average	36	17	5.75	7	6.75	4.75	5.5	6	5.5	7	6.75	12.5	23	16	18.5	3806.25
E2_10S3D	Sonar	36.7	30.3	19.1	13.8	13.1	10.7	13.1	11.2	9.7	14.8	13.3	17.8	20.8	48.5	77.3	6872.5
RC: 91.40	5mm	41	77	20	10	8	7	6.5	7	10.5	10	10.5	18	76	75	75	6775
T_p: 10.068	10mm	34	35	15	5	4	4	4.5	4.5	6	5.5	8	13	22	35	37	3650
$H_{m0,0}$: 1.202	average	37.5	56	17.5	7.5	6	5.5	5.5	5.75	8.25	7.75	9.25	15.5	49	55	56	5212.5
E3_12S3D	Sonar	52.7	75.3	27.4	26	9.3	6.8	9.8	13.1	11.2	13.6	11.9	12.7	12.3	21.2	60.3	6712.5
RC: 95.07	5mm	53	91	24	27	10	9	8	11.5	11	9	8	10	8	42.5	50.5	5975
T_p: 11.831	10mm	23	28.5	15	25	6	5.5	7	8.5	7.5	7	2	6	6.5	18	33.5	4262.5
$H_{m0,0}$: 1.070	average	38	59.75	19.5	26	8	7.25	7.5	10	9.25	8	5	8	7.25	30.25	42	5118.75
E4_14S3D	Sonar	68.8	9.4	11.2	9.8	10.4	9.8	4.1	12.6	13.7	12.6	12.2	18.8	28.5	49.2	57.3	6192.5
RC: 97.30	5mm	87	16	18	14	12	9.5	10	12	20	19	15	21	7	135	66	7250
T_p: 13.398	10mm	44	6	8.5	10	7	4.5	6	9	15	10	8.5	11	57	54	25	5687.5
$H_{m0,0}$: 1.074	average	65.5	11	13.25	12	9.5	7	8	10.5	17.5	14.5	11.75	16	32	94.5	45.5	6468.75

TEST SET F	Method	1	2	3	4	5	6	7	8	9	10	11	12	13	14	15	Area
F1_8S2D	Sonar	50.3	19.3	15.7	17.5	17.2	14.7	20	24.1	15	18.4	19.2	19.2	19.8	27.9	45	9152.5
RC: 88.92	5mm	55	41	38	23.5	24	22.5	27	35	33	33	34	28	41	36	60	14975
T_p: 7.758	10mm	24	16	11.5	13	11	12	14	16	18	18	19	16.5	20	20	45	7662.5
$H_{m0,0}$: 1.298	average	39.5	28.5	24.75	18.25	17.5	17.25	20.5	25.5	25.5	25.5	26.5	22.25	30.5	28	52.5	11318.75
F2_10S2D	Sonar	57.6	55.8	15.7	20.5	11.6	17.4	18.8	28.3	18.2	12.7	15.2	10.9	11.2	30.9	79	8352.5
RC: 94.80	5mm	69	44	32	21.5	14	22	17	30.5	27	15	14	15	10	43	86	9850
T_p: 10.068	10mm	43	26	15	14.5	11	14	9.5	13	13	7	7	8	5	27	21	5350
$H_{m0,0}$: 1.173	average	56	35	23.5	18	12.5	18	13.25	21.75	20	11	10.5	11.5	7.5	35	53.5	7600
F3_12S2D	Sonar	37.2	13.5	15.5	16.3	12.7	9.7	12	12.5	11.8	10.5	15.6	28.2	25.7	44	57.1	7495
RC: 97.06	5mm	40	18	17.5	14	16	9	9	17	16	13	12	20	24	86	61	7337.5
T_p: 11.831	10mm	23	11.5	12	10	10.5	6	5	10	9	7.5	6.5	15	16	30	29	4675
$H_{m0,0}$: 1.090	average	31.5	14.75	14.75	12	13.25	7.5	7	13.5	12.5	10.25	9.25	17.5	20	58	45	6006.25
F4a_14S2D	Sonar	86.1	58.5	18.1	14.1	12.7	9.3	9.4	11.9	9.8	18.5	15.4	16.5	42.2	42	47.5	7387.5
RC: 98.56	5mm	97	55	28	18	14	15.5	19	16	18.5	23	28.5	26	101	61	91	12150
T_p: 13.398	10mm	46	45	21	11	9	9.5	8	8	11	16.5	20	22	43	30	32	7350
$H_{m0,0}$: 1.115	average	71.5	50	24.5	14.5	11.5	12.5	13.5	12	14.75	19.75	24.25	24	72	45.5	61.5	9750

TEST SET G	Method	1	2	3	4	5	6	7	8	9	10	11	12	13	14	15	Area
G1_10S2T	Sonar	50.5	48.7	87.5	92.9	54.3	46.2	17.5	19.5	29.3	23.9	30.6	35	61.1	83.7	115	21175
RC: 85.98	5mm	43	57	163	99	64	56	50	55	87	91	88	115	162	106	191	43375
T_p: 10.068	10mm	26	27.5	56	36	17	20	18	27	37	54	40	33	52	33	102	16800
$H_{m0,0}$: 1.197	average	34.5	42.25	109.5	67.5	40.5	38	34	41	62	72.5	64	74	107	69.5	146.5	30087.5
G2_10S3T	Sonar	98.6	97.1	69.6	32.1	28.5	28.1	32.4	32.4	43.1	41.3	35.7	77.5	127.1	69.4	111.5	22472.5
RC: 84.64	5mm	90	92	34	22	23	28	28	30	44	46	51	85	127	134	121	21875
T_p: 10.068	10mm	67	59	20	15	14	17	18.5	20	23	25	24	44	55	64	97	11900
$H_{m0,0}$: 1.201	average	78.5	75.5	27	18.5	18.5	22.5	23.25	25	33.5	35.5	37.5	64.5	91	99	109	16887.5

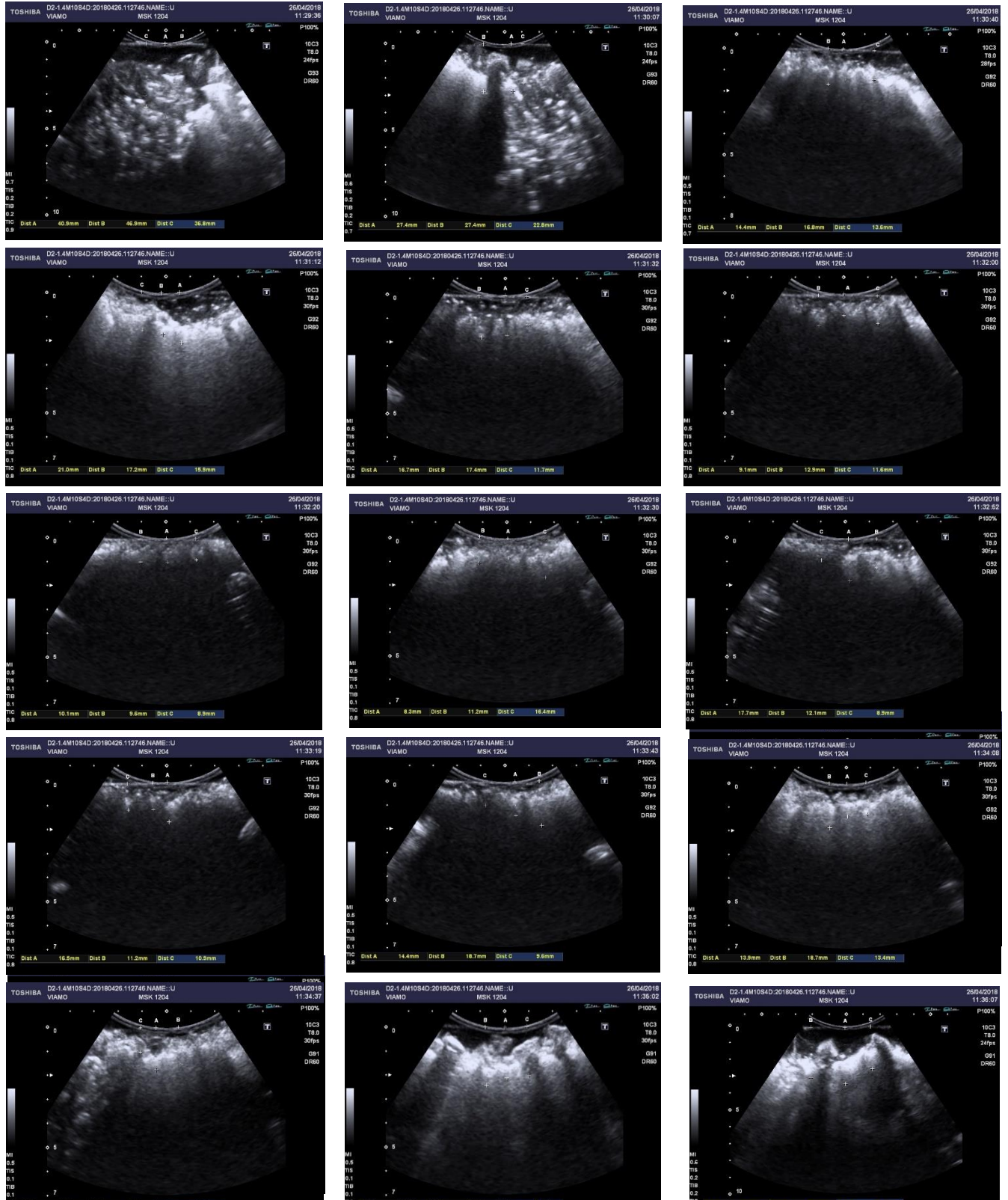| TEST SET H	Method	1	2	3	4	5	6	7	8	9	10	11	12	13	14	15	Area
H1_10S4D	Sonar	62.3	51.5	19.8	15	17.7	13.7	13.9	14.9	14.4	10.2	11.7	13.7	15.5	13.4	55.8	7142.5
RC: 90.31	5mm	88	90	75	31	87	87	92	88	90	78	90	81	97	87	94	40500
T_p: 10.068	10mm	45	33	45	21	39	39.5	25	28	31	24	27	25	36	27	38	15000
$H_{m0,0}$: 1.203	average	66.5	61.5	60	26	63	63.25	58.5	58	60.5	51	58.5	53	66.5	57	66	27750
H1.2_10S4D	Sonar	62.3	52	22.5	16	16.9	13.2	13.1	16	14.2	11.4	12.7	14.2	16.8	14.5	48.3	7367.5
H1.3_10S4D	Sonar	62	38.7	20.2	17.2	15.5	12.6	13.4	16.2	14.9	11.8	12.7	14.1	16.1	16.9	47.5	7327.5
H2_12S3D	Sonar	37.9	31.2	15.9	16.5	16.2	13.9	13.2	16.9	13.6	15	16.2	13.9	25.9	41	36.5	7815
RC: 93.96	5mm	51	30	28	27	30.5	24	27.5	22	28	22	25	23	53	83	73.5	13475
T_p: 11.831	10mm	33	18.5	16	17	19	23	18	17	17	20	18	17.5	28	39	36	9425
$H_{m0,0}$: 1.068	average	42	24.25	22	22	24.75	23.5	22.75	19.5	22.5	21	21.5	20.25	40.5	61	54.75	11450
H2.2_12S3D	Sonar	39.2	31.4	16	24.1	16.9	16.4	17.4	19.7	16.9	15.9	16	12.7	25.2	49.8	31.2	8830
H2.3_12S3D	Sonar	40.6	32.7	15.5	23.8	19.3	16.9	17.7	20.2	16.9	16.2	16	13.6	23.9	45.5	33.6	9015

Sonar Images of Test D2_10S4D

Figure 7-9: Images of sonar measurements for Test D2